Trinity College Dublin

The Impact of Electromagnetic Fields and Chemicals from Offshore Wind Farm Subsea Power Cables on Marine Environment

Trinity College Dublin
Coláiste na Tríonóide, Baile Átha Cliath
The University of Dublin

A Thesis Submission for the MSc (by research) in Civil, Structural and Environmental Engineering

4th of February 2022

Oluwasegun John Ohunyeye

Supervised by Dr Liwen Xiao

Trinity College Dublin

Declaration

I declare that this thesis has not been submitted as an exercise for a degree at this or any other university and it is entirely my own work.

I agree to deposit this thesis in the University's open access institutional repository or allow the Library to do so on my behalf, subject to Irish Copyright Legislation and Trinity College Library conditions of use and acknowledgement.

Name: Oluwasegun John Ohunyeye

Student Number: 19302301

Date: 04-02-2022

Acknowledgments

To begin with, I would like to thank God almighty for his love and protection throughout these years.

I want to express my most sincere gratitude to my fantastic supervisor Dr. Liwen Xiao, who was always generous with his time and wisdom. I genuinely appreciate all your efforts.

I wish to thank my parents, General Felix Ohunyeye and Mrs. Hannah Ohunyeye, and my sister, Sewa, who has always encouraged me to explore my ideas.

I would also like to say a massive thank you to Mary, who helped proofread my work.

Thank you all for your unwavering support.

Abstract

For many years, Subsea Power Cables (SPCs) have been installed across creeks and bays, connecting near-shore islands to the mainland. In more recent times, SPCs have been applied to supply power from offshore renewable energy installations to onshore substations, with little consideration for possible impacts of Electro-Magnetic Fields (EMFs) and chemicals from SPCs on marine species. Hence, this study unravelled the electromagnetic impacts by quantifying and characterising the EMFs produced by current and potential future SPCs. The Alternating Current cables produced magnetic field strengths ranging between 0.69 and 4.86 μT, and induced field strengths varying from 2.19×10^{-4} to 1.53×10^{-3} $\mathrm{V/m}$. On the other hand, the Direct Current cables produced magnetic fields of 56.20 – 105.59 μT and induced electric fields from 2.87×10^{-5} to 2.30×10^{-4} $\mathrm{V/m}$. The calculated intensities were then compared with the sensitivity threshold values of priority marine species with electromagnetic sensory capabilities, to establish the spectrum of species that are affected by the cables. In addition to this, an easy-to-use EMF estimation tool was developed to enable non-specialist users to model and estimate underwater cable emissions.

This study also investigated the toxicity of power cables: concentration of heavy metals (i.e. Al, Fe, Pb, Mn, As, Hg, Cd, Cu, and Ni) and abundance of microplastics released by four SPCs using different experimental procedures, an area of study which was hitherto relatively unresearched. The results revealed varying concentrations of the selected heavy metals. In addition, the study observed low levels of microplastic particles that were discharged by the cables. Collectively, the results provided new insights into the extent of pollution caused by SPCs. Finally, future research directions in this field were suggested.

Table of Contents

List of Figures

List of Tables

List of Acronyms and Abbreviations

H_2O_2	Hydrogen Peroxide
HNO_3	Nitric Acid
AC	Alternating Current
Al	Aluminium
As	Arsenic
ATSDR	Agency for Toxic Substances and Disease Registry
B-field	Magnetic Field
Cd	Cadmium
CIRC	Coaxially Integrated Return Cable
Cu	Copper
DC	Direct Current
E-field	Electric Felds
EHV	Extra High Voltage
EMFs	Electromagnetic Fields
ESCA	European Subsea Cable Association
EWEA	European Wind Energy Association
Fe	Iron
FOWTs	Floating Offshore Wind Turbines
HCl	Hydrochloric Acid
Hg	Mercury
HMs	Heavy Metals
HV	High Voltage
HVDC	High Voltage Direct-Current
ICNIRP	International Commission on Non-ionizing Radiation Protection
ICP-MS	Inductively Coupled Plasma Mass Spectrometry
ICP-OES	Inductively Coupled Plasma – Optical Emission Spectrometry
IGRF	International Geomagnetic Reference field
IRIS	Integrated Risk Information System
IRUG	Infrared and Raman User Group

LV	Low Voltage
Mn	Manganese
MPs	Microplastics
MRED	Marine Renewable Energy Devices
MV	Medium Voltage
NBDC	National Biodiversity Data Center
Ni	Nickel
NPWS	National Parks and Wildlife Service
OSS	Offshore Substation
OWET	Oregon Wave Energy Trust
OWFs	Offshore Wind Farms
Pb	Lead
PP	Polypropylene
RAIS	Risk Assessment Information System
RMS	Root Mean Square
RPM	Revolutions Per Minute
SPCs	Subsea Power Cables
SRC	Separate Return Conductor
SS	Onshore Substation
T_f	The Toxic Response Factor
WDP	Western Power Distribution

INTRODUCTION

1.0 Introduction

Growing efforts to mitigate the threat of global climate change has led to increased pressure to move away from energy production based on non-renewable fuels, such as natural gas, oil and coal, towards that of renewable resources (Gill et al., 2014; Pezy et al., 2020). On this basis, the need for a renewable energy source has given rise to an increase in the development and construction of Marine Renewable Energy Devices (MRED) all around the world (Otremba and Andrulwicz, 2014). Most developed countries make use of MREDs such as tidal energy or wave generators (tidal or wave turbines) and offshore wind farms (OWFs) for generating the maximum electric output possible (Uihlein and Magagna, 2016). However, of these technologies, the OWFs have proven to be by far the most sophisticated of them all (Wilding et al., 2017).

An operational OWF generates energy, which is transported from one point to the other, using subsea power cables (SPCs) (also called underwater power cables) (Andrulewicz and Otremba, 2011). Research conducted by Taormina et al. (2018) has shown that SPCs may permanently or temporarily have an impact on marine life and the natural environment, by disturbing their physical habitat and increasing the risk of entanglement. In other cases, SPCs may cause changes in artificial reef effects, chemical pollution, heat, noise, and electromagnetic field emissions (EMFs) (Petersen and Malm, 2006; Taormina et al., 2018).

In the early eighteenth century, the world's first subsea power cable (SPC) was laid across the Isar River, which cuts through Austria and Germany (Republic, 2020). Since then, SPCs have improved significantly with respect to installation techniques, cable dimensions, and materials used (Dunham et al., 2015). Similar to-shore-based transmission lines, SPCs are designed to use either alternating current (AC) or direct current (DC) transmission systems for connecting autonomous grids (Leibfried and Zoller, 2020). They could be potentially applied to supply power to subsea

observatories, islands, and oil and gas marine platforms (Taormina et al., 2020). Currently, over 70% of the world's high voltage direct-current (HVDC) cables are located in the continent of Europe (Ardlean and Minnebo, 2015).

As aforementioned, SPCs like any other human activities or man-made installation may disrupt marine life, by introducing various harmful pollutants into the marine environment. However, Taormina et al. (2020) considers the emission of EMFs as a major concern in comparison to the other environmental incidences. According to Nyqvist et al. (2020), electromagnetic fields can be divided into magnetic and electric fields. Electric and magnetic fields are naturally occurring forces of nature (Albert et al., 2020). Many marine organisms are able to detect these fields due to their magneto-sensitive or electro receptive features (Wiltschko and Wiltschko, 2005). On the other hand, submarine power cables produce artificial fields that may alter or mask natural electric and magnetic cues, which could affect various ecological processes such as homing, predation, feeding migrations or spawning, and the ability to detect sexual mates (Tricas and Gill, 2011).

Despite there being a gradual increase in ongoing research efforts to understand the effects of electric and artificial magnetic fields on marine fauna, analysis conducted appears to be based on only single cable configurations (Vattenfall AB, 2010; Hutchinson et al., 2021a). In real life applications, an OWF would typically have different cable configurations (e.g. Static AC and/or DC cables, or Dynamic AC cables) and voltages (Weerheim, 2018). Indeed, there may be a need to use higher voltage cables in certain sections and lower voltage cables in other sections, depending on the production and distribution requirements of the wind farm. To date, the most detailed study that provides both qualitative and quantitative information and analysis on EMFs produced by different cable configurations was conducted by Tricas and Gill (2011) for the US Department of Interior. Notably, Hutchinson et al. (2021b) stated that

there is a need for researchers to improve the current knowledge base on SPC transmission, by predicting the likely EMFs that may be produced by future larger capacity SPCs. In a different study, the author emphasised on the need for more elaborate EMF studies that include all aspects of magnetic and induced electric field modelling for AC and DC cables (Hutchinson et al., 2021a).

Apart from the EMFs that are generated by SPCs, the earth (i.e. particularly the ocean) itself creates its own local magnetic field, which may be altered by the EMFs from the cable (Tricas and Gill, 2011). This local magnetic field serves as an artificial global positioning system (GPS) for marine species (Wiltschko and Wiltschko, 2005), and therefore, should not be ignored (Tricas and Gill, 2011).

According to Hutchinson et al. (2021b), it is of utmost importance that future studies consider the influence of the earth's local magnetic field when modelling or predicting EMFs produced by SPCs. In addition, there is currently no freely available tool that can be used to estimate or predict EMFs from different SPCs. An easy-to-use EMF calculation tool will help the Irish public to predict EMFs from SPCs, without needing a technical background in physics/modelling.

Besides the ever-growing environmental concerns over the impact of EMFs on the marine environment, underwater cables have also been identified as a source of chemical pollution (Taormina et al., 2018). Cable components include plastics (e.g. polypropylene) and heavy metals, which have the potential to degrade (plastics or microplastics) or dissolve (heavy metals) and spread into the environment when SPCs have been damaged or abandoned (Meibner et al., 2006). To Taormina et al.'s (2018) best knowledge, no scientific studies have been conducted to determine how harmful these SPC-related pollutants may prove to be to marine organisms.

Improving our understanding of the cumulative impacts that SPC-related EMFs and Chemicals compounds may have on the marine environment, would be of benefit to both the public, and marine and energy companies, allowing them to make more comprehensive and informed decisions before applying for foreshore licenses.

1.1 Rationale for Conducting this Research

Fossil based energy production contributes to the emission of greenhouse gases globally. For this reason, European Union (EU) countries have begun making efforts to reduce their carbon and energy footprint (Ivanova et al., 2017) by promoting renewable power production such as wind power (Thomson, 2016). For example, the United Kingdom (UK) has prevented the emission of 36 million tonnes of greenhouse gases (within a 6-year period) by generating power from wind farms (Thomson, 2016). The country boasts of over 39 operational offshore wind farms, more than any other country in Europe (Sonnichsen, 2020). In comparison, Ireland has just 1 operational offshore wind farm (Curran, 2019). However, after years of neglect, energy firms have come up with a huge turn around as they prepare to invest over €5.9 billion into offshore wind projects in Ireland (O'Halloran, 2019). This development should significantly boost Ireland's energy generation and sales capacity in the coming years. Also, as offshore wind projects continue to increase, so will SPCs in the Irish sea, hence the need to further understand its potential environmental impacts to the marine environment. For this reason, the Irish Sea was chosen as a case study in this research.

1.2 Aims and Objectives

The aim of this project was to investigate the impact of electromagnetic fields and chemicals from offshore wind farm submarine power cables on marine species in the Irish Sea.

The specific objectives of this study were to:

- Quantify and characterise the EMFs produced by current and potential future subsea power cables.
- Design an easy-to-use EMF assessment tool.
- Identify priority marine organisms in the Irish sea that may be sensitive to either magnetic or electric fields.
- Determine the concentration of heavy metals released by SPCs.
- Determine the abundance of microplastics released by SPCs.

LITERATURE REVIEW

2.0 Literature Review

2.1 Introduction

Electromagnetic fields and its various sources, as well as the design characteristics of submarine power cable and its chemical pollutants are reviewed in this chapter.

2.2 Electromagnetic Fields

In physics, a field is frequently used to refer to the influence that an object has on its surrounding environment (McMullin, 2002). For instance, an apple is able to fall to the ground as a result of the force of the earth's gravitational field. Similarly, within our planet, several magnetic (B-field) and electric fields (E-field) occur (Singh et al., 2008). On a daily basis, organisms could be exposed to the influence of these invisible areas or forces of energy (Lewczuk et al., 2014). The human body is no exception to this, as it uses its own electric field as a source of communication by allowing the free flow of information between cells and tissues (WHO, 2005).

Apart from this natural occurrence, magnetic and electric fields are typically created whenever an object has electric charges flowing through it (WHO, 2007). Notwithstanding, electric fields are also able to exist even when an electric current is not in use (WHO, 2007). The electric field depends on the voltage, whilst the magnetic field depends on the current (Hydro Quebec, 2011). When identified individually, an increase in either voltage or current will result in a concurrent increase in the strength or magnitude of the field (McManus and Department of Energy, 1988). The quantity unit for the magnetic field strength is tesla (T) or gauss (G) and for the electric field strength, volts per meter (V/M) (National Grid, 2018).

In connection with subsea cables, the strength of a cable's field is also affected by the voltage and current flowing through it (Scott et al., 2018).

Aside from this, Tricas and Gill (2011) noted that cables are also affected by other parameters such as its' design characteristics (e.g. the use of an alternating or direct current cable, the twisting and bending of the conductors, and the arrangement of the phase conductors) and the length of the space that separates the observer (human or marine organisms) from the cable. To date, magnetic, and electric field have been analysed separately, but when combined, they can be referred to as electromagnetic fields (EMFs) (Lewczuk et al., 2014).

EMFs are characterised by their frequency (WaterProof Marine Consultancy et al., 2016). In Ireland, most of Europe and Asia, Southern South America, Australia and Africa, electricity varies at a frequency of 50 Hz (ESB, 1999). Simply put, current flowing through any electrical appliance and power cable in these countries will have to alternate back and forth 50 times every second, whereas in America and Canada, the frequency of these fields is 60 Hz (Ansari and Hei, 2000). These time-varying frequencies are called alternating current (AC) fields which are typically produced by electrical power systems (e.g. power cables), sources in the environment, and organisms (Including humans and marine species) (Tricas and Gill, 2011). Besides the 50 and 60 Hz frequencies, electrical power systems are also accompanied by weak and very low harmonic fields, which are fractions or integer multiples of the original frequency (Tricas and Gill, 2011). Magnetic, and electric fields are also characterised by static or direct current (DC) fields, which have a frequency of 0 Hz, as it does not vary significantly over time (CMACS, 2003). The DC current flows continuously in one direction and can also be created the same way as AC fields are produced (ESB, 1999).

2.3 Natural Sources of Electromagnetic fields in the Irish Sea

There are three fundamental natural sources of EMFs in the aquatic environment; motionally induced electric fields that are produced by the movement of organisms or currents, bioelectric fields (generated by marine organisms), and the geomagnetic field created by the earth (Hutchison et al., 2020). These are reviewed below.

2.3.1 The Geomagnetic Field

The geomagnetic field, also called the earth's DC magnetic field (or the earth's main field), is a geophysical phenomenon, which originates from the earth's deep interior and extends out into space (Buffett, 2014). Within the earth's core, electricity is created by the movement of a liquid metal or electrically conductive material (Beggan, 2019; BGS, 2020), in a similar way to hydroelectric power plants, which converts the energy from flowing water into electricity. The electric current flows back and forth around the middle of the planet in a wide-reaching loop, that in turn creates a large magnetic field that surrounds the earth (with intensities varying between 25-65 μT) (Figure 1). (Hutchison et al., 2020). This "magnetic screen" protects and prevents the earth's atmosphere from getting destroyed by the sun's magnetic field (Lowrie, 2007).

The geomagnetic field has a dipole structure and resembles the magnetic field of a bar magnet, wherein its poles are closely positioned with the earth's own geographic poles (true north-south direction) (Figure 1) (Campbell, 2003). This unique feature explains why a compass needle aligns itself relative to the magnetic north-south direction, and not the geographic poles (United States Department of Energy, 2013).

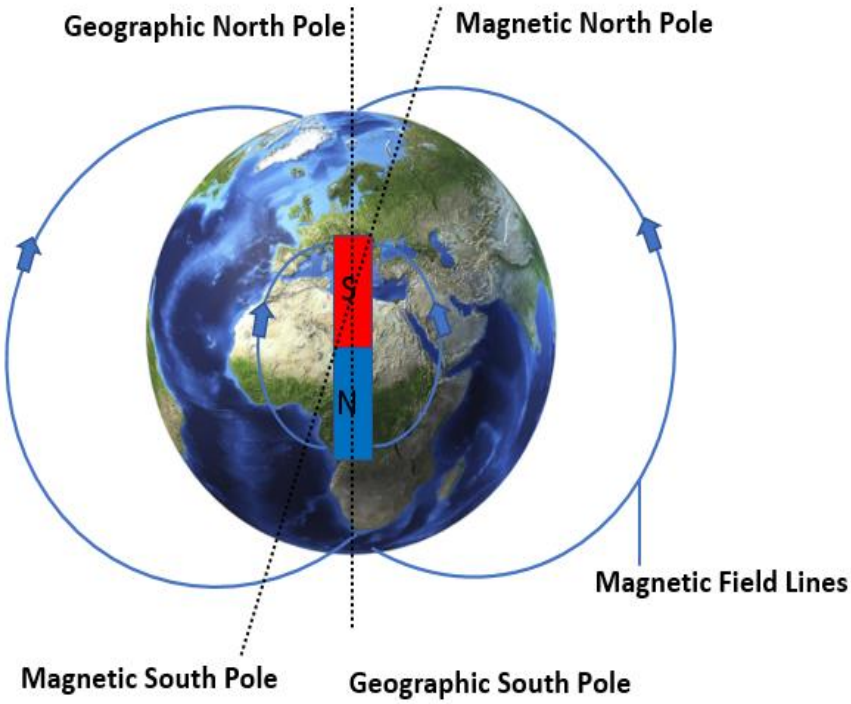

Figure 1: The variation between the geomagnetic poles (magnetic north-south direction) and the geographic poles (true north-south direction) (Modified from Coyne, 2018).

A vital attribute of the earth's magnetic field is that it is a vector quantity; an attribute not shared by many other measured environmental phenomena (Lowrie, 2007). In addition to this, for each location on earth, the geomagnetic field is described in terms of its' angles of inclination and declination, as well as its field strength (or intensity) (Tauxe, 2010). The earth's inclination at any given point is the angle between the horizontal plane and the total field vector (Schubert, 2007) (Figure 2). Hereas, the earth's declination is the angle between geographical north and magnetic north (McLean, 2020).

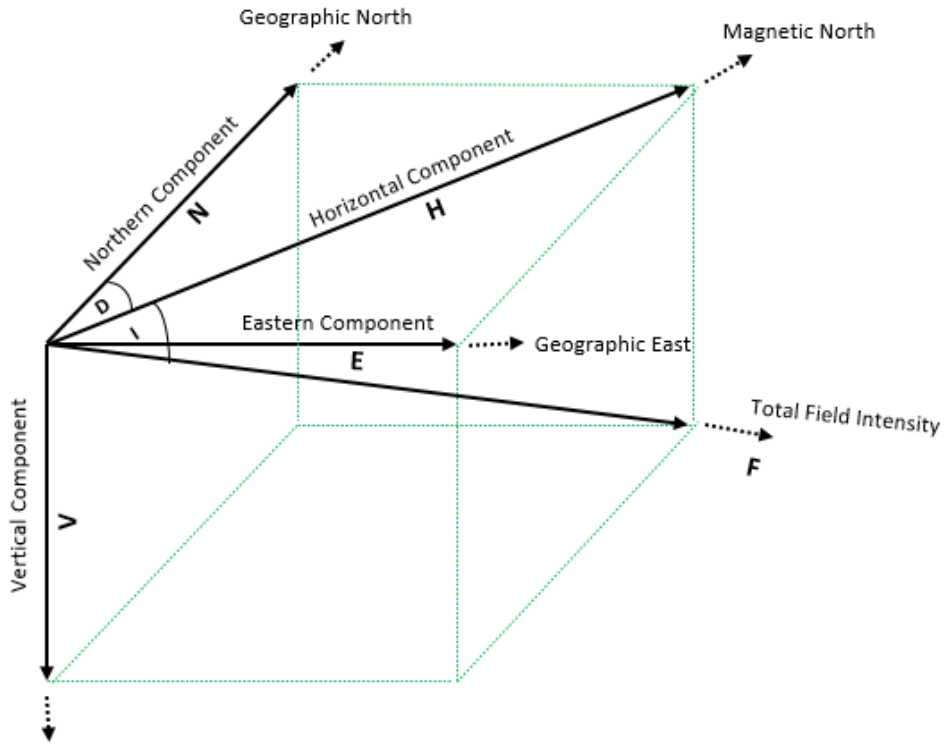

Figure 2: Schematic representation of the earth's magnetic field vector components. The geomagnetic field is described by the following parameters: Declination angle (D), Inclinational angle (I), Vertical field component (V), Northern field component (N), Horizontal field component (H), Eastern field component (E), Total magnetic intensity (F). (Modified from Campbell, 2003).

According to Poletti (2020), the field strength of the geomagnetic field is characterised by three vector components acting at right angles to each other, along the X, Y and Z axes (Figure 2). Any increase or decrease in the intensity of any component (X, Y or Z) would in turn result in an increase or decrease in the strength of the field. Total Field Strength =$(\mathrm{X}^2 + \mathrm{Y}^2 + \mathrm{z}^2)^{0.5}$.

Furthermore, EMFs researchers at the United States Department of Energy (2013) have suggested that the total strength of the earth's magnetic field might be affected by the presence of various ferromagnetic sources (e.g. mineral deposits, pipelines, sunken ships, and

onshore structures), which cause local distortions to the geomagnetic field.

Channell and Vigliotti (2019) have identified the geomagnetic field as a potential source of information for numerous life forms (e.g. humans, microorganisms, marine or terrestrial species) for navigation or orientation over various spatial distributions. Wang et al. (2019) provided some evidence that the human brain possesses special magnetic sensors (or magnetoreceptors) that permit orientation through the earth's magnetic field. These sensors help us understand our surroundings – knowing that there is a building on the left, and there's a circular intersection that we need to drive around. In the marine environment, the influence of the earth's magnetic field can be observed in elasmobranchs (e.g. shark, sawfish, skates and rays) marine mammals (Kalmijn, 1982), Fishes (Walker et al., 1992; Moore and Riley, 2009), and invertebrates (Lohmann and Willows, 1987). Indeed, most of these species either respond, orient, or sense changes in the earth's magnetic field (Putman et al., 2013).

2.3.2 Bioelectricity and Bioelectric Fields

Bioelectricity refers to the electrical potential and current produced or occurring within the cells and tissues of living organisms (Mitcheson and Stanfield, 2013). The transmission of nerve impulses, irregular distribution of charged ions, and contraction of the heart are all examples of bioelectric fields (Rizwan et al., 2019). In an article published by McCaig et al. (2009), bioelectric fields were reported to be associated with the wound healing process in animals. In fact, Aganta and Inoue (2012) advocate this view and state that animals such as the salamander are able to regenerate brain tissue, lower jaws, limbs and even, hearts. In comparison to animals, Ikeuchi et al's. (2016) findings show that the vast majority of plants possess even higher regenerative capacity. For example, the *Acetabularia* plant is cable of regenerating its apical whorl

shape from apical stalks that have had their nucleus removed (Mandoli, 1998).

Some marine species use their bioelectric fields for communicating, and locating other organisms, pray and objects (Pals and Van SchaickZillesen, 1982). For sharks, these activities are mediated through the tuberous electro sensory organ (Peters et al., 2002). Sharks also possess a different electroreceptor organ, called the ampullae of Lorenzini (Moller, 1995). This organ is used in detecting very weak electric fields produced by conspecifics and prey (Kalmijn and Adrianus, 1972; Bedore and Kajiura, 2013) and can sense electric fields as little as 0.01 microvolts per centimetre (μV/cm) (Pals and Van SchaickZillesen, 1982).

2.3.3 Induced Electric Fields

Motionally induced electric fields (or Secondary EMFs) are created by the movement of charges in seawater through the earth's static magnetic field (Xu et al., 2018). Albert et al. (2020) notes that these induced electric fields are primarily influenced by the movement and direction of conductive marine organisms or ocean currents (or tidal flow) relative to the earth's magnetic field. Hence, moving seawater creates localised and widespread electric fields (Tricas and Gill, 2011).

Over the years, marine and oceanography researchers have conducted extensive predictive studies to better understand the variation and intensity of naturally induced electric fields around the ocean. One of these researchers is Kalmijn (1982), who was able to provide estimations of the likely electric field intensities that marine species might encounter when travelling through shallow waters (Tricas and Gill, 2011). The researcher found that these intensities could range between 0.05 and 0.5 μV/cm. Owing to this discovery, Poléo et al. (2001) took things further by measuring the electric field intensity in the English Channel. The value reported was less than 0.31 μV/cm. This value still falls within the same

detection threshold measured by Kalmijn (1982). On the other hand, higher estimates of about 0.75 μV/cm have been measured over muddy seabed's (Pals et al., 1982), and 0.93 μV/cm during geomagnetic storms (Brown et al., 1979). These localised electric fields are important to marine species because they may serve as position (or neighbourhood) indicators and, hence, provide an electric map of the aquatic environment (Pals and Zillesen, 1982).

2.4 Man-Made Sources of Electromagnetic Fields in the Irish Sea

Anthropogenic sources of EMFs are partly introduced into the aquatic environment by marine installations (e.g. offshore platforms or bridges), marine vessels, shipwrecks, and submarine pipelines (Tricas and Gill, 2011; Hutchinson et al., 2020). As reported by Redlarski et al. (2015), these sources of environmental pollution pose a greater risk to the existence of marine species than any of the natural sources of EMFs aforementioned. Notwithstanding, Ardelean and Minnebo (2015) have identified undersea telecommunication and power cables as the most dominant sources of EMF pollution in the marine environment. Presently, these cables have a total length that exceeds $10^6\mathrm{km}$ of land space on the seabed (Albert et al., 2020), largely composed of telecommunication cables (Carter et al., 2009). Even though telecommunication cables span across a larger area of the seabed, their EMF emissions are significantly smaller than those of subsea power cables (Meißner et al., 2006), which are reviewed in Section 2.5.

2.5 Subsea Power Cables (SPCs)

2.5.1 Design Characteristics

SPCs come in various lengths, shapes, and sizes. However, due to their diverse applications, cables are usually selected based on their designed voltage rating and the design constraints of the project (e.g. grid layout, route length, soil type, insulation type, and transmission capacity) (Gilbertson, 2000). SPCs are categorised into four major voltage groups which include, low voltage (LV) (up to 1000 V), medium voltage (MV) (1000 V-36 KV), high voltage (HV) (36-230 kV), and extra high voltage (EHV) (over 230 kV) (EC, 2020). In this thesis, MV and HV SPCs were focused upon, because these voltages are more applicable to offshore wind farm developments (Weerheim, 2018). The design characteristics for MV (AC), HV (AC and DC), and dynamic power cables are discussed in the following sections.

2.5.1.1 Static AC Cables

AC undersea cables are used for transmitting power from one static (or bottom fixed) wind turbine to the next, forming together a string of inter-array (turbine) cable connections (EWEA, 2020) (Figure 3a and 3b). These cables carry voltages in the range of 24 to 36 kV (Wright et al., 2002) that flows into a nearby offshore substation (OSS) (INNOSEA, 2020). Like the substations used for general overhead power lines, the OSS receives, converts, and redistributes the power generated. It is one of the most important components of a wind farm (Tricas and Gill, 2011). In other applications, AC cables are used for carrying larger voltages of up to 220 kV (Prysmian Group, 2020) from the OSS to an onshore substation (SS) (INNOSEA, 2020).

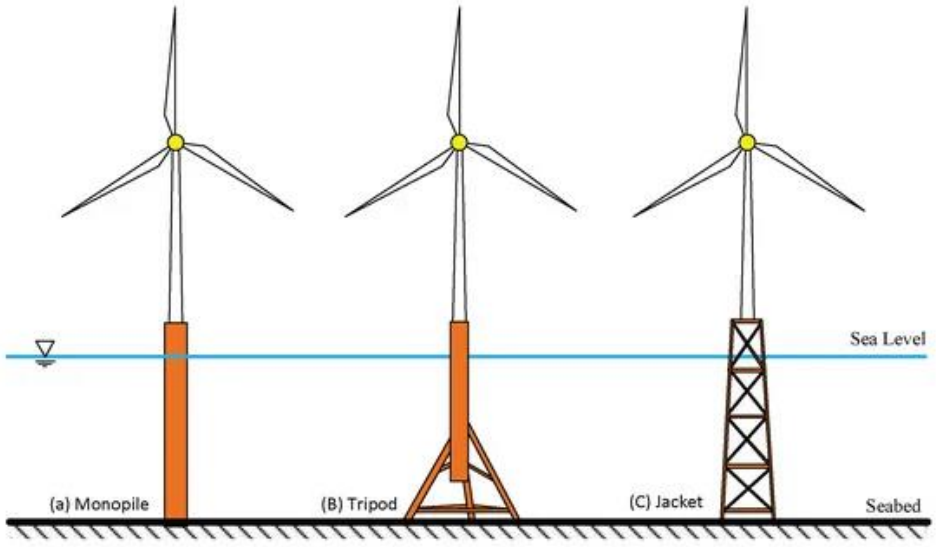

Figure 3a: Different types of static wind turbine structures (Plodpradit, 2019).

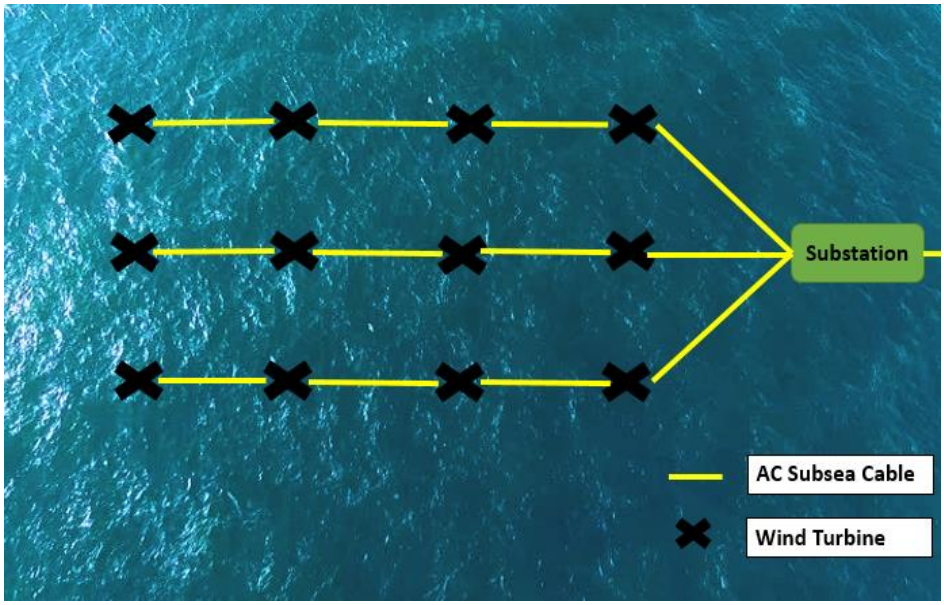

Figure 3b: A distribution of inter-array cables.

The structure of AC underwater cables can be divided into two parts; single-core (one phase) and three-core (three phase) configurations (Liu et al., 2021). The former consists of a cable with only one conductor. In contrast, the three-phase cable is made up of identical conductors that exist either as three isolated cables, or as a bundle that contains three cables (ESCA, 2021).

A study was conducted by Liu (2019) to assess the suitability of the single and three-core cables for subsea engineering applications. Results from Liu's research showed that the three-core cable performed better than the single-core cable with regards to area (i.e. the area needed to lay the cable), circuit safety and unit cost. Wright et al. (2002) notes that the selection of the three-core cable helps to lower the cost of cable laying. In addition, three-core cables have been reported to generate weaker EMFs around an AC cable (Wright et al., 2002). Owing to some of these reasons, the bundled three-core cable has become increasingly sought after and is applied often to underwater transmission projects (Benatoand Paolucci, 2005). An example of a typical bundled three-core AC cable is shown in Figure 4.

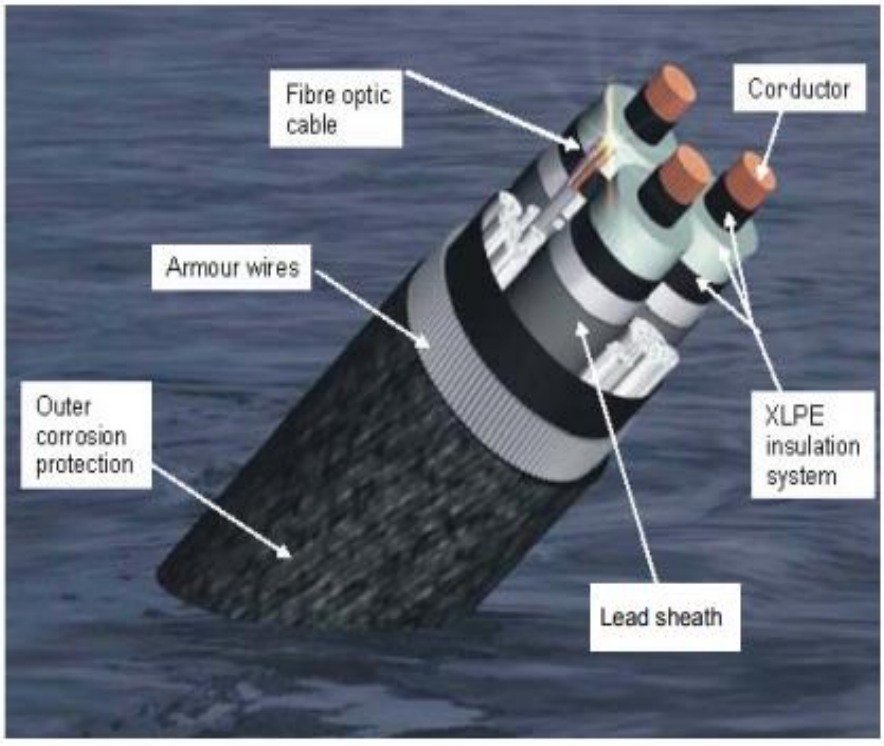

Figure 4: Configuration of a bundled three-core AC subsea power cable (Tricas and Gill, 2011).

The cable's electrical conductor is fabricated from aluminium or copper wires (Fahem, 2018). The cross-sectional area is generally less than 1200 mm^2, although bigger sizes (e.g. 2400 mm^2) have been designed occasionally to carry higher voltages (Fahem, 2018). The conductors are protected by an electrical insulation material which is surrounded by a non-conductive and conductive metallic cover (Tricas and Gill, 2011). This protective sheath is put in place to ground the cable. It is also completely effective at preventing any generated E-field from permeating through the cable to the surrounding environment (OWET, 2011).The only disadvantage that comes with using this sheath is that it is only somewhat effective at blocking and absorbing B-fields produced by the cable (Stolan, 2009; Tricas and Gill, 2011). Unfortunately, this is because it is not presently feasible from a cost and design perspective to totally reduce the B-field. Consequently, with no strong insulation material in place, the B-field gets released into the environment (Woodruff et al., 2013). In some installations the cable may be equipped with a fibre optic cable, which is used to carry information from one point to another across stretches of the ocean (Wright et al., 2002).

The outer material of the cable consists of a metallic armour layer and an outer serving (often a polymer material) (Weerheim, 2018). Once a cable is ready for use, it is usually laid on the seabed by using cable ship (Carter et al., 2009) (Figure 5). In other occasions, they might be buried to protect against tsunamis, ocean currents, anchoring, trawling and other marine activities (Albert et al., 2020; Wang et al., 2021).

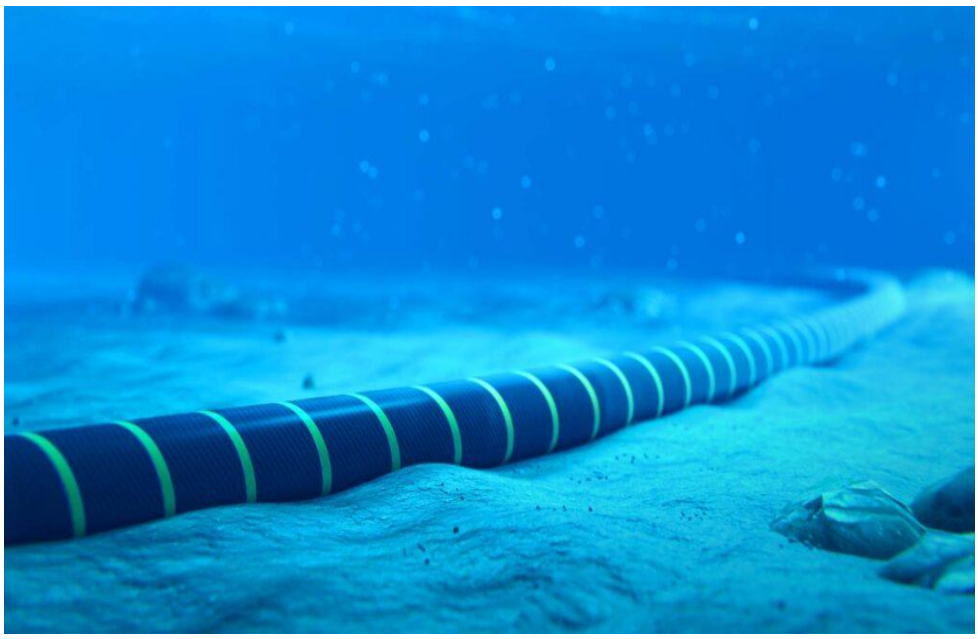

Figure 5: A subsea cable laid on the seabed (Lesaint, 2021).

According to Wright et al. (2002), AC cables are arguably the most economical and mature underwater transmission technology. In spite of these advantages, HVAC cables are generally limited to only near shore applications of less than 80 Km (ESCA, 2021). For longer distances and higher voltage capacity, HVDC cables are typically used to reduce cost (Öhmanet al., 2007; INNOSEA, 2020).

2.5.1.2 Static DC Cables

As OWFs become larger and more detached from the shore, the general consensus for using the HVDC cable in place of the HVAC cable to transmit large amounts of power to the shore-based substation becomes easier to justify (Kirby et al., 2002). The HVDC cable is able to carry voltages that could be as high as 800kV (Tang, 2013) with very low dissipative losses (Liu et al., 2021). In physics, energy losses are generally defined as the difference between the energy entering and leaving a distribution network (WDP,2021). In the context of AC and DC cables (used in OWF applications), electrical losses occur when current fails to flow through the complete cross-section of the conductor (Ardelean and Minnebo, 2015). This is particularly true for AC cables, as current tends to gravitate

towards the conductor's surface, which lowers the utilised cross-section and therefore, increases energy losses and resistance (Bardalai et al., 2019; INNOSEA, 2020) (Figure 6). In comparison, there is a uniform distribution and flow of electrical current in DC cables (Ardelean and Minnebo, 2015). Nevertheless, this does not completely make them exempt from losses, as they may occur at a very low rate (Wright et al., 2002).

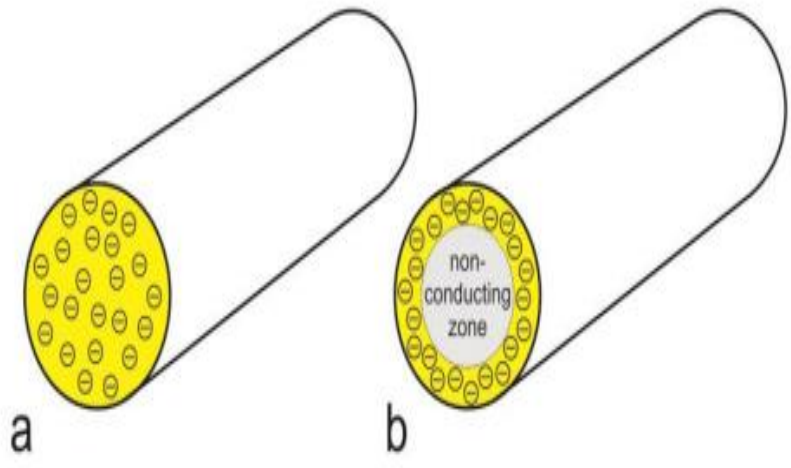

Figure 6: Current flow through the (a) AC and (b) DC cable (Ardelean and Minnebo, 2015).

There are two major types of HVDC cable systems: monopolar and bipolar (ESCA, 2021). In the monopolar system, power is transmitted from one end using a single HVDC conductor and returned by the other on a LV separate return cable (SRC) (Alstom, 2010). The SRC is strapped to the main cable and is laid as one whole cable (Tricas and Gill, 2011). In other occasions, a monopolar cable may be designed with a coaxially integrated return cable (CIRC) (Maekawa et al., 2002). According to Hirano et al. (2021), this configuration allows both the reduction of the cost and environmental impact on the nearby surroundings of the cable. Lastly, monopolar HVDC cables may be designed as a single power cable, which uses the ground or sea electrodes as its return path (Ardelean and Minnebo, 2015; Kamalapur and Arakeri, 2020). However, Tricas and Gill

(2011) note that this design feature tends to generate high B and E-fields. Koops (2000) added that the use of the cable may also lead to an increase in the emission of gases and other environmental pollutants. The different arrangements of the cables are shown in Figure 7.

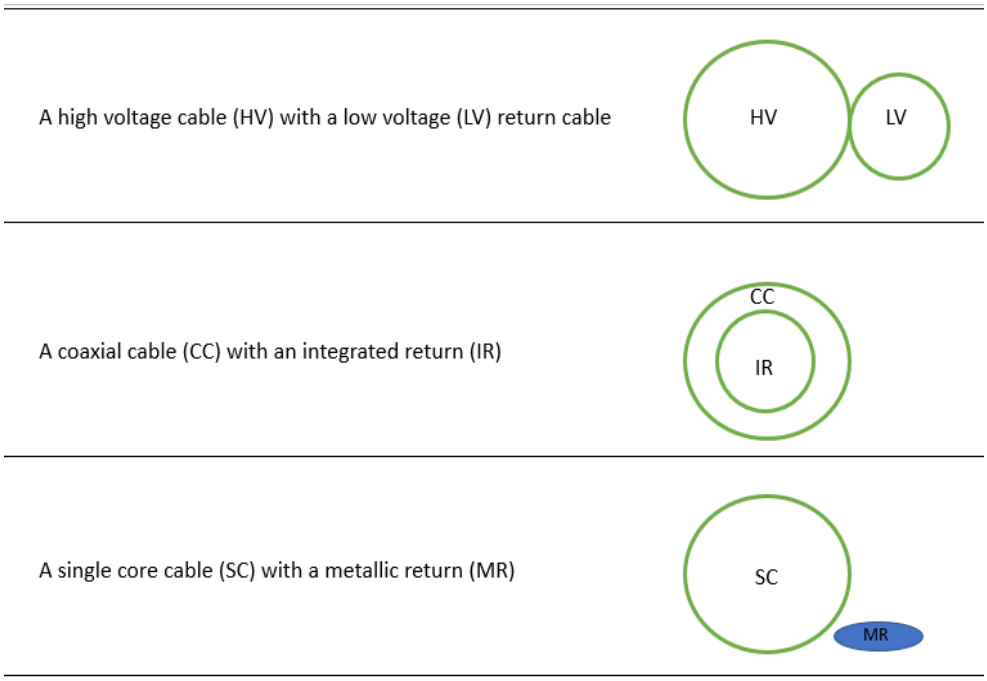

Figure 7: Configuration of different monopolar cable systems (modified from Ardelean and Minnebo, 2015).

The second type of the HVDC cable (i.e. Bipolar systems) system consists of two same size conductors with opposite polarity (i.e. positive and negative) (Gordonnat and Hunt, 2020) (Figure 8). In some designs, sea electrodes may be used as a backup current return path, in the case that a conductor becomes faulty or gets damaged (Wright et al., 2002; Gordonnat and Hunt, 2020). This means that they are able to function as both monopolar and bipolar cables. From an economic standpoint, bipolar cables are not totally cost effective (Kamalapur and Arakeri, 2020). However, they raise fewer environmental concerns in comparison to monopolar systems, making them the more popular option for HVDC applications (Wright et al., 2002). The structural configuration of a typical bipolar cable consists of a copper conductor protected by an insulation, steel armouring and outer serving (Gordonnat and Hunt, 2020). The

functions and characteristics of these components have been discussed in Section 2.5.1.1.

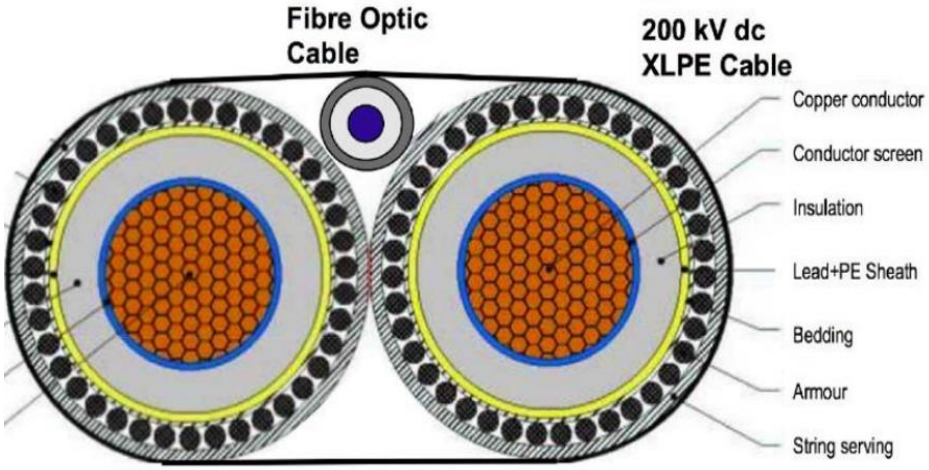

Figure 8: The structure of a 200kV HVDC bipolar subsea cable (Kavet et al., 2016).

2.5.1.3 Dynamic Cables

As aforementioned, OWFs are progressing and moving further from the shore. However, this new development is presenting the need for a more dynamic and flexible wind turbine structure (Young et al., 2018). This is because conventional bottom-fixed turbines are mainly suitable for use in water depths ranging from 50 to 60 m, due to economic and structural constraints (Weerheim, 2018). In a bid to address this challenge, floating offshore wind turbines (FOWTs) have been developed for deep sea applications (e.g. between 50-200 m of water depth) (Carbon Trust, 2017). Unlike bottom-fixed wind turbines, FOWTs are unable to make use of static AC and DC cables (for power transmission) because of the dynamic environmental forces that exist within the water column, hence, a dynamic cable will be required (Weerheim, 2018).

Presently, the design configuration of the dynamic cable is not significantly different to that of the static cable. Identical to static AC cables, all dynamic cables are designed as three AC conductors (i.e. three cores in a bundle) (Weerheim, 2018) (Figure 9). However, this restricts them to only inter turbine applications as they cannot be used as export cables (Rentschler et al., 2020). Nevertheless, some major differences still exist between dynamic and static cables. Firstly, dynamic cables are protected by two metallic armours (Rentschler et al., 2020). This double armouring helps to prevent damage during installation and operation by increasing the bending and torsional stiffness of the cable (Alcorn and O'sullivan, 2013). Dynamic cables have larger conductors, which help in reducing the induced heat generated by the cable (INNOSEA, 2020). In terms of the cost (i.e. cost per metre of the cable), dynamic cables are significantly more expensive than convention subsea power cables (INNOSEA, 2020).

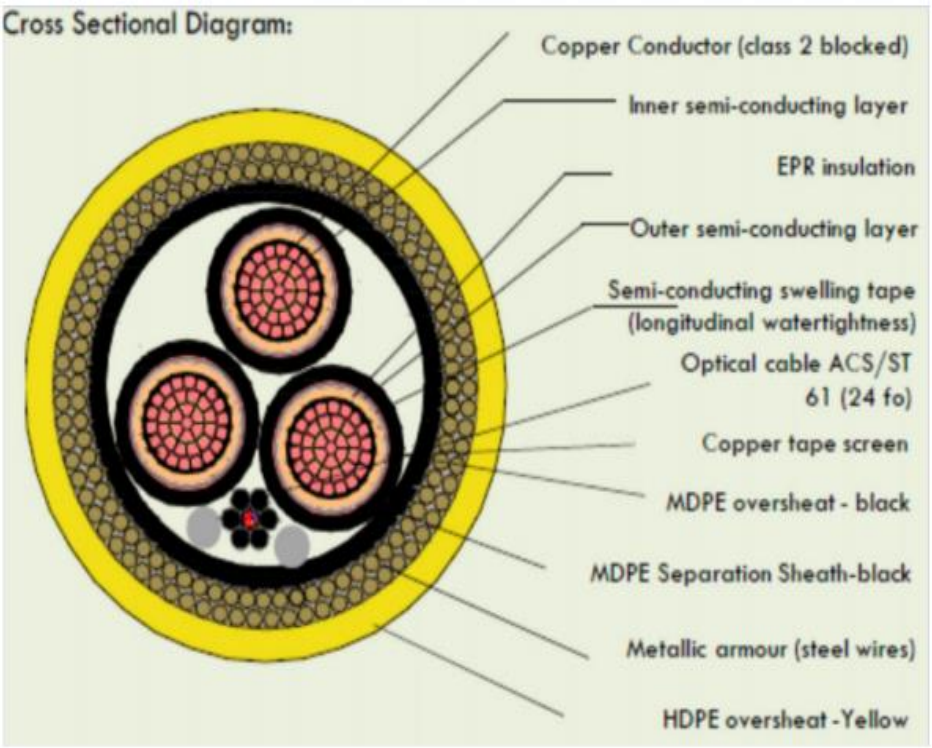

Figure 9: The structural configuration of a typical dynamic power cable (Cavaleiro, 2012).

While static cables are laid on the seabed, dynamic cables on the other hand are installed underneath FOWTs, which leaves them suspended and ultimately exposes them to extreme loads and stress in the water column (Zhao et al., 2021). In general, there are six major dynamic cable hanging configurations, namely, the steep wave, lazy wave, free hanging (catenary), steep S, lazy S, and Chinese lantern (INNOSEA, 2020) (Figure 10). The selection of any configuration is primarily influenced by factors such as environmental and site constraints, cost, and water depth (Weerheim, 2018; INNOSEA, 2020). The benefits and drawbacks of each hanging configuration are summarised in Tables 1a and b.

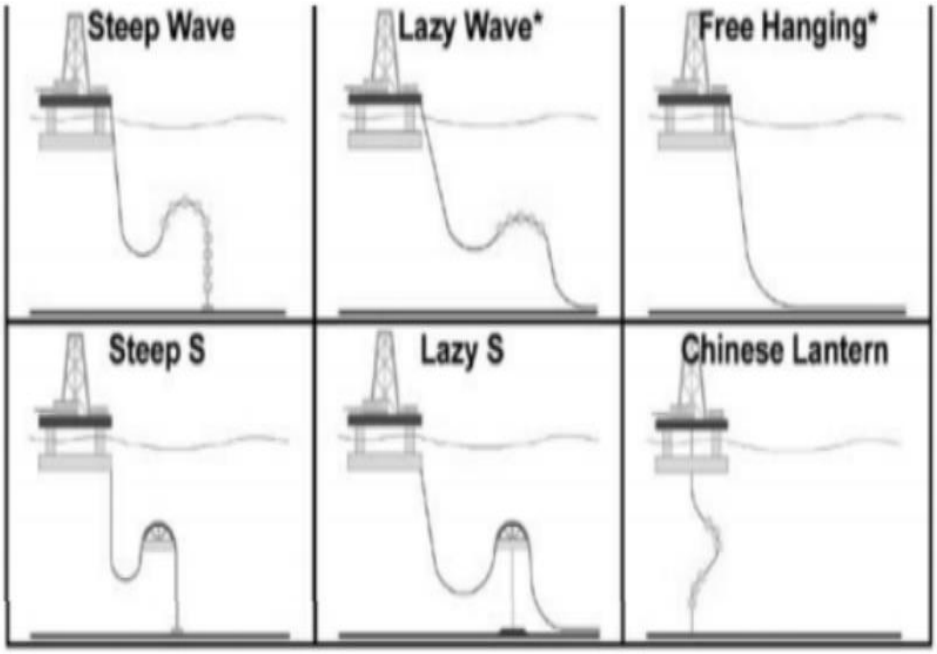

Figure 10: Different dynamic cable hanging configurations for FOWT structures (Clausenand D'Souza, 2001).

Table 1a: A summary of the advantages and disadvantages of different dynamic cable hanging configurations (modified from Weerheim, 2018; INNOSEA, 2020).

Name	Steep Wave	Lazy Wave	Free Hanging
Description	- Cable makes use of buoyancy modules at its midwater section. - The cable has a steeper slope than the Lazy wave system.	- Cable makes use of buoyancy modules at its midwater section. The buoyancy modules provide lift and help to reduce the top tension loads.	- Cable hangs in a similar fashion to a catenary curve.
Advantages	- Very popular and widely accepted for offshore wind applications. - Minimal changes in the shape of the cable over time. - Accommodates a fair number of marine species	- Accommodates a substantial number of marine species. - Simple design to install. - Used more often in comparison to other configurations.	- Simplest design to install. - Very affordable. - Does not require buoyancy modules.
Disadvantages	- No control over the lateral movement of the platform.	- No control over the lateral movement of the platform.	- Very high tension at the connection points.

	- Buoyancy module is needed to support the cable.	- Buoyancy module is needed to support the cable.	- Risk of buckling at the seabed joint under extreme loads.

Table 1b: A summary of the advantages and disadvantages of different dynamic cable hanging configurations (modified from Weerheim, 2018; INNOSEA, 2020).

Name	Steep S	Lazy S	Chinese Lantern
Description	- Cable has a very steep slope at its midwater.	- Cable makes use of a midwater buoy instead of buoyancy modules. - This design is very similar to the lazy wave configuration.	- Cable hangs vertically from the bottom of the floating platform with buoyancy modules positioned at the middle of the cable.
Advantages	- Minimal changes in the shape of the cable over time.	- Accommodates a reasonable number of marine species. - Good for dynamic applications. - Minimal changes in the	- Affordable solution. - May accommodate a reasonable number of marine species.

		shape of the cable over time.	
Disadvantages	- Very expensive to install.	- Very expensive to install.	- Most complex design. - Unsuitable for applications where extreme loads are present.

2.6 Microplastics and Chemical Pollutants

Plastic pollution is a worldwide phenomenon. Cozar et al. (2014) refers to this present day in the history of humanity as the plastic age. This is because plastic products are ever present in our daily life, due to their high durability, light weight, and very low cost (Barnes et al., 2009). Yet, a huge portion of the plastic we produce ends up in different depths of the ocean (Jambeck et al., 2015; Zhang et al., 2020). Fontana et al. (2020) refers to this development as a pressing environmental issue that needs to be addressed. Brown et al. (2011) supports the authors assertion as he notes that the average manufactured plastic is non-biodegradable, which implies that if improperly disposed of, could pollute our oceans for decades or even centuries to come. On the other hand, when biodegradable plastics are used, the amount of degradation depends on the density, polymer, shape, and application of the plastic itself (Eriksen et al., 2014).

For static SPCs, a polymer material (e.g. polypropylene (PP)) is generally used as the outer protective layer of the cable (Weerheim, 2018). The cable and its tightly wrapped covering are typically exposed to various natural threats at all water depths e.g. shark attacks (Márquez, 2020), volcanic activities, waves and currents, tsunamis, and submarine earthquakes (ICPC, 2011). The occurrence of these activities may cause the outer material to abrade or tear (ICPC, 2011). In other cases, the cable may break or might get buried by these natural hazards (ICPC, 2011). Though not scientifically proven (to the best knowledge of the author), one may wonder if the abrasion or tear of the outer serving could lead to the progressive fragmentation and disintegration of the plastic material into tiny pieces, which may then contribute to the release of microplastic pollutants into the ocean.

Microplastics (MPs) are generally defined as tiny particles that have dimensions, which range from roughly 1 µm to 5 mm (Arthur et al., 2009).

These ever-increasing pollutants have been spotted/reported in mussels and crabs (Farrell and Nelson, 2013), sandhoppers, crustaceans, fish, and sea turtles (Cole et al., 2011). As observed by Verla et al. (2019), MPs tend to block the digestive system of marine species, which may affect their eating pattern or lead to death. Additionally, plastics themselves tend to contain endocrine disruptors (i.e. hormonal active agents), as well as chemical contaminants and additives that may be harmful at very low concentrations to marine species (Gallo et al., 2018). Conversely, MPs may contribute to the chemical pollution of the sea because of their ability to house and transport pollutants such as organic chemicals, and heavy metals (HMs) (Santana-Viera, 2021) due to their large surface area-to-volume ratio (Verla et al., 2019).

The term heavy metal is a generic term use to define metals and metalloids whose specific density is approximately $5\ \mathrm{g/cm^3}$ or elements with an atomic weight above $40.4\ \mathrm{g/mole}$, which is the atomic weight of normal calcium (Duffus 2001; Sani, 2011). They can also be said to be metals having an atomic density greater than 4 g/cm³ (Orosun et al., 2020). Since toxicity and heaviness are inter-related, metalloids such as arsenic that are toxic at low-level of exposure are regarded as a heavy metal (ATSDR, 2007; Orosun et al., 2020). Heavy metals, when present in the aquatic ecosystem (sea) can cause various health hazards on the aquatic animals, ranging from mild irritation of organs to death (Jiwan and Ajayi, 2011; Ali et al., 2019). Some mobile benthic species like crabs can migrate from the toxic environment to a new one, whereas sessile (bivalves, tubeworms etc.) and sensitive species (such as slower growing or fragile species) will be more impacted (OSPAR, 2012).

SPCs themselves contain heavy metals that include lead, copper, as well as many other pollutants, which have the potential to dissolve and contaminate the marine environment when a cable is damaged (Taormina et al., 2018). According to Taormina et al. (2018), no scientific studies have been conducted to determine the risk and severity of such

SPC-related pollutants. It is therefore imperative to explore the level of heavy metals enrichment due to the presence of the SPCs.

Methodology

3.0 Methodology

3.1 Modelling

3.1.1 Introduction

In this Section, the EMFs produced by typical AC and DC SPCs are modelled to better understand the magnitude and spatial extent of EMFs from current and proposed cable systems.

3.1.2 Magnetic Field Equation for Static AC Cables

As introduced in Section 2.2, the strength of the magnetic field produced by a cable depends primarily on design configuration and current flowing through the cable. Indeed, the magnitude of the B-field at any point in space is the resultant of all the contributing sections or elements of a current-carrying SPC conductor (Fernandez and Patrick, 2021). The B-field is directly proportional to current and inversely proportional to the distance between the position of the cable's conductors and a reference point on the horizontal and vertical planes (x, y). The Biot-Savart equation describes these relationships (Moore, 1997).

$$B = \frac{\mu_0 I}{2\pi r} a_r \qquad \text{(Equation 3-1)}$$

Where μ_0 is the relative permeability of free space; I the current; r the perpendicular distance between the conductors and the reference points and a_r the unit directional vector.

Equation 3-2 to 3-7 shows the horizontal (B_x) and vertical (B_y) components of the B-field generated by the cable's conductors (Jayalakshmi and Deepa, 2016). These revised equations were used in creating the B-field models. As discussed in the literature review, most AC SPCs are designed using 3 conductors. For this reason, the B-field

contribution from the conductors have been divided into 3 segments (i.e. 3 horizontal and 3 vertical).

$$Bx_1 = -R \times [\frac{(Rhy_1 - Yp_1)}{(Rhx_1 - Xp_1)^2 + (Rhy_1 - Yp_1)^2}] \quad \text{(Equation 3-2)}$$

$$Bx_2 = -R \times [\frac{(Rhy_2 - Yp_2)}{(Rhx_2 - Xp_2)^2 + (Rhy_2 - Yp_2)^2}] \quad \text{(Equation 3-3)}$$

$$Bx_3 = -R \times [\frac{(Rhy_3 - Yp_3)}{(Rhx_3 - Xp_3)^2 + (Rhy_3 - Yp_3)^2}] \quad \text{(Equation 3-4)}$$

$$By_1 = R \times [\frac{(Rhx_1 - Xp_1)}{(Rhx_1 - Xp_1)^2 + (Rhy_1 - Yp_1)^2}] \quad \text{(Equation 3-5)}$$

$$By_2 = R \times [\frac{(Rhx_2 - Xp_2)}{(Rhx_2 - Xp_2)^2 + (Rhy_2 - Yp_2)^2}] \quad \text{(Equation 3-6)}$$

$$By_3 = R \times [\frac{(Rhx_3 - Xp_3)}{(Rhx_3 - Xp_3)^2 + (Rhy_3 - Yp_3)^2}] \quad \text{(Equation 3-7)}$$

Where Rh_y is the reference height on the vertical axis; Y_p the vertical position of the conductors; Rh_x the reference height on the horizontal axis and X_p the horizontal position of the conductors. The parameter R can be expressed as a function of the magnetic permeability of free space (μ_0) and nominal current (I_M) flowing through the cable (Jayalakshmi and Deepa, 2016):

$$R = \frac{\mu_{0(I_{RJ}+nI_{IJ})}}{2\pi} \quad \text{(Equation 3-8)}$$

Where I_{RJ} is the actual part of the current through the nth conductor and I_{IJ} the imaginary part of the current through the nth conductor (Jayalakshmi and Deepa, 2016). The current in each conductor is given by,

$$I_A = I_M \cos(\omega t + \emptyset_A) \quad \text{Where, } \emptyset_A = 0 \quad \text{(Equation 3-9)}$$

$$I_B = I_M \cos(\omega t + \emptyset_B) \quad \text{Where, } \emptyset_B = \emptyset_A + 120^0 \quad \text{(Equation 3-10)}$$

$$I_C = I_M \cos(\omega t + \emptyset_C) \quad \text{Where, } \emptyset_C = \emptyset_A - 120^0 \quad \text{(Equation 3-11)}$$

The parameter ω is the angular frequency of supply and $\emptyset$ the phase angle or displacement, which describes the angular difference between each conductor when they reach their maximum or zero values. For a three-phase circuit, the phase angle is always 120^0 (Fernandez and Patrick, 2021).

The root-mean-square (RMS) value of alternating current in each conductor is given by (Jayalakshmi and Deepa, 2016).

$$I_{RA} = \frac{I_M}{\sqrt{2}} \cos(\omega t + \emptyset_A) \quad \text{(Equation 3-12)}$$

$$I_{IA} = \frac{I_M}{\sqrt{2}} \sin(\omega t + \emptyset_A) \quad \text{(Equation 3-13)}$$

$$I_{RB} = \frac{I_M}{\sqrt{2}} \cos(\omega t + \emptyset_B) \quad \text{(Equation 3-14)}$$

$$I_{IB} = \frac{I_M}{\sqrt{2}} \sin(\omega t + \emptyset_B) \quad \text{(Equation 3-15)}$$

$$I_{RC} = \frac{I_M}{\sqrt{2}} cos\ (\omega t + \emptyset_C)$$ (Equation 3-16)

$$I_{IC} = \frac{I_M}{\sqrt{2}} sin\ (\omega t + \emptyset_C)$$ (Equation 3-17)

In the three-phase system, the current flowing through each conductor can be broken into its in-phase and out-phase components (Fernandez and Patrick, 2021). This means that each conductor will have an in-phase and out-phase B-field in the horizontal and vertical direction (i.e. $B_{xin-phase}, B_{xout-phase}, B_{yin-phase}, B_{yout-phase}$). For this to occur, equations 3-2 to 3-7 evolves to the equations below for the 3 conductors in the cable (Jayalakshmi and Deepa, 2016).

$$B_x = \sqrt{\left\{\sum_{i=1}^{n} B_{xin_i}\right\}^2 + \left\{\sum_{i=1}^{n} B_{xout_i}\right\}^2}$$ (Equation 3-18)

$$B_y = \sqrt{\left\{\sum_{i=1}^{n} B_{yin_i}\right\}^2 + \left\{\sum_{i=1}^{n} B_{yout_i}\right\}^2}$$ (Equation 3-19)

The total B-field in the cable is given by,

$$B_{field} = \sqrt{{B_x}^2 + {B_y}^2}$$ (Equation 3-20)

3.1.2.1 Magnetic Field Modelling Approach and Assumptions for Static AC Cables

In this project, 10 AC SPCs (i.e. 5 medium voltage and 5 high/extra high voltage cables) were shortlisted and selected for analysis based on the availability of sufficient information needed to characterize the EMF levels produced by the cables (Table 2). The first 5 MV cables were applied for use in an inter-array cable setting, whilst the next 5 are used as export cables. This is obvious, because cables A-E have a relatively lower voltage capacity in comparison to the others. Detailed information about the cables and where they have been deployed has been deliberately omitted due to intellectual property rights concerns.

Table 2: An overview of the 10 AC SPCs.

Cable name	Cable type	Year commissioned	Country	Installed Capacity (MW)	Voltage (kV)	Nominal cross-sectional area (mm^2)
A	MVAC	2013	UK	270	33	185
B	MVAC	2018	UK	367	33	150
C	MVAC	2018	UK	367	33	500
D	MVAC	2007	UK	348	34	500
E	MVAC	2021	UK	406	36	630
F	HVAC	2010	Norway	40	115	300
G	HVAC	2019	Greece	154	150	800
H	HVAC	2009	Belgium	325	170	1000
I	HVAC	Planning stage (2022)	Netherlands	1500	220	1000
J	HVAC	2019	China	N/A	500	1000

The B-field levels from the 10 cables were calculated using the revised Biot-Savart equation discussed in the Section 3.1.2. According to Exponent (2014), the application of the equation is particularly

appropriate for very straight and long conductors such as the one's used for SPC-related projects. Due to the length and complexity of the equations, the B-field levels for the 10 cables were computed and modelled using the MATLAB programming software. This simple and user-friendly software was chosen because it allows the user to compute very complex equations without the need of having to write extremely long codes. The input information to the software were data regarding the conductor's configuration, line phasing, and current output. The MATLAB code and information about the cable's geometry (i.e. conductor configuration) are found in Figure 11 and Appendix A, Table A-1 respectively.

```
format shortg
h1 = 0; % middle reference height Y direction
h2 = 0; % left reference height Y direction
h3 = 0; % right reference hight Y direction
x = [-60,-50,-40,-30,-20,-10,0,10,20,30,40,50,60]; % measurement point on x
axis from cable (x=x1=x2=x3)
xm1 = 0; % Lateral position of the middle conductor from x=0, y=o (m), along
the west-east plane
xm2 = 0; % Lateral position of the left conductor from x=0, y=o (m)
xm3 = 0; % Lateral position of the right conductor from x=0, y=o (m)
ym1 = 0; % y Position of middle conductor
ym2 = 0; % y Position of left conductor
ym3 = 0; % y Position of right conductor
Im = 530; % Current flowing through cable (A)
uo = (((12.566)*(10)^-7)); % Permeability of free space (Tm/A)
Ira = (Im/sqrt(2))*cosd(0); % Current root mean square for middle conductor (A)
(angular peak frequency and time were calculated manually) cos(0)
Iia = (Im/sqrt(2))*sind(0); % Current root mean square for an imaginary middle
conductor (A) sin(5.215)
Irb = (Im/sqrt(2))*cosd(120); % Current root mean square for left conductor (A)
cos(-119.97+120)
Iib = (Im/sqrt(2))*sind(120); % Current root mean square for an imaginary left
conductor (A) sin(-118.406+120)
Irc = (Im/sqrt(2))*cosd(-120); % Current root mean square for right conductor
(A) cos(+119.97-120)
Iic = (Im/sqrt(2))*sind(-120); % Current root mean square for an imaginary
right conductor (A) sin(+121.54-120)
Bxa_real_part= -(uo/(2*pi))*Ira*[(h1-ym1)./(((x-xm1).^2)+((h1-ym1).^2))]; %
Magnetic contribution from the real part of current through the middle
conductor
Bxa_Imag_part= -(uo/(2*pi))*Iia*[(h1-ym1)./(((x-xm1).^2)+((h1-ym1).^2))]; %
Magnetic contribution from the Imaginary part of current through the middle
conductor
Bxb_real_part= -(uo/(2*pi))*Irb*[(h2-ym2)./(((x-xm2).^2)+((h2-ym2).^2))]; %
Magnetic contribution from the real part of current through the left conductor
Bxb_Imag_part= -(uo/(2*pi))*Iib*[(h2-ym2)./(((x-xm2).^2)+((h2-ym2).^2))]; %
Magnetic contribution from the Imaginary part of current through the left
conductor
Bxc_real_part= -(uo/(2*pi))*Irc*[(h3-ym3)./(((x-xm3).^2)+((h3-ym3).^2))]; %
Magnetic contribution from the real part of current through the right conductor
Bxc_Imag_part= -(uo/(2*pi))*Iic*[(h3-ym3)./(((x-xm3).^2)+((h3-ym3).^2))]; %
Magnetic contribution from the Imaginary part of current through the right
conductor
Bya_real_part= (uo/(2*pi))*Ira*[(x-xm1)./(((x-xm1).^2)+((h1-ym1).^2))]; %
Magnetic contribution from the real part of current through the middle
conductor
Bya_Imag_part= (uo/(2*pi))*Iia*[(x-xm1)./(((x-xm1).^2)+((h1-ym1).^2))]; %
Magnetic contribution from the Imaginary part of current through the middle
conductor
Byb_real_part= (uo/(2*pi))*Irb*[(x-xm2)./(((x-xm2).^2)+((h2-ym2).^2))]; %
Magnetic contribution from the real part of current through the left conductor
Byb_Imag_part= (uo/(2*pi))*Iib*[(x-xm2)./(((x-xm2).^2)+((h2-ym2).^2))]; %
Magnetic contribution from the Imaginary part of current through the left
conductor
Byc_real_part= (uo/(2*pi))*Irc*[(x-xm3)./(((x-xm3).^2)+((h3-ym3).^2))]; %
Magnetic contribution from the real part of current through the right conductor
Byc_Imag_part= (uo/(2*pi))*Iic*[(x-xm3)./(((x-xm3).^2)+((h3-ym3).^2))]; %
Magnetic contribution from the Imaginary part of current through the right
conductor
Bx_final_real= Bxa_real_part + Bxb_real_part + Bxc_real_part; % Total
horizontal magnetic field from the real part of the 3 conductors
Bx_final_imag= Bxa_Imag_part + Bxb_Imag_part + Bxc_Imag_part; % Total
horizontal magnetic field from the Imaginary part of the 3 conductors
By_final_real= Bya_real_part + Byb_real_part + Byc_real_part; % Total vertical
magnetic field from the real part of the 3 conductors
By_final_imag= Bya_Imag_part + Byb_Imag_part + Byc_Imag_part; % Total vertical
magnetic field from the Imaginary part of the 3 conductors
Bx_final= sqrt(Bx_final_real.^2 + Bx_final_imag.^2); %Total magnetic field in
the x
By_final= sqrt(By_final_real.^2 + By_final_imag.^2); %Total magnetic field in
the y
B_total = sqrt (Bx_final.^2 + By_final.^2) % Magnetic field in the cable
(Tesla)
```

Figure 11: Parameters and code for AC magnetic field calculation.

In reality, the 10 cables were designed to be used at different offshore wind farms with varying loading and operational requirements. The cables were also laid in different marine environments (e.g. varying water depths and topography's) which makes it a challenge to critically compare the B-fields produced by all the cables. For these reasons, calculations were performed for 3 major modelling scenarios that represent a vast range of potential installation configurations and loading conditions that apply to all the cables.

The first case represents the typical configuration of a standard subsea cable that has been laid on the seabed, with an assumed load current of 200 amperes (A), which is referenced to a standard height of 1m above the cable. According to standard practice from the IEEE (2019), power lines should be referenced to a height of 1m above the ground surface. As aforementioned in the literature review, SPCs are sometimes buried to protect the cable from damage. For this reason, a second case was created to determine the B-field values produced by the cables if they were to simulate buried conditions.

Case two describes the scenario where the cables have been trenched to depths of 5m and 10m below the seabed surface and measured to a default reference height of 1m. The cables were assumed to be carrying loads of 200 A.

The third case study represents a scenario wherein the maximum magnetic field was calculated for all the cables at the seabed with the default reference height. The cable was modelled to carry loads of 300, 400, 500, 600 and 800 A. The three modelling cases are summarized below in Table 3.

Table 3: Modelling conditions in Case 1, 2 and 3.

Conditions	Case 1	Case 2	Case 3
Burial depth (m)	0	5 and 10	0
Cable load (A)	200	200	300, 400, 500, 600 and 800
Reference height on the Y-axis (m)	1	1	1

Additional assumptions made in relation to the B-field modelling are:

- The current flowing through each conductor within the cable is assumed to be balanced (Magnitude of current in conductor 1= Magnitude of current in conductor 2= Magnitude of current in conductor 3).
- The conductors are parallel to each other.
- The protective effects of the cables armouring, and anticorrosion sheaths were ignored to simplify the model.
- B-field was modelled at 90 degrees to the cable (Perpendicular to the line).

3.1.3 Induced Electric Field Equation for Static AC Cables

As discussed in Section 2.2, electric fields are generated whenever a cable has electric charges flowing through it. This means that a charged conductor will produce electric fields around its vicinity. However, as noted by Vattenfall AB (2010), the original electric fields produced by an SPC tends to be completely attenuated and absorbed by the shielding and electric isolation materials that are wrapped around the cable. For this reason, the original electric fields produced by the cables were deemed negligible were ignored.

On the other hand, a different type of electric field exists around SPCs (Tricas and Gill, 2011). This electric field is referred to as the induced electric field (iE-field), which is created when the field strength or density of the magnetic field becomes altered in an electrically conducting material (Vattenfall AB, 2010). In AC cables, the natural time changing flow of electrical current within the cable will induce an electric field around the cable (Huang, 2005). Also, iE-fields can be created by the movement of marine species across SPCs (Tricas and Gill, 2011).

With regards to AC SPCs, an equation was developed by the CMACS (2003) to help users evaluate the iE-fields produced near a SPC. The formula adopted for this calculation is given by (CMACS, 2003):

$$E_{field} = 2 \times \pi \times P_{frequency} \times B_{field} \quad \text{(Equation 3-21)}$$

Where $P_{frequency}$ is the power frequency and B_{field} the magnetic flux density.

With regards to the iE-fields produced as a result of the movement of a marine species around the cable, the Lorentz's law described below was applied (Tricas and Gill, 2011):

$$E_{field} = \frac{F}{q} \quad \text{(Equation 3-22)}$$

and

$$F = qvB_{field} \sin\theta \quad \text{(Equation 3-23)}$$

Where F is the force; q the electric charge; v the velocity of the charge; B_{field} the magnetic field and $\sin\theta$ the sine of the angle θ between the vectors of the B_{field} and v.

3.1.3.1 Induced Electric Field Modelling Approach and Assumptions for Static AC Cables

Since the intensity of the iE-field depends on the magnitude of the B-field, the B-field was calculated for the 10 cables (Table 2) based on the assumptions that; the cables were laid on the surface of the seabed, the magnetic field was measured at the heights of 1 m above the ground, and the SPC had a load current of 200 A. The estimated B-field intensity was then used in modelling two different scenarios for which an iE-field may be produced. The MATLAB code developed for this analysis can be found below in Figure 12.

```
Power_frequency= 50; % (Hertz) Frequency used in
Europe and Asia
V= 2; % (m/sec) Charge or water velocity
Angle= 90; % (Degrees) Angle between the direction of
the charge and the magnetic field
Electric_field1= 2*pi*Power_frequency*B_total% (V/m)
Induced Electric field around the cable (without
considerng the movement of water through the magnetic
field).
Electric_field2= V*B_total*sind(Angle) % (V/m) Induced
electric field generated as a result of the movement
of sewater through the magnetic field
InducedTotal= Electric_field1+Electric_field2
```

Figure 12: Code for AC induced electric field calculation.

The first case (called case A) describes a scenario where the iE-field is produced by the AC cable after assuming a power frequency value of 50 Hz. This value was chosen because electricity in Ireland varies at a frequency of 50 Hz (ESB, 1999). Equation 3-21 was used in simulating the iE-field model for case A. Case B illustrates a scenario where a marine specie crossing a cable induces an electric field around the cable. The marine specie was assumed to be travelling at a speed of 4 m/s (Tricas and Gill, 2011). Equations 3-22 and 3-23 were used to produce the models for case B. The two cases are summarized below in Table 4.

Table 4: Modelling conditions in Case A and B

Scenario	Conditions	
Case A	• Frequency = 50 Hz	• Cable burial depth = 0 m
Case B	• Velocity = 4 m/s • Angle= 90 Degrees	• Reference height above ground= 1m • Loading=200 A

In relation to the iE-field modelling, the following assumption was made:

- Induced electric fields generated as a result of the non-perfect shielding of the cable were ignored.

3.1.4 Magnetic Field Equation for Static DC Cables

The B-fields attributable to a load on a SPC can be calculated by applying the fundamental principles of the Biot-Savart law described in Section 3.1.2. However, the equations (i.e. Equations 3-2 to 3-19) used to model the B-fields produced by the AC cables cannot be used in calculating the magnetic fields for the DC cables. This is because of the differences in the design configuration of both cables. The magnetic fields produced by a DC cable can be divided into its northern, eastern, and vertical components. According to Kavet et al. (2016), for bipolar cables, each component can be described by the following equations:

$$B_{CableNorth} = \frac{I}{5} \times \sin\emptyset \times \left\{ \frac{(h+a) - \left(\frac{S}{2}\right) \times \sin(\theta)}{((x - \left(\frac{S}{2}\right) \times \cos(\theta))^2 + ((h+a) - (\frac{S}{2}) \times \sin(\theta))^2} - \frac{(h+a) + \left(\frac{S}{2}\right) \times \sin(\theta)}{((x + \left(\frac{S}{2}\right) \times \cos(\theta))^2 + ((h+a) + (\frac{S}{2}) \times \sin(\theta))^2} \right\} \quad \text{(Equation 3-24)}$$

$$B_{CableEast} = \frac{I}{5} \times \cos \emptyset \times \left\{ \frac{(h+a) - (\frac{S}{2}) \times \sin(\theta)}{((x - \left(\frac{S}{2}\right) \times \cos(\theta))^2 + ((h+a) - (\frac{S}{2}) \times \sin(\theta))^2} - \frac{(h+a) + (\frac{S}{2}) \times \sin(\theta)}{((x + \left(\frac{S}{2}\right) \times \cos(\theta))^2 + ((h+a) + (\frac{S}{2}) \times \sin(\theta))^2} \right\} \quad \text{(Equation 3-25)}$$

$$B_{CableVertical} = \frac{I}{5} \times \left\{ \frac{(x) - (\frac{S}{2}) \times \cos(\theta)}{((x - \left(\frac{S}{2}\right) \times \cos(\theta))^2 + ((h+a) - (\frac{S}{2}) \times \sin(\theta))^2} - \frac{(x) + (\frac{S}{2}) \times \cos(\theta)}{((x + \left(\frac{S}{2}\right) \times \cos(\theta))^2 + ((h+a) + (\frac{S}{2}) \times \sin(\theta))^2} \right\} \quad \text{(Equation 3-26)}$$

Where $B_{CableNorth}$ is the northern component of the cables B-field; $B_{CableEast}$ the eastern component of the cables B-field; $B_{CableVertical}$ the vertical component of the cables B-field; I the current; h the reference measurement height on the y axis;a the burial depth of the cable; s the conductor spacing; x the lateral distance of the reference measurement point on the x axis; $\emptyset$ the profile angle (i.e. the angle with which the user views the cable relative to the east-west coordinate plane) and θ the twist angle, which refers to the angle of cable placement (Figure 13).
The magnitude of the B-field produced by the cable is calculated as,

$$B_{CableTotal} = [(B_{CableNorth})^2 + (B_{CableEast})^2 + (B_{CableVertical})^2]^{0.5} \quad \text{(Equation 3-27)}$$

Apart from the EMFs that are generated by the SPCs, the earth itself creates its own local DC magnetic field, which may be altered by the magnetic field from the cable (Tricas and Gill, 2011). This local magnetic field serves as an artificial GPS for marine species and therefore, should not be ignored when calculating the B-fields from SPCs (Wiltschko and

Wiltschko, 2005; Tricas and Gill, 2011). Hence, the contribution from the geomagnetic field is given as (Kavet et al., 2016),

$$B_{GeoTotal} = [(B_{GeoNorth})^2 + (B_{GeoEast})^2 + (B_{GeoVertical})^2]^{0.5} \quad \text{(Equation 3-28)}$$

Where $B_{GeoTotal}$ is the resultant geomagnetic field; $B_{GeoNorth}$ the northern component of the earths B-field; $B_{GeoEast}$ the eastern component of the earths B-field and $B_{GeoVertical}$ the vertical component of the earths B-field.

The combined B-field profile (from the cable and earth) is calculated as (Kavet et al., 2016),

$$B_{Total} = [(B_{CableNorth} + B_{GeoNorth})^2 + (B_{CableEast} + B_{GeoEast})^2 + (B_{CableVertical} + B_{GeoVertical})^2]^{0.5} \quad \text{(Equation 3-29)}$$

The presence of the cable in the earth will cause the strength of the local B-field near the cable to deviate from the magnitude of the original geomagnetic field around that area (Tricas and Gill, 2011). The Net, that is, the deviation, is given by (Kavet et al., 2016),

$$B_{Net} = B_{Total} - B_{GeoTotal} \quad \text{(Equation 3-30)}$$

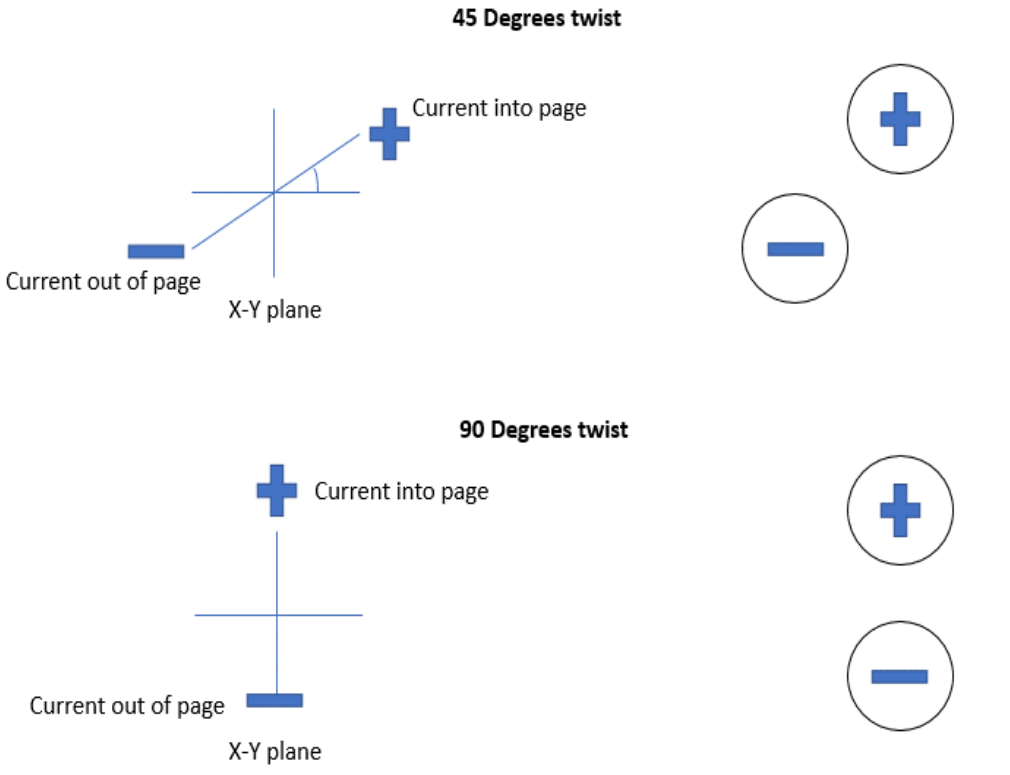

Figure 13: A schematic representation of the twist angle for a bipolar DC SPC (Modified from Kavet et al., 2016).

3.1.4.1 Magnetic Field Modelling Approach and Assumptions for Static DC Cables

In this study, 5 bipolar DC SPCs were selected for analysis based on the availability of sufficient information needed to characterize the EMF levels produced by the cables (Table 5). As aforementioned in the literature review (section 2.5.1.2), DC SPCs are divided into monopolar and bipolar systems. The latter configuration was chosen because the newly built cables are predominantly bipolar (Ardelean and Minnebo, 2015). The owners of the cables plan to lay them in the coming years.

Table 5: An overview of the 5 DC SPCs.

Cable name	To be commissioned in	Location	Power (MW)	Voltage (KV)	Conductor spacing (m)
1	2024	Germany	900	±320	0.1
2	2025	North Sea	1400	±500	0.5
3	2022	North Sea	1200	±500	0.7
4	2028	North Sea	1400	±500	0.9
5	2021	North Sea	1400	±550	1

The B-fields produced by the 5 cables were calculated using the equations described in Section 3.1.4. The MATLAB code developed for this analysis can be found in Figure 14.

```
format long
X = [0];% (m) Distance away from cable centreline
I = 1650;% (A) Current through cable
A = 6;% (m) Total vertical distance to the measurement point from the
cable
S = 0.135;% (m) Separation between the two cables
P = 90;% (Degrees) Profile angle of the cable relative to the east and
west direction
T = 90;% (Degrees) Cable twist angle between the centre of the two
cables in the x-y plane
U = 1.25668*10^-6;% (Tm/A) Permeability of free space
Uo = (U/(2*pi))*10^9;% (nTm/A)
Bgn = 18345.4;% Magnitude of the geomagnetic field in the Northern
direction
Bge = -4694.3; % Magnitude of the geomagnetic field in the Eastern
direction
Bgv = 50084;% Magnitude of the geomagnetic field in the Vertical
direction
Bcn =Uo*((I/5)*sind(P))*(((A)-(S/2)*sind(T))./[(((X)-
(S/2)*cosd(T)).^2)+((A)-(S/2)*sind(T)).^2]-
[((A)+(S/2)*sind(T))./((((X)+(S/2)*cosd(T)).^2)+(((A)+(S/2)*sind(T)).^2
))]);% Magnetic field due to the current on the cable in the northern
direction
Bce =Uo*((I/5)*cosd(P))*(((A)-(S/2)*sind(T))./[(((X)-
(S/2)*cosd(T)).^2)+((A)-(S/2)*sind(T)).^2]-
[((A)+(S/2)*sind(T))./((((X)+(S/2)*cosd(T)).^2)+(((A)+(S/2)*sind(T)).^2
))]);% Magnetic field due to the current on the cable in the eastern
direction
Bcv = Uo*(I/5)*(((X)-(S/2)*cosd(T))./[(((X)-(S/2)*cosd(T)).^2)+((A)-
(S/2)*sind(T)).^2]-
[((X)+(S/2)*cosd(T))./((((X)+(S/2)*cosd(T)).^2)+(((A)+(S/2)*sind(T)).^2
))]);% Magnetic field due to the current on the cable in the vertical
direction
B_Totalcable = ((((Bcn).^2)+((Bce).^2)+((Bcv).^2)).^0.5);% Magnitude of
the total field from the cable (only)
B_Geotal =((((Bgn).^2)+((Bge).^2)+((Bgv).^2)).^0.5);% Magnitude of the
total geomagnetic field (only)
B_total = ((((-Bcn+Bgn).^2)+((Bce+Bge).^2)+((-Bcv+Bgv).^2)).^0.5)%
Magnitude of the total field (from the cable and the earth)
B_net = B_total-B_Geotal; % Difference between Magnitude of the total
field and the magnitude of the geomagnetic field
```

Figure 14: Parameters and code for DC magnetic field calculation

The first DC case (called Case 4 or the fourth magnetic field case) represents the configuration of a standard DC cable that has been laid on the seabed, with an assumed load current of 1800 A. The cable twist and profile angles were assumed to be 90 and 0 Degrees respectively. In general, the B-field above a cable is calculated along profiles perpendicular to the survey line (i.e. at 90 degrees) (Tricas and Gill, 2011). The 0-degree cable twist was chosen based on the assumption that both cables (i.e. the bipolar SPC) are on the same plane (Figure 13).

The magnetic field was initially calculated without considering the influence of the geomagnetic field. After this was done, a new B-field model was created. The new model took into account the influence of the geomagnetic and how it interacts with the B-field produced by the cable. As aforementioned in the introductory section of the project, Ireland has been chosen as a case study. Thus, geomagnetic field values were obtained from a location north of the Irish Sea (Table 6). Coordinates of the position were inputted into the latest International Geomagnetic Reference Field (IGRF) Model (IGRF, 2021). The IGRF model was then used to generate the three-dimensional coordinates of the geomagnetic field at that location.

To better understand the influence of the total magnetic field (i.e. B-field from cable + B-field from the earth) on the geomagnetic environment, a new scenario was modelled. In scenario 5, the magnetic field deviation (see Equation 3-30) was estimated for the location north of the Irish sea, following the same assumptions described above. In addition, a new model was created for comparison using coordinates south of the Irish Sea (Table 6).

Table 6: Coordinates of the geomagnetic field positions

	Locations	
Latitude and Longitude	**North of the Irish Sea**	**South of the Irish Sea**
North	53°55'49.3''	52°19'41.9''
West	6°05'18.6''	6°17'52''

The sixth and final magnetic field case study represents a scenario where the cables have been buried at a depth of 0.5 m and positioned at the following angles: 0, 90 and 180 degrees. The same assumptions in scenario 4 were used in creating this model. The three cases are summarized in Table 7.

Table 7: Modelling conditions in Case 4, 5, and 6

Conditions	**Case 4**	**Case 5**	**Case 6**
Cable load (A)	1800	1800	1800
Burial depth (m)	0	0	0.5
Profile angle (Degrees)	90	90	90
Twist Angle (Degrees)	0	0	0, 90, and 180
location of geomagnetic field position	North of the Irish Sea	North and south of the Irish Sea	North of the Irish Sea
Reference height on the Y-axis (m)	1	1	1

Additional assumptions made in relation to the B-field modelling are:

- The protective effects of the cables armouring, and anticorrosion sheaths were ignored to simplify the model.

- Conductor spacing was assumed since the projects are currently still in the planning phase. However, in a similar project, 0.5-1 m conductor spacing was assumed (Tricas and Gill, 2011).

3.1.5 Induced Electric Field Modelling Approach and Assumptions for Static DC Cables

Since DC cables do not directly induce electric fields, iE-fields may be produced by the movement of marine species across the cable. Hence, Equation 3-22 was adopted for this study. Since the intensity of the iE-field depends on the magnitude of the B-field, the B-field was first calculated for the 5 cables based on the assumptions adopted in case 4. The estimated B-field intensity was then used in modelling one scenario for which an iE-field may be produced. Case C illustrates a scenario where a marine species crossing a cable induces an electric field around the cable. The marine specie was assumed to be travelling at a speed of 4 m/s (at 90 degrees). Equations 3-22 and 3-23 were used to produce the models for case C.

In relation to the iE-field modelling, the following assumption was made:

- The background field was ignored in these calculations in order to reduce the complexity of the model.

3.1.6 EMF Tool Design

As aforementioned in the introductory section of the report, there is currently no freely available tool that can be used to estimate or predict the EMFs that may be produced by SPCs. For this reason, a simple excel tool (called DolphDetch EMF) was developed to assist the Irish public in estimating the EMFs produced by 3-core AC and bipolar DC power cables. All the equations applied in this project were used in designing the tool. A copy of the tool has also been submitted alongside the dissertation.

3.2 Marine Species

3.2.1 Introduction

This section describes the procedure that was used in identifying the marine organisms in the Irish sea that may be sensitive to either magnetic and/or electric fields.

3.2.2 Identification of Priority Species in the Irish Sea

An important objective of this project was to identify priority species in the Irish sea that may be sensitive to EMFs produced by underwater cables. Three major challenges were faced whilst making efforts to achieve the objective. To begin with, there are thousands of marine species in the Irish Sea, which make it nearly impossible for the researcher to identify the sensory capabilities for each species within the time frame of this study. According to Tricas and Gill (2011), there is a considerable disparity in terms of the quantity and quality of data available on the sensory capabilities of each marine species in the ocean. The final challenge related to this objective is that studies on sensitivity to EMFs have only focused on a few species (Hutchinson et al., 2021b). Indeed, EMF senses have been reported for some marine fishes (e.g. Elasmobranchs), mammals, reptiles (including turtles) and invertebrate species (Tricas and Gill, 2011). Hence, information about the sensitivity of Irish marine species to electric or magnetic fields was inferred based on the availability of data.

In previous studies, researchers tend to focus on the species that are most likely to interact with SPCs (Gill et al., 2005). These tend to be the species that live around areas where a cable will be laid. However, realistically, some marine species tend to migrate from one point to the other at different times during the year (Lascelles et al., 2014). Also, in Ireland, offshore wind farm structures are planned to be installed at

different locations in the Irish Sea (4C Offshore, 2021). This implies that different marine species may potentially be affected by SPCs. Thus, this study focuses on a wide range of species that live in the Irish sea.

To begin with, a preliminary list containing all the marine species in Ireland was compiled through a rigorous, cautious, and cumulative process. Species were organised into major groups and subgroups based on their taxonomical classification. Once this was completed, the following species of concern were then added to a smaller list: fishes, mammals, reptiles, and invertebrates. Critically endangered, endangered, and vulnerable species were also added to the new refined list. The new list was further reduced to a listing of priority species. Species were only added to the priority list if they met one of the following criteria:(1) there is direct evidence of EMF sensory capability and (2) when evidence of EMF sensitivity isn't available, a suspected species must come from the same family as another species for which EMF sensitivity has been documented. Data regarding the various marine species were obtained primarily from the websites of the following organisations: National Biodiversity Data Center (NBDC), National Parks and Wildlife Service (NPWS) (Including the Irish red list for endangered species) and the department of public expenditure and reform (open data unit) (NBDC, 2021; NPWS, 2021; DGE, 2021).

3.3 Heavy Metals

3.3.1 Introduction

This Section presents the reagents used, instruments employed, and the analytical procedures adopted for the HM analysis. The experiment was conducted based on the assumption that a SPC is damaged or broken, and has some, if not all of its cross-sectional area exposed. As aforementioned in the literature review section, the cables are typically designed with copper or aluminum conductors, which may pollute the marine environment if left exposed when damaged or abandoned.

3.3.2 Sample Preparation and Analysis

Underwater power cables of different diameters and ages (i.e. New, 12 days, 15 years and, 34 years) were collected from a marine company in Ireland. The age of a cable refers to the amount of time the cable has spent in the ocean. For example, the 12 days old cable was laid in the ocean for 12 days before being removed. In addition, three cables (i.e. New, 15 years, and 34 years) are made of copper electrodes (conductors), while the fourth (i.e. 12 days) was designed using aluminum conductors. Information regarding the cable components is presented in Table 8.

Table 8: The design characteristics of the SPCs.

Design characteristics	New Cable	12 Days	15 Years	34 Years
Conductor diameter (cm)	1.50	5.00	3.00	1.50
Cable diameter (cm)	10.50	27.00	11.00	9.00
Cross sectional Area (Cm^2)	86.60	572.63	95.05	63.63
Insulator diameter (cm)	2.50	8.00	N/A	3.00
Conductor	Copper	Aluminium	Copper	Copper

Figure 15a: A picture of the 4 subsea power cables

Figure 15b: The experimental set up

The SPCs were cut into similar lengths of approximately 7 cm and buried in plastic vessels (buckets) containing 8 liters of seawater (Figures 15(a) and (b)). Before submerging the cables, a background sample (or control sample) was collected. The background sample served as a benchmark for the other samples since it was unaffected by the releases from the cables. After this had occurred, the cables were submerged and monitored for six months and one year, respectively. Seawater samples were also collected at six months and one year, respectively. The samples (i.e. background, six months, and one year) were collected in suitable 100 ml glass test containers.

The samples were filtered to remove any suspended particle using a 0.45 µm membrane. The filtered samples were digested by adding 9 ml of concentrated nitric acid (HNO_3) and 3 ml of hydrochloric acid (HCl) to 100 ml of the samples as recommended by Creed et al. (1994). The resulting mixture was heated on a hot plate (at 90^0) for 55 minutes (Enyoh and Isiuku, 2020). A few millimeters of deionized water were then added to the reduced mixture, which was then re-filtered into 100 ml standard flasks and transferred into glass bottles for elemental analysis using the inductively coupled plasma optical emission spectrometry (ICP-OES) and inductively coupled plasma mass spectrometry (ICP-MS) instrument (Alomary and Belhadj, 2007; Bonta et al., 2016).

Throughout the experiment, all glass vessels were cleaned with detergents and then rinsed thoroughly with deionized water (18.2 MΩ). This is necessary to remove any form of contamination. The standard solutions were prepared by diluting a 1,000 mg/l multi-element solution (ICP-Multi-element Standard, Merck). All chemicals and reagents used for the experiment were of analytical grade.

The entire content of mercury (Hg) and arsenic (As) in the seawater samples was analyzed with an ICP-MS attached to the intuitive WinLab32 software system, which helps the user to analyze samples and report data

(Zhang & Hu, 2011; Bonta et al., 2016). The whole content of Aluminum (Al), Cadmium (Cd), Copper (Cu), Iron (Fe), Lead (Pb), Manganese (Mn) and, Nickle (Ni) in the seawater samples was analyzed using the ICP-OES (software v4.1.0b443, GBIP v1.7b2) instrument. Device calibrations were ensured using the recommended procedures provided by the device manufacturers. The standard solution was prepared using deionized water.

3.3.3 Estimation of the Cables Contribution to Heavy Metal Pollution Potential

The amount of the HMs released per centimeter square of the cable was estimated using the equation below. It is necessary to estimate this consequential adjustment because the cables were of different sizes. This will help to improve one's understanding of the contribution of each cable, irrespective of size.

$$Amount\ of\ Hm\ realeased\ per\ cm^2\ of\ cable = \frac{Amount\ of\ Hm\ released\ from\ cable}{Cable\ crossectional\ area}$$

(Equation 3-31)

Where,

$$\pi\frac{D}{4} = Cable\ cross\ sectional\ area$$

$$D = Diameter\ of\ the\ cable$$

$$Amount\ of\ HM\ released\ from\ cable$$

$$= Heavy\ metal\ concentration\ in\ seawater\ after\ submersion$$

$$- heavy\ metal\ concentration\ before\ submersion\ (control)$$

3.4 Microplastics

3.4.1 Introduction

As discussed in the literature review section, the outermost covering of a typical underwater cable is composed of a polymer material, which means that there is a possibility that SPCs may contribute to the MP pollution of the ocean. However, at present, no scientific studies have been conducted to determine the likelihood of that occurring. As a result, two experiments (static and dynamic) were carried out to investigate and identify any potential MPs that underwater power cables may release.

The first experiment (static) represents a scenario where a cable has been isolated from other external disturbances in the ocean in order to easily identify the MPs that may be released from the cable. The cable samples used for the HMs test were also used in this study. The static experiment was conducted based on the assumption that the polymer materials wrapped around the cables are reasonably held together (Figure 5). It was assumed that the cables would not experience any significant external force in the ocean. This is true for this experiment because the cables were placed in plastic buckets filled with seawater. Although the entire cross-sectional area of the cables was fully exposed, the contributions from its internal components were ignored because the polymer material around the cable would be the primary source of MP contamination as it is in direct contact with the ocean. Therefore, it was assumed that the cable was perfectly sealed on both ends.

As aforementioned (in Section 2.6), the outermost covering of a SPC is typically exposed to numerous threats in the ocean (e.g. waves, current and, shark attacks), which may cause it to abrade or tear (Figure 16). In the case of this occurrence, the exposed cable fibers or strands may disintegrate over time if exposed to agitation caused by currents and

waves that circulate the ocean. For this reason, the dynamic experiment was conducted to determine how likely it is for the loose cable strands to contribute to the MP pollution of the ocean. The experimental procedures that were applied have been detailed in the sections below.

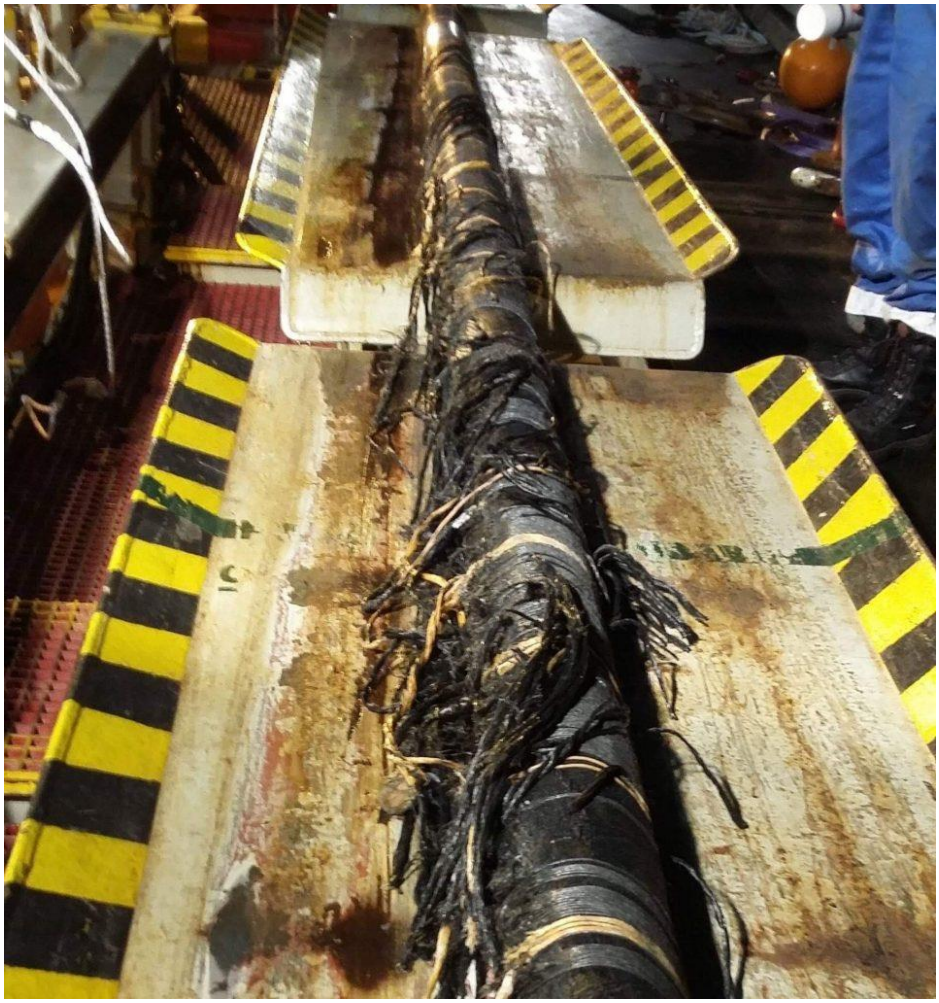

Figure 16: An abraded SPC (Cathie Group, 2018).

3.4.2 Sample Preparation and Analysis

3.4.2.1 The Static Experiment

In the static experiment, seawater samples (80 ml) were collected from the four buckets containing the four subsea cables (i.e. New, 12 days, 15 years, and 34 years) that had been buried for one year. Each 80 ml sample was stored in a 100 ml glass test bottle. Glass bottles were chosen over plastic bottles to minimize the risk of enrichment of the potential MPs from the plastic container. After that, the samples were digested using 5 ml of 30% hydrogen peroxide(H_2O_2) for 24 hours in the 100 ml glass test bottle. In other seawater experiments, different researchers have used larger volumes (e.g. 50 ml – Depending on the volume of the sample) of hydrogen peroxide to digest the organic matter in their samples (Tamminga et al., 2019; Zheng et al., 2021). However, 5 ml was used for this experiment because no major organic materials were identified in any samples. After complete digestion, 20 ml of the mixture was filtered unto a $0.8\,\mu m$ gold nitrocellulose membrane using a vacuum pump (Fisher Scientific) with a glass filtration device. The entire quantity of the mixture was not filtered because the researcher wanted to make it easy to identify any potential MP particles.

The filtered membrane was carefully placed into each sample's square (24x24 mm) and rectangular (24x50 mm) shape cover glass. The cover glass was then sealed between a sterile petri dish (60x15 mm) and stored at room temperature for further analysis. Throughout this experiment, all the samples were handled with extreme care to avoid any form of MP contamination. Cotton lab coats and nitrile gloves were worn to maintain the aseptic technique and to prevent cross-contamination. All the apparatus used were rinsed four times with deionized water to avoid any form of contamination. More importantly, the beaker and filtration funnel were cleaned for 30 minutes (at $40^0\ C$) using an ultrasonic bath (Bandeline Sonorex digital).

The potential MPs in the samples were identified using a Raman microscope spectrometer (Renishaw InVia). The Renishaw (WiRE 3.4) software was used for the experiment. This system was equipped with the following tools: a microscope (NT-MDT), a 532-nm laser and, a cooled charged coupled device. Before any sample was tested, the system was calibrated using a silicon wafer. Then, the size and quantity of MPs were determined using ImageJ.

3.4.2.2 The Dynamic Experiment

For the dynamic experiment, newer cable samples were obtained by measuring and cutting 7 cm long cable fibers (or strips) from the bodies (i.e. the outer covering) of each of the original cables (Figure 17). The new samples were thoroughly cleaned with soap and water and rinsed four times with deionized water to minimise any risk of contamination that may occur during the experiment. This was done because some of the cables had been in the ocean for very long periods. After drying the samples, 80 ml of deionized water was poured into 100 ml glass bottles. Deionized water was used because it contains much fewer impurities than seawater. Once this had been completed, the new cable samples were carefully transferred into glass bottles using a sterile stainless-steel tweezer.

Figure 17: The new cable samples

Thereafter, each bottle was positioned tightly in the middle of a horizontal shaker (Stuart reciprocating shaker), where its speed was set to 250 revolutions per minute (RPM) for 15, 45, and 90 minutes, respectively (Figure 18). The shaker had a 90-minute time limit, making it impossible to test the samples for longer. After the first 15 minutes, the cable fiber was removed and placed in a clean petri-dish while the seawater sample was stored at room temperature for further analysis. 80 ml of deionized water was then added into a new 100 ml glass bottle. The stored fiber was then inserted into the bottle for the 45-minute experiment. The previously mentioned procedure was then repeated for the 45- and 90-minute tests. 20 ml of the samples were then filtered following the same procedures outlined in the static experiment. The same quality control and contamination protection measures were also adopted for this study. In addition, the samples were also analyzed using similar methods as described above.

Figure 18: The main experimental setup for the dynamic experiment

3.4.2.3 Risk of MP Contamination

The risk of MP contamination was determined by applying Equation 3-32, as described by Kabir et al. (2021). The equation considers the chemical composition and concentration of MPs in the seawater samples (Liu et al., 2019).

$$H_i = \sum(\frac{P_{ji}}{C_i} \times S_j)$$

(Equation 3-32)

Where P_{ji} is the number of each single MP polymer identified in a sample, C_i the total number of MPs in a sample, and S_j the chemical toxicity coefficient or risk scores. For instance, the S_j for PP is 1 (Lithner et al., 2021).

Results

4.0 Results

4.1 Introduction

In this chapter, the calculated EMF profiles for various cables are presented. The marine species in the Irish sea that may be sensitive to EMFs are reported. Also, the results from the experimental analysis of heavy metals and microplastics are presented.

4.2 Magnetic Field Calculations

4.2.1 Case 1 (AC SPCs)

In the first case study, the magnetic field levels from the 10 AC SPCs were calculated based on the scenario where the cables were laid on a seabed, with an assumed nominal load of 200 A. The magnetic field strength produced by the cables is shown in Figure 19.

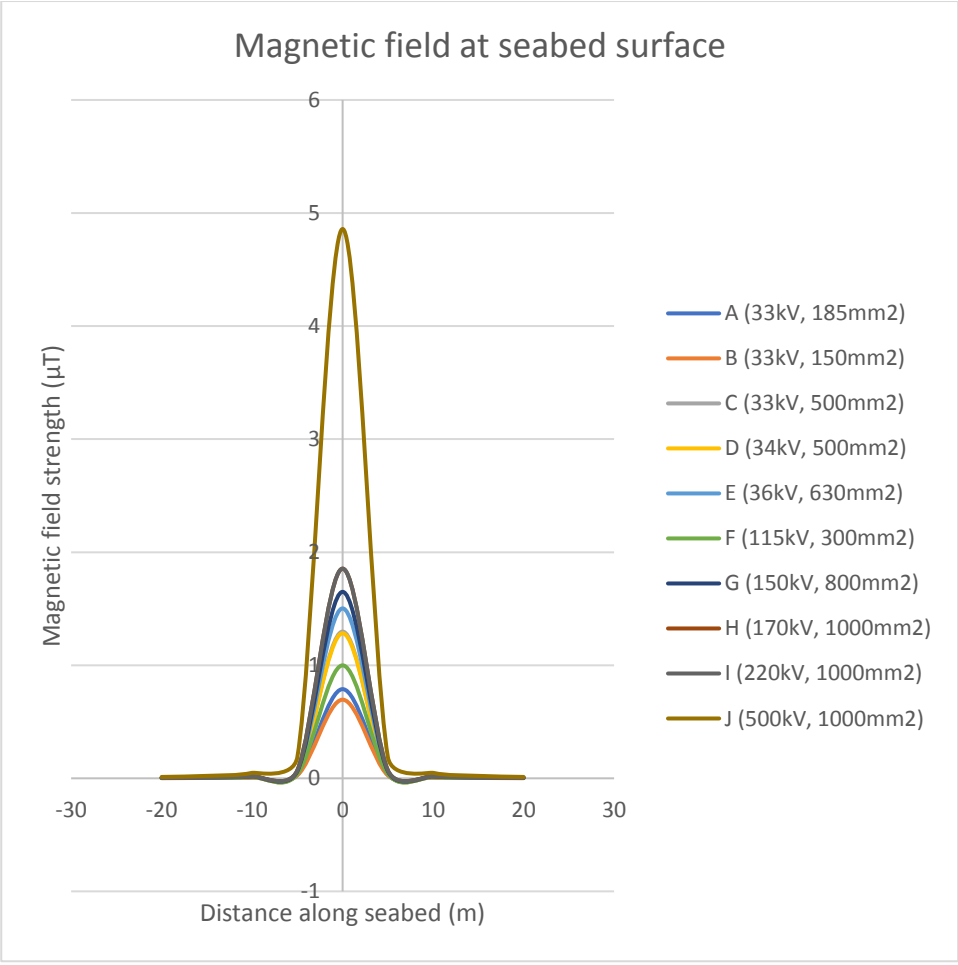

Figure 19: Case 1. The magnetic field strength over the 10 AC SPCs.

The highest magnetic field strength was 4.86 μT, which was produced by the 500 kV, 1000 mm^2 Cable (i.e. 500 kV cable with a nominal cross-sectional area of 1000 mm^2), and the lowest from the 33 kV, 150 mm^2:0.69 μT, at the centerline of the cable. The order of magnetic field strengths was as follows: B (33V, 150 mm^2) < A (33 kV, 185 mm^2) < F (36 kV, 630 mm^2) < D (34 kV, 500 mm^2) < E (36 kV, 630 mm^2) < G (150 kV, 800 mm^2) < H (170 kV, 1000 mm^2) < I (220 kV, 1000 mm^2) < C (33 kV, 500 mm^2) < J (500 kV, 1000 mm^2). The magnitude of the magnetic fields increased with an increase in the cross-sectional area of the cable. Figure 20 shows the average modelled magnetic field strength for the 10 AC SPCs. The 10 cables have a mean strength of 1.68 μT. An average magnetic field profile was estimated because of the variation in the configuration of the 10 cables. The results for this scenario were tabulated in Appendix A, Table A-2 and A-3.

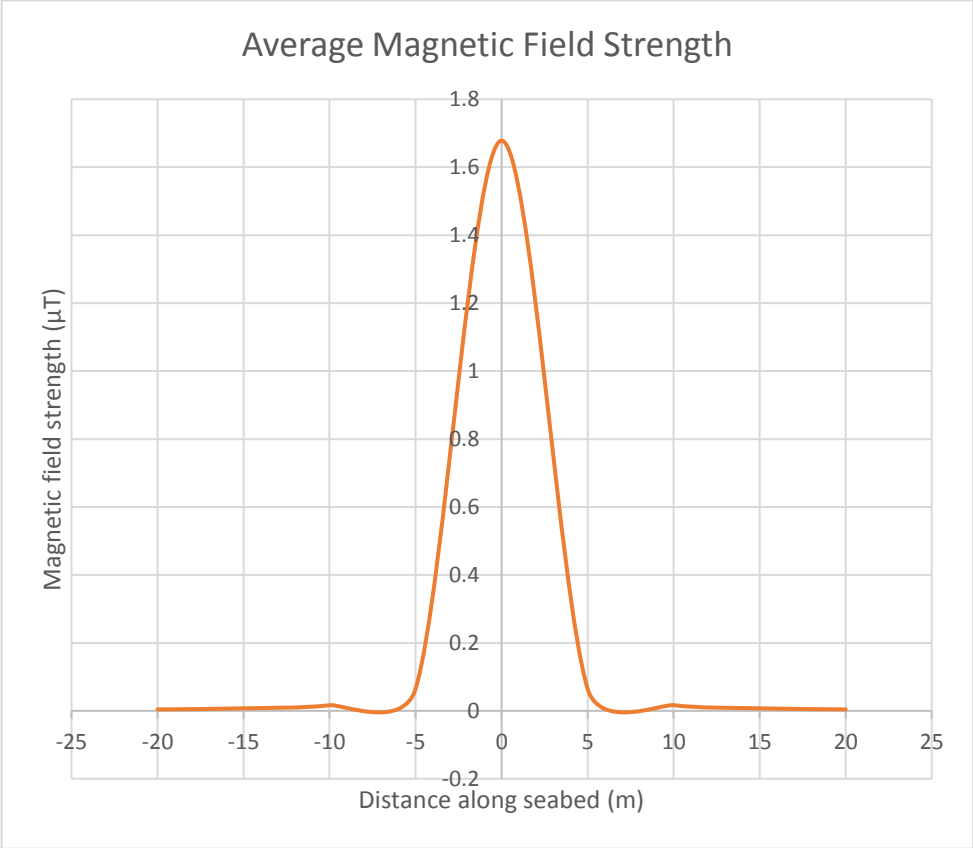

Figure 20: Case 1. The average magnetic field strength over the 10 AC SPCs.

4.2.2 Case 2 (AC SPCs)

The second case study represents the scenario where the cables have been trenched to depths of 5 and 10 m below the seabed surface. Like Case 1, the cables were assumed to be carrying loads of 200 A. Figures 21 and 22 depict the magnetic field calculated for this case study. When the cable was kept 5 m below the seabed (Figure 21), the 500 kV, 1000 mm^2 cable (Cable J) had the greatest magnetic field strength of 0.14 μT, while the 33kV, 150 mm^2 cable (Cable B) had the lowest magnitude of 0.02 μT. The magnetic field levels were rapidly decaying with distance along the seabed. For example, at 25 m and 50 m from the centerline, the maximum magnetic field level fell to 0.007 μT and 0.002 μT. respectively. The results can be found in Appendix A, Table A-4.

On the other hand, a similar trend was observed when the cable was buried 10m below the seabed (Figure 22). At distances of 25 and 50 m to either side of the cable, the maximum magnetic field level diminished to 0.0065μT and less than 0.002μT. Also, the Cable J had a reduced magnetic field strength of 0.04 μT, whilst Cable B had a magnetic field strength of 0.006 μT. The results are provided in Appendix A, Table A-5.

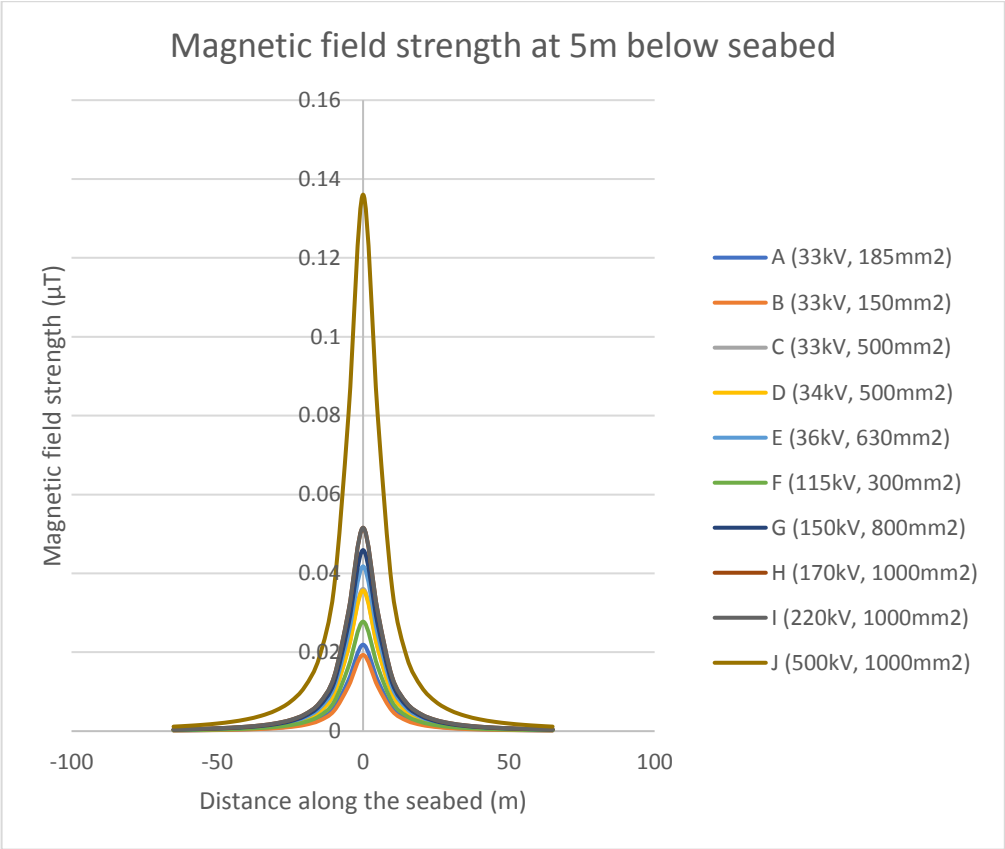

Figure 21: Case 2. Modelled magnetic field strength at 5 m below seabed.

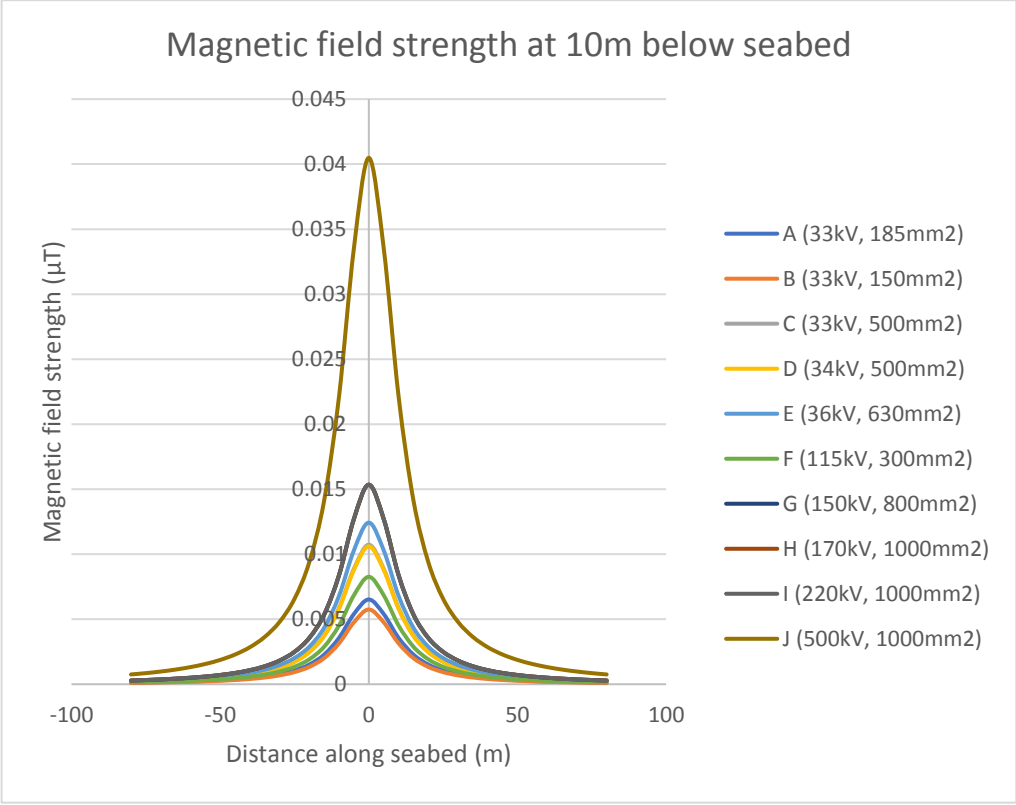

Figure 22: Case 2. Modelled magnetic field strength at 10m below seabed.

4.2.3 Case 3 (AC SPCs)

In case 3, the magnetic field was calculated at the centreline of each cable (i.e. the maximum point) for various loading conditions. It was assumed that the following loads passed through the cables: 200, 300, 400, 500, 600, 800 A. The calculation results are shown in Table 9. Overall, the magnetic field strength increased with increasing amperage from 200 (1.68±1.13 µT) to 800 (6.71±4.51 µT). This result is expected because the magnetic field is directly proportional to the current flowing through the cable (Equation 3-1). This means that an increase of the amperage by four times would also result in an increase of the magnetic field strength by the same magnitude. The following pattern was observed for all the loading conditions: J > I /H > G > E > C > D > F > A > B.

Table 9: Calculated magnetic field values at the centerline of the 10 SPCs.

Load (A)	A (33Kv, 185 mm2)	B (33kV, 150 mm2)	C (33kV, 500 mm2)	D (34kV, 500 mm2)	E (36kV, 630 mm2)	F (115 kV, 300 mm2)	G (150 kV, 800 mm2)	H (170 kV, 1000 mm2)	I (220 kV, 1000 mm2)	J (500 kV, 1000 mm2)
	microTesla (µT)									
200	0.79	0.70	1.30	1.28	1.50	1.00	1.65	1.85	1.85	4.86
300	1.18	1.04	1.95	1.92	2.25	1.50	2.47	2.78	2.78	7.29
400	1.58	1.39	2.59	2.57	3.01	2.00	3.30	3.71	3.71	9.72
500	1.97	1.74	3.24	3.21	3.76	2.50	4.12	4.64	4.64	12.15
600	2.37	2.09	3.89	3.85	4.51	3.00	4.95	5.56	5.56	14.58
800	3.15	2.78	5.19	5.13	6.01	4.00	6.60	7.42	7.42	19.43

4.2.4 Case 4 (DC SPCs)

In this case study, the magnetic field profiles of 5 DC SPCs were modelled. The models were created to provide information about the magnitude of the magnetic fields that may be produced by 5 prospective DC cables that are carrying a load current of 1800 A. In the first instance, the magnetic field was calculated without considering the influence of the geomagnetic field (Figure 23). In the second scenario, the researcher calculated the magnetic field produced by the cable and earth (i.e. the B-field and Geomagnetic field) (Figure 24). The geomagnetic field at 53°55'49.3'' (Northern Latitude) and 6°05'18.6'' (Western Longitude) was used in this calculation, corresponding to the geomagnetic components shown in Table 10.

Table 10: Magnitude of the geomagnetic field at the location north of the Irish Sea

Component	Strength (μT)
Northern	18.3
Eastern	-0.7
Vertical	45.9
Total	49.5

When the geomagnetic field was absent (Figure 23 and Appendix A, Table A-6), cable 5 (i.e. the 550 kV cable with a spacing of 1 m) produced the highest magnetic field of 57.60 μT (at its centre). On the other hand, after taking into account the influence of the geomagnetic field, the calculated value rose to 105.59 μT (Figure 24 and Appendix A, Table A-7). Interestingly, the lowest magnetic field was produced by the cable that had a spacing of 0.1 m. In a similar fashion, the average magnetic field was lowest in the absence of the geomagnetic field (39.49 μT) (Figure 25), and highest in the presence of the geomagnetic field (87.50 μT) (Figure 26). The results are provided in Appendix A, Table A-8 and A-9.

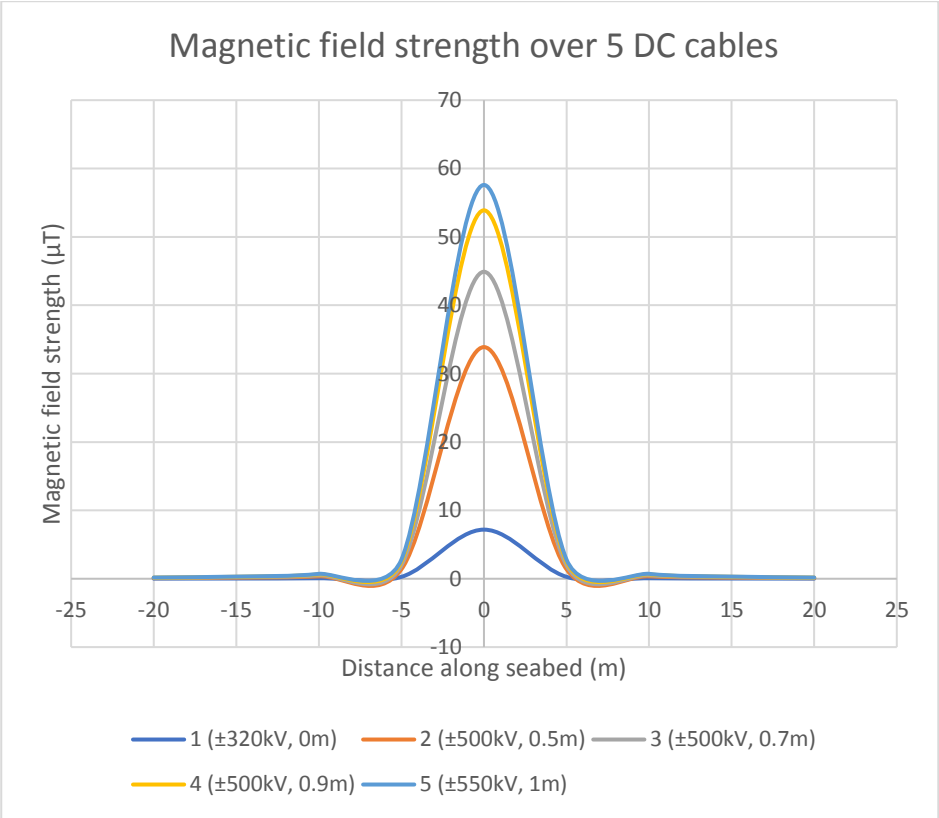

Figure 23: Case 4. Calculated magnetic field produced by 5 DC SPCs (without considering the influence of the geomagnetic field).

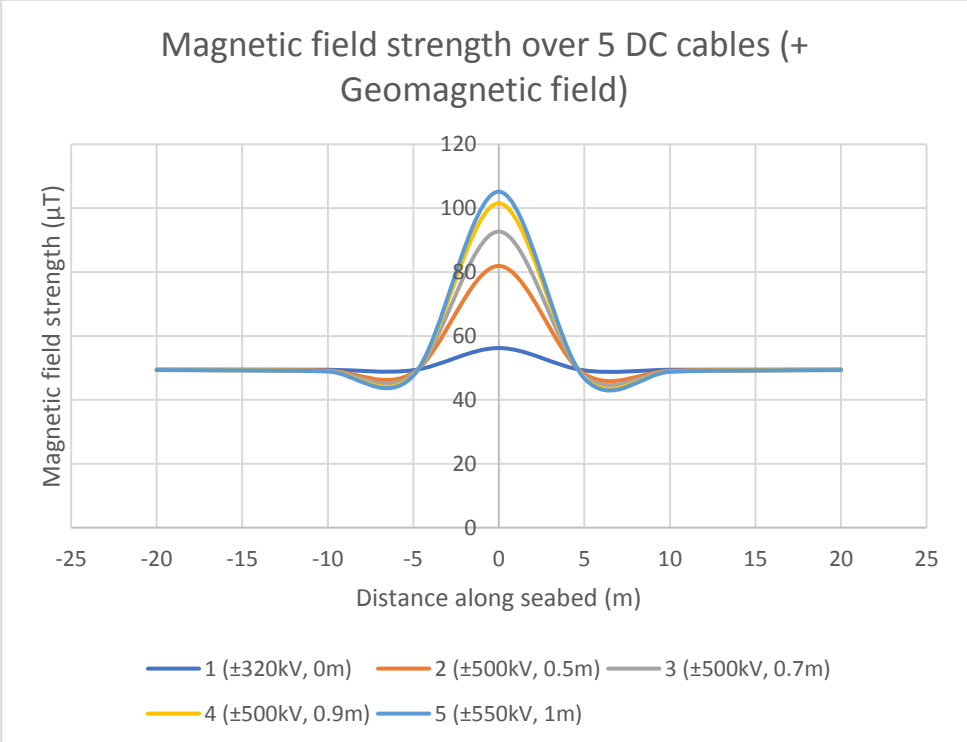

Figure 24: Case 4. Total magnetic field produced by 5 DC SPCs and the earth.

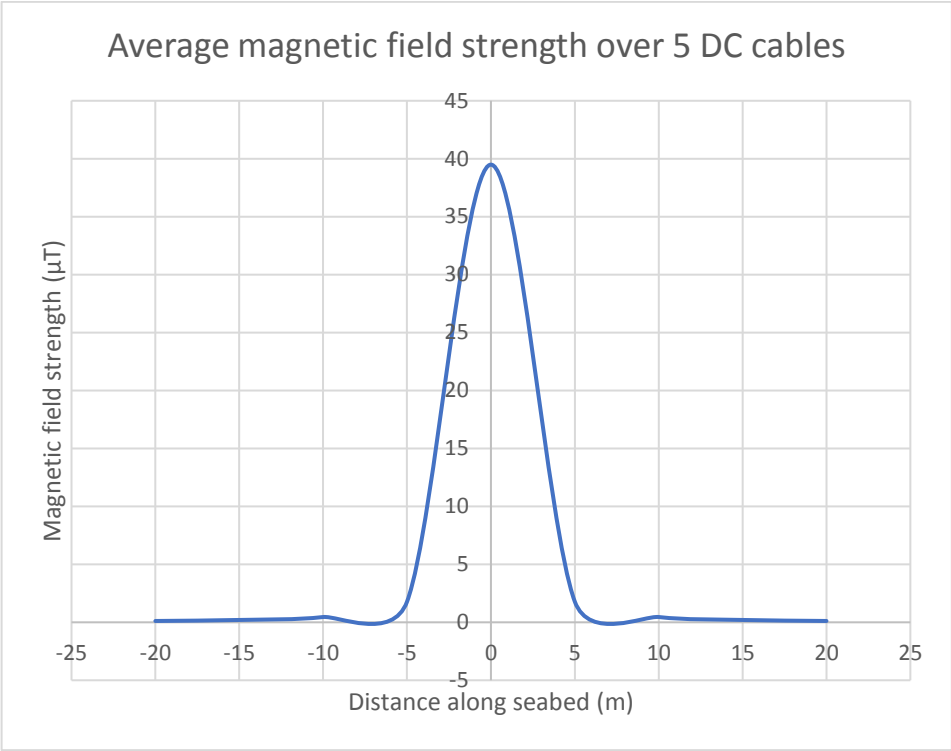

Figure 25: Case 4. Average magnetic field produced by 5 DC SPCs (without considering the influence of the geomagnetic field).

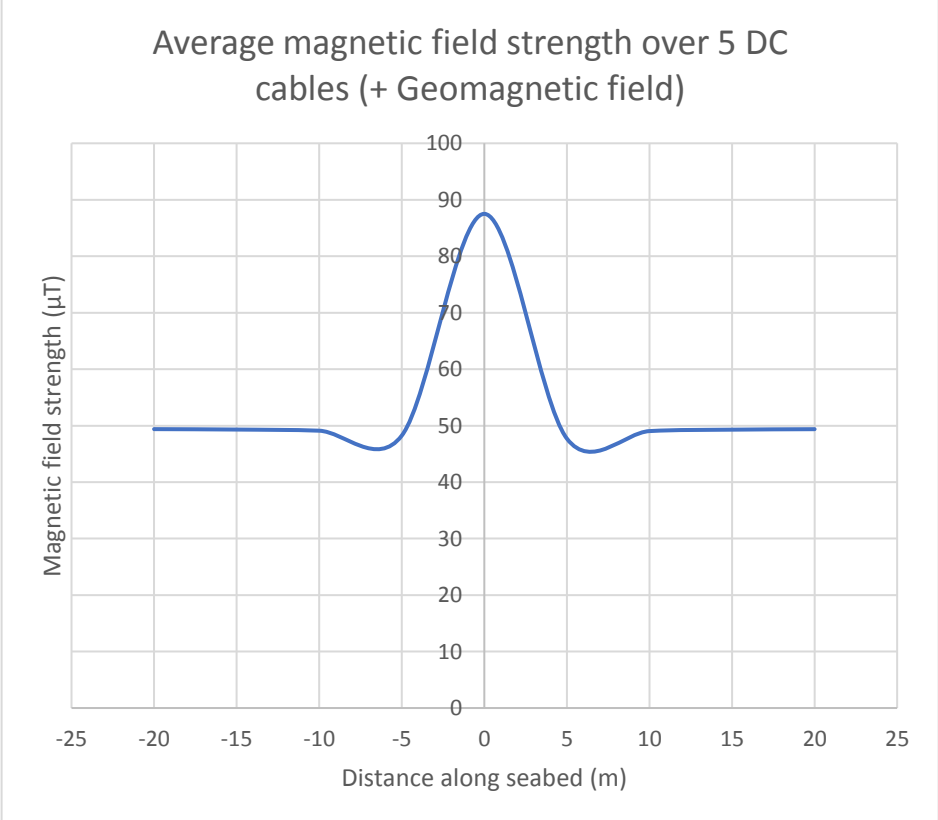

Figure 26: Case 4. Average magnetic field produced by 5 DC SPCs and the earth.

4.2.5 Case 5 (DC SPCs)

As aforementioned in Section 3.1.4, the presence of the cable in the ocean will cause the strength of the local magnetic field near the cable to deviate from the magnitude of the original geomagnetic field around that area (Tricas and Gill, 2011). For the five cables, the average geomagnetic field deviation was calculated at a location north and south of the Irish Sea (Table 6). The geomagnetic components at the northern location were described in the case above. However, at the southern location, the geomagnetic field had a total magnitude of about 49.02 μT, with a northern component of about 19.2 μT; a component pointing east with a magnitude of -0.67 μT; and a vertical component with a field strength of about 45.1 μT. The average geomagnetic deviation at the two locations is presented in Table 11. The highest deviations of 38.02 μT (northern location) and 37.84 μT (southern location) were recorded at the centerline of the cables. The values (at both locations) decreased considerably with increasing distance from the cable. The results for this scenario were tabulated in Appendix A, Table A-10 and A-11.

Table 11: The average geomagnetic deviation caused by the cables at two different locations

Distance along seabed - axis (m)	40	30	20	10	0	-10	-20	-30	-40
Deviation north of the Irish sea (μt)	-0.03	-0.05	-0.11	-0.45	38.0	-0.38	-0.10	-0.05	-0.03
Deviation south of the Irish sea (μt)	-0.03	-0.05	-0.11	-0.45	37.8	-0.38	-0.10	-0.05	-0.03

4.2.6 Case 6 (DC SPCs)

The sixth case study represents a scenario where the cables have been buried at a depth of 0.5 m and positioned at different angles. Typically, SPCs may be positioned at different angles because of various project or site constraints (i.e. the presence of pipes, other cables, rocks etc.). In this case study, the 5 DC SPCs were modelled by assuming that the cables were positioned at 0, 90 and 180 degrees. The average magnetic field profile is depicted in Figure 27.

The highest magnetic field of 67.6 μT was produced when the cables were positioned horizontally with the positive current going into the page. When the position of the cables was reversed, the maximum magnetic field decreased by about 51.3%. Likewise, the magnetic field value decreased by 29.7% when the supply conductor was positioned on the top of the receiving conductor. The results are provided in Appendix A, Table A-12, A-13, and A-14.

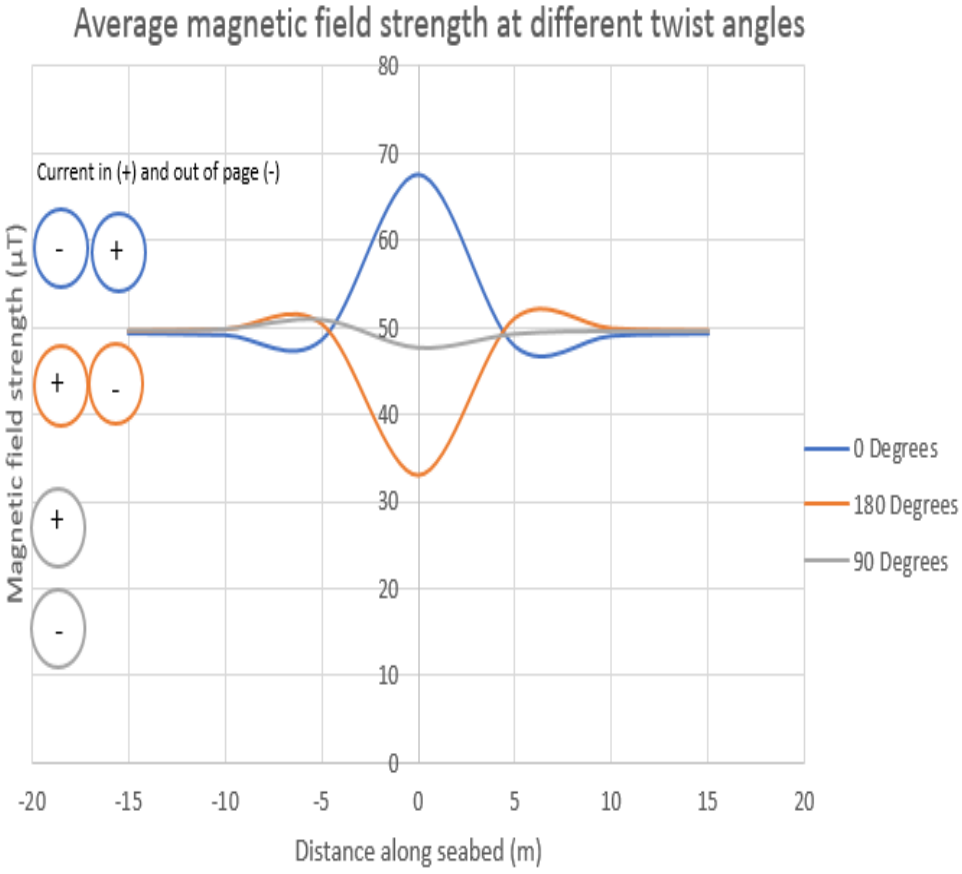

Figure 27: Case 6. Average magnetic field strength for 5 DC SPCs positioned at different angles.

4.3 Induced Electric Field Calculations

4.3.1 Case A and B (AC SPCs)

Case A describes the scenario where an induced electric field is produced over the 10 AC SPCs as a result of the alternation of the cables conductors (Figure 28). To create this model, a power frequency value of 50 Hz was assumed. Similar to the observations made in the previous cases, the maximum induced electric field was recorded at the centre of the cables (at point 0 m). The induced electric field was highest over cable J (1.5×10^{-3} V/m) and lowest over cable B (2.19×10^{-4} V/m). The 10 cables have a mean induced electric field strength of 5.3×10^{-4} V/m (Figure 29). At distances of 5 m and 15 m to either side of the cable, the average

magnetic field level diminishes to 2.03 × 10^{-5} V/m and less than 2.35 × 10^{-6} V/m. The results are tabulated in Appendix A, Table A-15 and A-16.

The second case (i.e. Case B) illustrates a scenario where a marine species crossing the 10 AC cables induces an electric field around them (Figure 30). The marine species was assumed to be travelling at a speed of 4 m/s. The magnitude of the induced field produced by the movement of the species is highest over cable J (1.94 × 10^{-5} V/m) and lowest over cable B (2.78 × 10^{-6} V/m). The cables have a mean electric field strength of 6.7 × 10^{-6} V/m (at 0 m) which fades completely at a distance of ± 10 m from the centreline of the cable (Figure 31). The results are included in appendix A, Table A-17 and A-18.

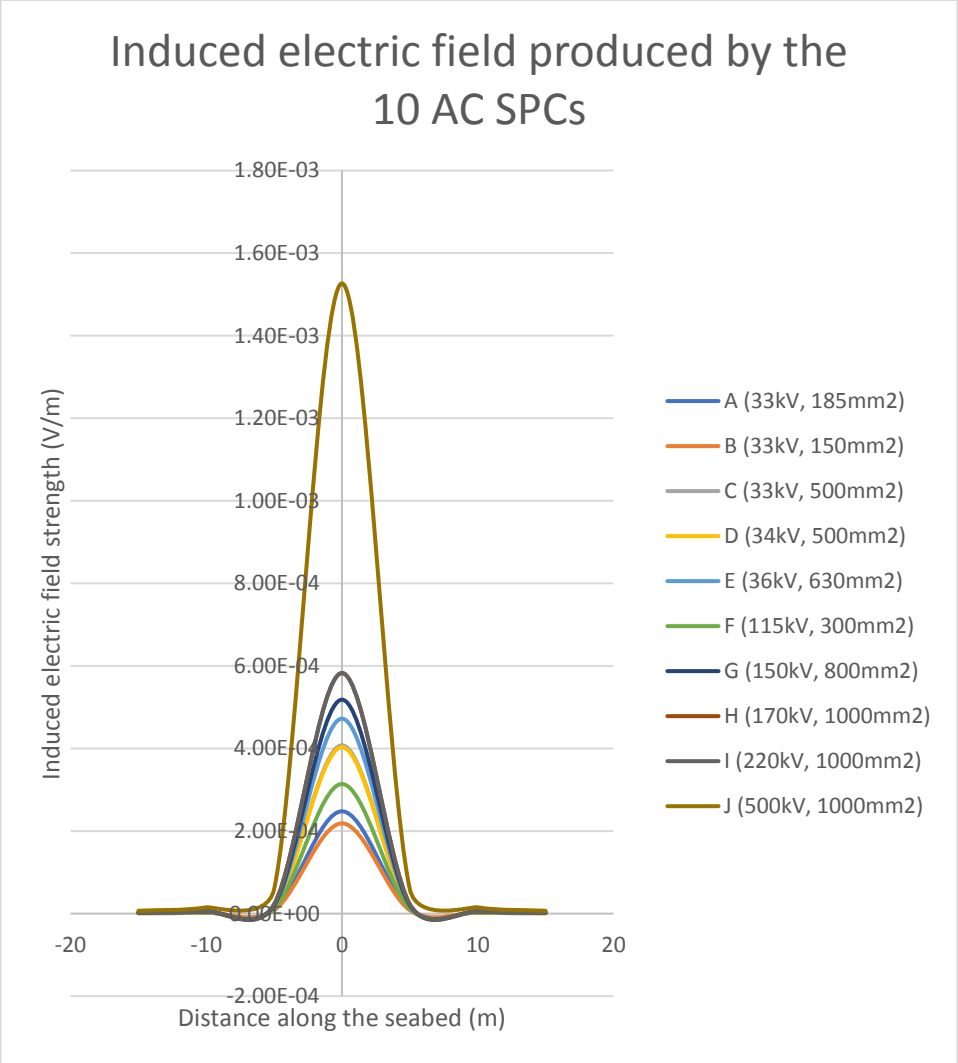

Figure 28: Case A. The induced electric field produced by the 10 AC SPCs.

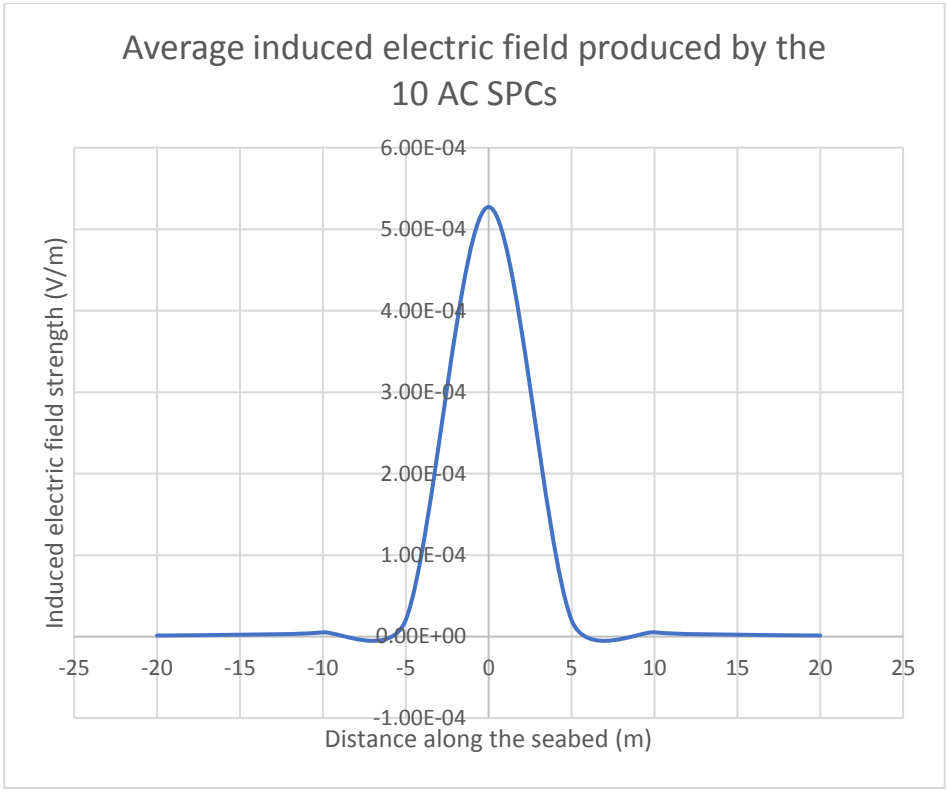

Figure 29: Case A. The average induced electric field produced by the cables.

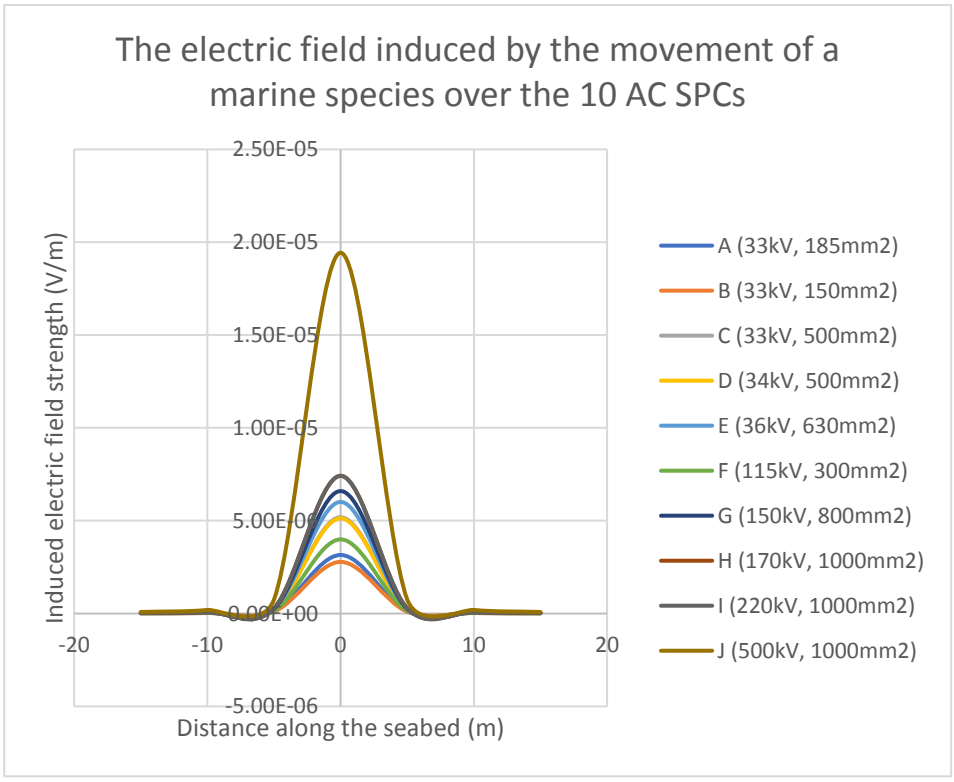

Figure 30: Case B. The electric field induced over the 10 AC cables by a marine species travelling at a speed of 4 m/s.

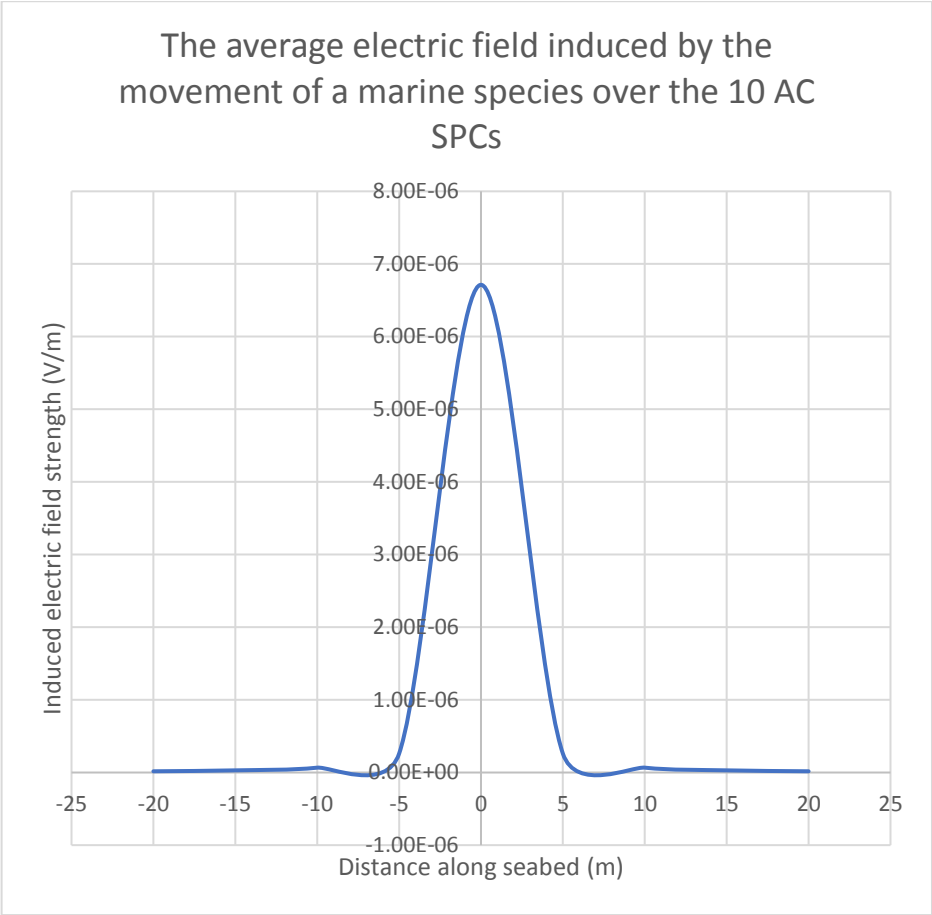

Figure 31: Case B. The average electric field induced over the 10 AC cables by a marine species travelling at a speed of 4 m/s.

4.3.2 Case C (DC SPCs)

In this case, a simulation was created to determine how the movement of a marine species in the ocean will induce electric fields around 5 DC SPCs. The cables where modelled based on the assumption that a species was traveling at a speed of 4 m/s over the cables. The order of electric field strength was as follows: cable 5 (2.30×10^{-4} V/m) > 4 (2.16×10^{-4} V/m)> 3 (1.8×10^{-4} V/m)> 2 (1.35×10^{-4} V/m)> 1 (2.87×10^{-5} V/m) (Figure 32). The species induces an average magnetic field level of 1.58×10^{-4} V/m over the cables (Figure 33). The results are tabulated in Appendix A, Table A-19.

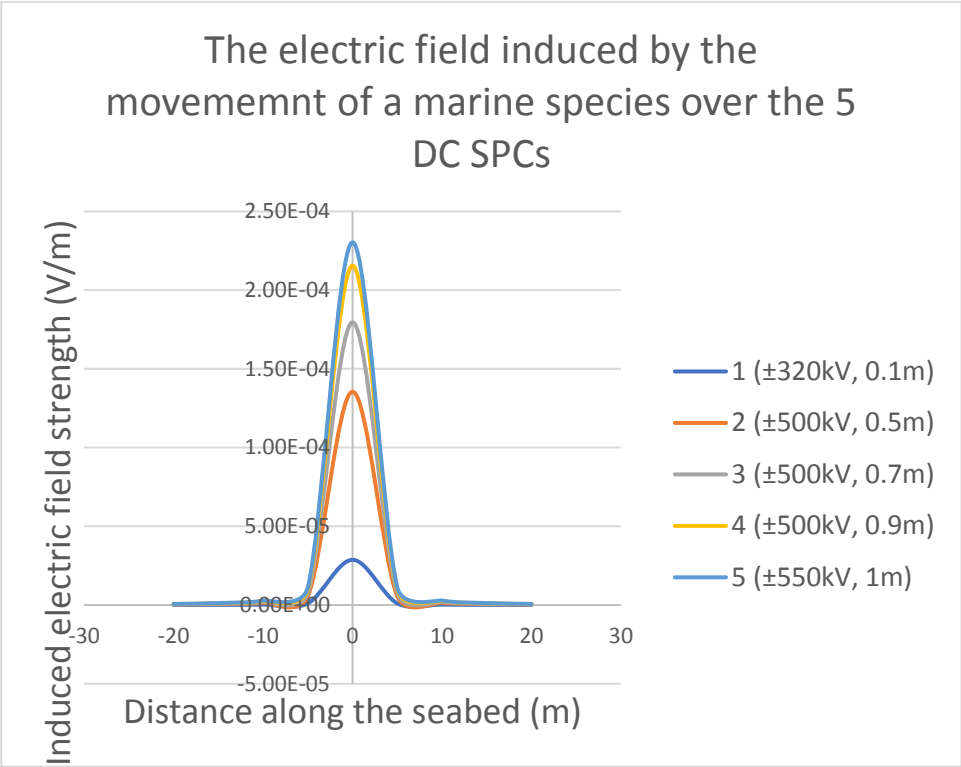

Figure 32: Case C. The electric field induced over the 5 DC cables by a marine species travelling at a speed of 4 m/s.

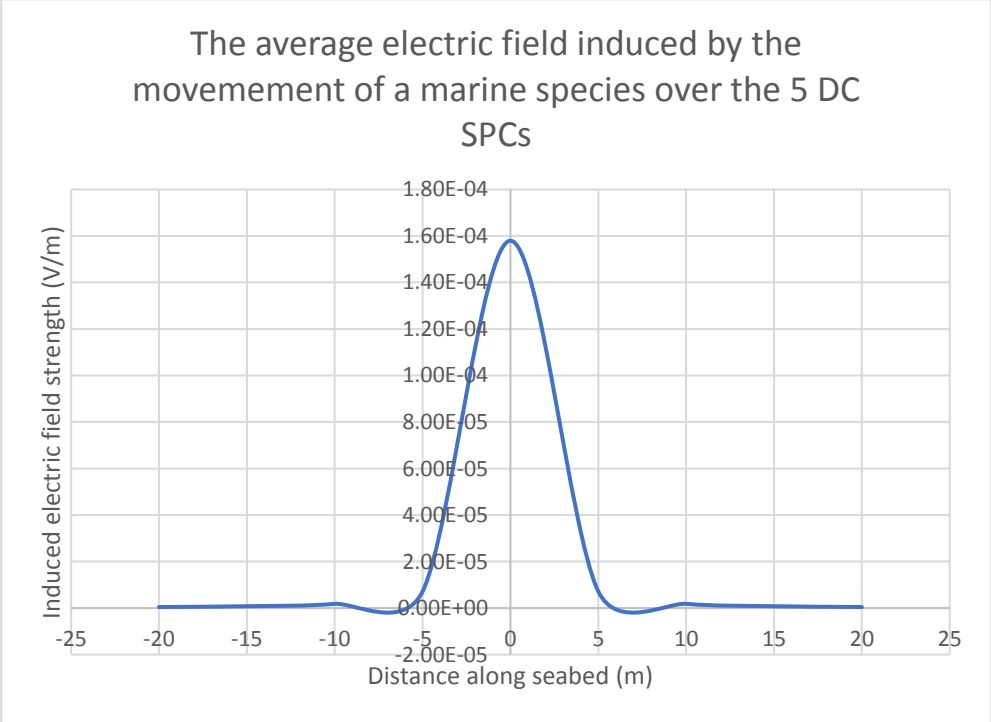

Figure 33: Case C. The average electric field induced over the 5 DC cables by a marine species travelling at a speed of 4 m/s.

4.4 Marine Species Result

4.4.1 Electro- and Magneto-sensitive Marine Species

An objective of this project was to identify priority marine species in the Irish Sea that may be sensitive to electric and/or magnetic fields. Through a comprehensive literature search, 26 Irish marine species were found to possess electromagnetic sensory abilities (Table 12). From the 26 species, 7 are mammals (2 dolphins and 5 turtles), 13 are elasmobranchs (8 sharks, 2 rays and 3 skates), and 6 are fishes. Out of the 26 species, 30% (8 species) can detect magnetic fields, whilst 19.2% (5 species) have electro sensory capabilities. Conversely, 58% of the species are able to detect both magnetic and electric fields. On average, the magneto-sensitive species have sensory thresholds varying between 12.6 nT to 7400 μT, whereas electrosensitive species are able to detect between <1 nV/cm and 2 μV/cm. The refined list can be found in Appendix B, Table B-1.

Table 12: Electro (EF) and magneto (MF) sensitive species in the Irish Sea.

Main Group	Subgroup	Ordinary Name	Taxon Name	Mf/Ef Exposure Threshold	Proof	Citation
Mammals	Dolphin	Bottle-nose Dolphin	Tursiop truncatus	1a)N/A (MF) 1b) 0.05 µT (GM)	1)Quicker behavioural response to magnetic cues 1b) Evidence of Geomagnetic field perception	(Kremers et al., 2014) (Kuznetsov et al., 1990)
Mammals	Dolphin	Common Dolphin	Delphinus delphis	1a)N/A (MF) 1b) 0.05 µT (GM)	1a) Magnetite found in skull. 1b) Evidence of Geomagnetic field perception.	(Zoeger et al., 1981; Kirschvink 1990)
Reptiles	Turtles	Leatherback	Dermochelys coriacea	1)N/A (GM)	1)An experimental study provides evidence of geomagnetic field perception in the absence of light	(Lohmann and Lohmann 1993)
Reptiles	Turtles	Loggerhead	Caretta caretta	1a)0.005 TO 7400 µT (MF and GM)	1)Proven in the lab by exposing them to pulsed fields.	(Tricas and Gill, 2011)

Main Group	Subgroup	Ordinary Name	Taxon Name	Mf/Ef Exposure Threshold	Proof	Citation
Reptiles	Turtles	Hawksbill	Eretmochelys imbricata	1)0.005 TO 7400 µT (MF and GM)	No direct study has been carried out on the Eretmochelys imbricata. Hence, its sensory values have been assumed to fall within the same range as that of the Caretta caretta	
Reptiles	Turtles	Kemp' s Ridley	Lepidochelys kempii	1)v0.005 TO 7400 µT (MF and GM)	Same as the above.	
Reptiles	Turtles	Green Turtle	1Chelonia mydas	1) 45-49 µT (MF) 1b)N/A (GM)	1a) An artificial arena was setup to monitor its orientation. 2)Evidence of Geomagnetic field	(Lohmann et al., 2004)
Elasmobranch	Sharks	Spurdog	Squalus acanthias	1) N/A (MF) 2) <1 nV /cm (EF)	1)Magnetic field perception suggested by Gill 2)Proof of response to weak electric field	(Gill et al., 2005) (Jordan et al., 2011)

Main Group	Subgroup	Ordinary Name	Taxon Name	Mf/Ef Exposure Threshold	Proof	Citation
Elasmobranch	Sharks	Tope	Galeorhinus galeu	1)N/A (MF) 2) 0.005 -0.01 µV/cm (0.0005-0.001 mV/m) (EF)	1) Magnetic field perception suggested by Gill 2)Proof of EF suggested by Tricas and Gill. No direct study has been carried out on Galeorhinus galeus, hence it is assumed to have the same sensory value as Mustelus canis.	(Gill et al., 2005)
Elasmobranch	Sharks	Nurse hound or large-spotted dogfish	Scyliorhinus stellaris	1)N/A (MF)	Magnetic field sensitivity suggested by Gill	(Gill et al., 2005)
Elasmobranch	Sharks	Portuguese dogfish	Centroscymnus coelolepis	N/A (EF)	Proof of electric field perception suggested by Tricas and Gill	(Tricas and Gill, 2011)
Elasmobranch	Sharks	Basking shark	Cetorhinus maximus	1)N/A (MF) 2)N/A (EF)	1)Magnetic field perception suggested by Gill 2) The inclination of its electro sensory pores makes it possible to catch its preys	(Gill et al., 2005) (Kempster and Collin, 2011)

Main Group	Subgroup	Ordinary Name	Taxon Name	Mf/Ef Exposure Threshold	Proof	Citation
Elasmobranch	Sharks	Small-spotted catshark	Scyliorhinus canicula	1)N/A (MF) 2a) 0.01 µV/cm (0.001 mV/m) (EF) 2b)N/A (EF)	1)Evident changes in its behavioural pattern 2a) Its response to feeding 2b) The ampullae were sensitive to electric currents when subjected to certain temperatures	(Gill et al., 2009) (Kalmijin 1971; Bromm et al., 1975)
Elasmobranch	Sharks	Porbeagle shark	Lamna nasus	2 µV/cm (EF)	1)Electric field perception suggested by Tricas and Gill 2)No direct study has been carried out on Lamna nasus, hence its assumed to have the same sensory range as Cephaloscyllium isabellum.	(Tricas and Gill, 2011)
Elasmobranch	Sharks	Common smooth-hound	Mustelus mustelus	N/A (EF)	Electric field perception suggested by Tricas and Gill	(Tricas and Gill, 2011)
Elasmobranch	Rays	Thornback ray	Raja clavata	1) 0.35 G 2) (35µT) (MF) 2) 0.01 µV/cm (0.001 mV/m) (EF)	1) Response in the nervous system 2) Its electrical response to feeding	(Brown and Ilyinsky, 1978) (Kalmijin, 1971)

Main Group	Subgroup	Ordinary Name	Taxon Name	Mf/Ef Exposure Threshold	Proof	Citation
Elasmobranch	Skate	Longnose skate	Dipturus oxyrinchus	1)N/A (MF)	1) Magnetic field perception suggested by Gill	(Gill et al., 2005)
Elasmobranch	Ray	Undulate ray	Raja undulata	1)N/A (MF)	1) Magnetic field perception suggested by Gill	(Gill et al., 2005)
				2)N/A (EF)	2) Electric field perception suggested by Gill	(Gill et al., 2005)
Elasmobranch	Skate	white skate	Rostroraja alba	1)N/A (MF)	1) Magnetic field perception suggested by Gill	(Gill et al., 2005)
				2)N/A (EF)	2) Electric field perception suggested by Gill	(Gill et al., 2005)
Elasmobranch	Skate	Common (blue) Skate	Dipturus batis	1)N/A (MF)	1) Magnetic field perception suggested by Gill	(Gill et al., 2005)
				2) N/A (EF)	2) Electric field perception suggested by Gill	(Gill et al., 2005)

Main Group	Subgroup	Ordinary Name	Taxon Name	Mf/Ef Exposure Threshold	Proof	Citation
Ocean fishes	Fish	Pollock	Pollachius virens	0.3 mV/cm (30 mV/m) ((EF)	No direct study has been carried out on the Pollachius virens. Hence, its sensory values have been assumed to fall within the same range as that of the Gadua morhua.	(Tricas and Gill, 2011)
Ocean fishes	Fish	Brown trout	Salmo trutta	1)0.15 – 4.2 mT (150-4200 µT) (MF)	1) Their mode of attraction using the magnetite in their skull	(Formicki et al., 2004)
Ocean fishes	Fish	European seabass	Dicentrarchus labrax	1)N/A (MF)	1) Traces of magnetite found in the skull of the sea bass.	(Tanski et al., 2011)
Ocean fishes	Fish	Atlantic cod	Gadus morhua	1a)0.3 mV/cm (30 mV/m) (EF) 1b)2 µV/cm (200 mV/m) (EF)	1a) N/A 1b)Their behavioural conduct	(Bullock and Fessard, 1974) (Gill et al., 2005)

Main Group	Subgroup	Ordinary Name	Taxon Name	Mf/Ef Exposure Threshold	Proof	Citation
Ocean fishes	Fish	European plaice	Pleuronectes platessa	1)N/A (GM)	1) an experimental study of its orientation provided evidence of a geomagnetic perception	(Metcalfe et al., 1993)
				2)N/A (EF)	2) Proof of electric field perception suggested By Gill	(Gill et al., 2005)
Ocean fishes	Fish	European eel	Anguilla anguilla	1a)12.63 to 192.4 nT (0.0126-0.192 μT) (MF)	1a) Experimental study conducted provided evidence of magnetic field sensitivity. In addition, no GF value has been recorded, hence Anguilla anguailla is assumed to fall within the same GF threshold as the Anguilla japonica.	(Formicki et al., 2004)
				1b) N/A (MF)	1b) behavioural orientation	(Tesch 1974; Enger et al., 1976)
				2)N/A (EF)	2)Experimental study of the species heartrate provides proof of electroreception.	

4.5 Heavy Metals Results

4.5.1 The Concentration of Heavy Metals in the Seawater Samples

The results of the analysis of the HMs reveal varying concentrations of the selected HMs that are higher than the control values, and their regulatory limits (in some cases). The results are provided in Table 13 and Figures 34 (a) to (i).

Table 13: The results of the heavy metals analysis for the 6 month and 1-year submersion (ECE, 1998; USEPA, 2011; WHO; 2011).

Metals	Background Concentration (µg/l)	New Cable (µg/l)	12 Days (µg/l)	15 Years (µg/l)	34 Years (µg/l)	WHO	USEPA	ECE
Al_{1year}	10	96.4	2140	130	47.4	-	-	-
Al_{6mnth}		52.9	67.5	36.6	16.5			
Cd_{1year}	0.1	0.2	34.1	0.5	0.2	30	50	50
Cd_{6mnth}		0.4	91.8	0.7	0.4			
Cu_{1year}	4	27.8	6.8	449	130	2000	1300	2000
Cu_{6mnth}		47.9	47.9	97.8	105			
Fe_{1year}	7.2	45.9	587	174	269	300	300	200
Fe_{6mnth}		57.9	16.7	192	7.2			
Pb_{1year}	1.7	3	5240	1.7	2.1	10	15	10
Pb_{6mnth}		1.7	223	3.5	1.7			
Mn_{1year}	0.7	391	96.2	238	36.7	100	50	50

Mn_{6mnth}		143	23.7	180	216			
Ni_{1year}	0.2	3	9.9	2.3	2.3	70	700	70
Ni_{6mnth}		5.2	20	5.8	5.3			
Hg_{1year}	0.05	3	0.05	0.65	2	6	6	-
Hg_{6mnth}		0.2	0.05	0.05	1			
As_{1year}	0.05	0.05	3	2	0.05	10	10	10
As_{6mnth}		1	2	1	0.05			

For each sample containing emissions from a cable (i.e. New, 12 days, 15 years, and 34 years), the concentration of Al appears to increase between six months and one year. The highest concentration of Al was recorded in the 12 days sample (2140 µg/l), and the lowest in the 34 years sample (47.4 µg/l).

Unlike Al, the concentration of Cd in all the samples appears to reduce between 6 months and one year. In the first six months, the 12 days cable released the highest concentration of Cd (91.80 µg/l). However, the value got reduced by more than half after the next six months. Similar observations were noted after measuring the concentration of Ni in all samples.

Overall, the concentration of Cu ranges from 47.9-105 µg/l and 6.80-449.00 µg/l at six months and one year, respectively. The highest concentration of Cu was emitted by the 15 (449 µg/l) and 34 (130 µg/l) years SPCs between six months and one year. On the other hand, the concentration of Cu decreased over time in other examined samples. A similar variation was observed for Fe. The mean concentration of Pb, As, and Hg increases over time in all samples. In the cases where the

concentrations are below the instrument's detection limit, the limit of detection was used.

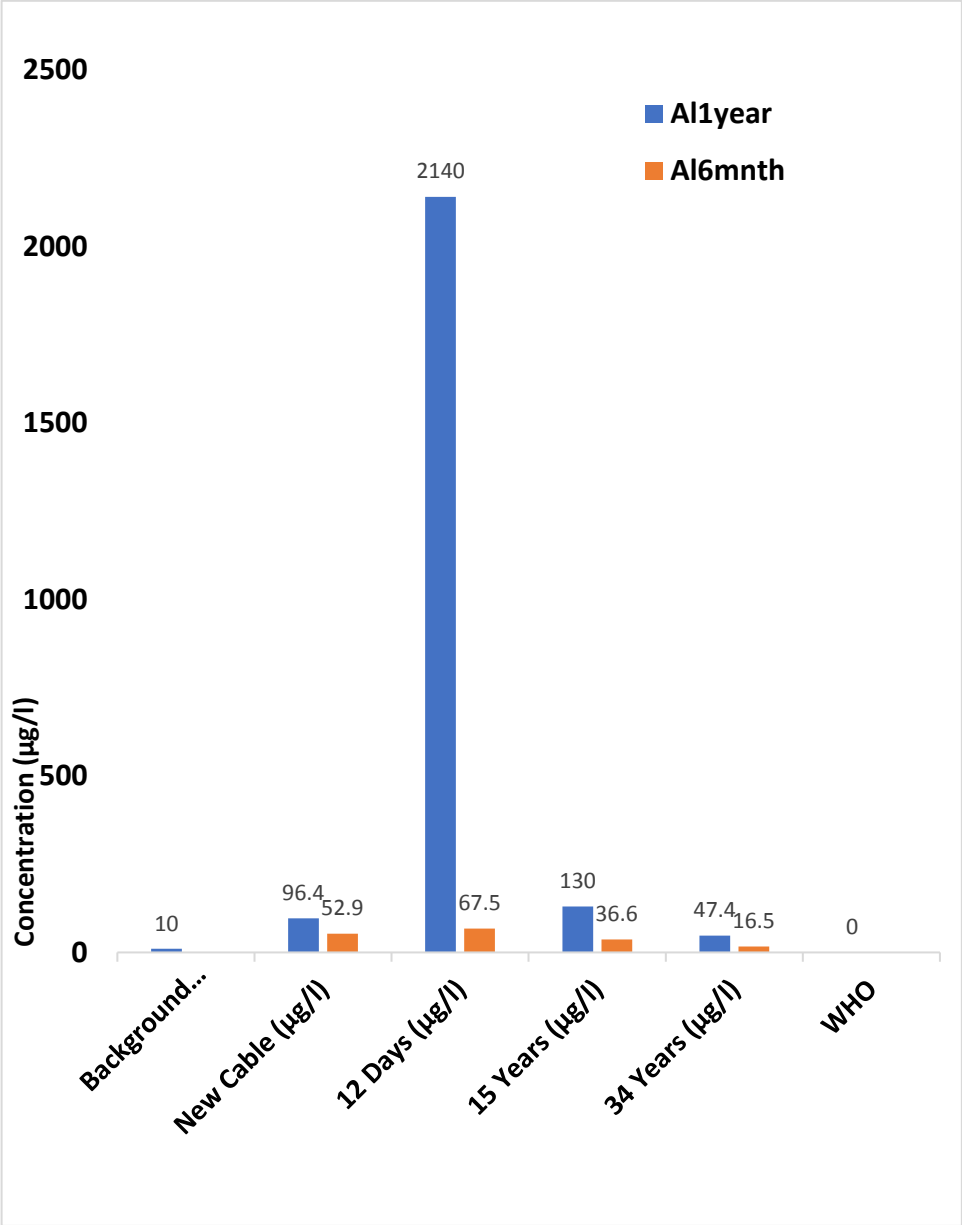

Figure 34a: The concentration of Aluminum (Al) in the samples.

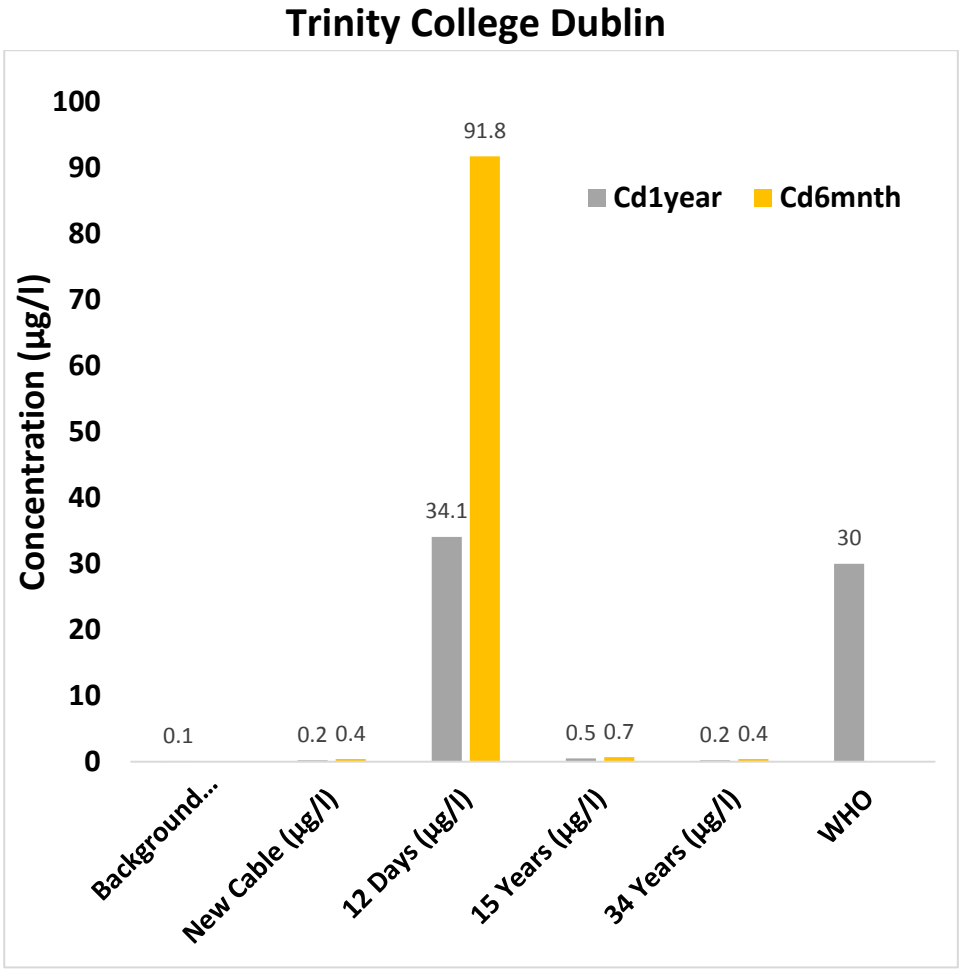

Figure 34b: The concentration of Cadmium (Cd) in the samples.

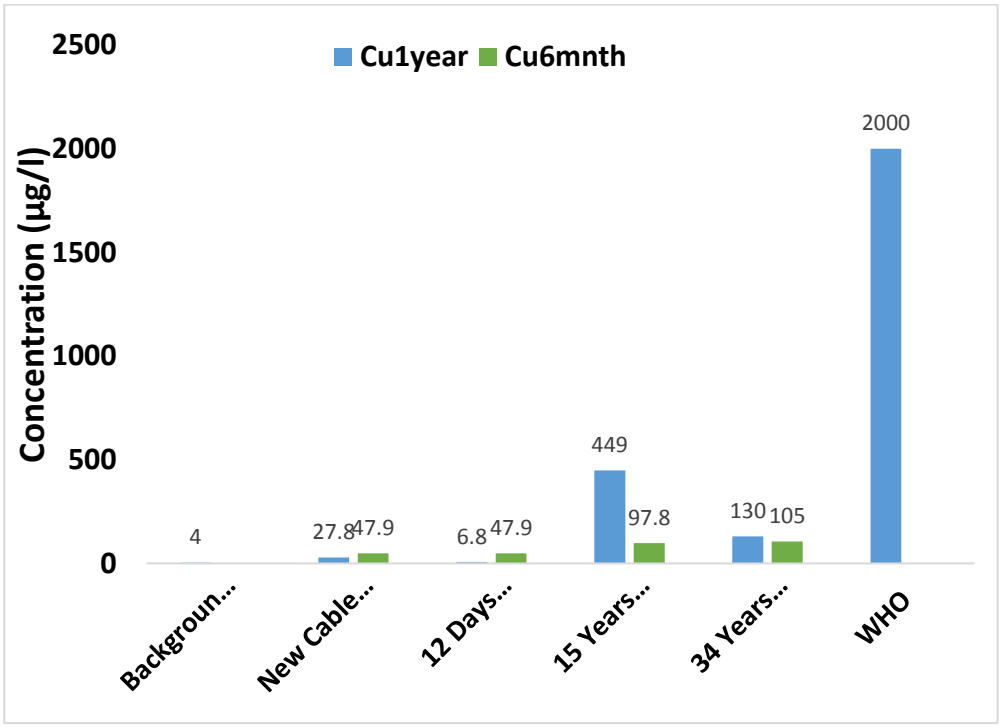

Figure 34c: The concentration of Copper (Cu) in the samples.

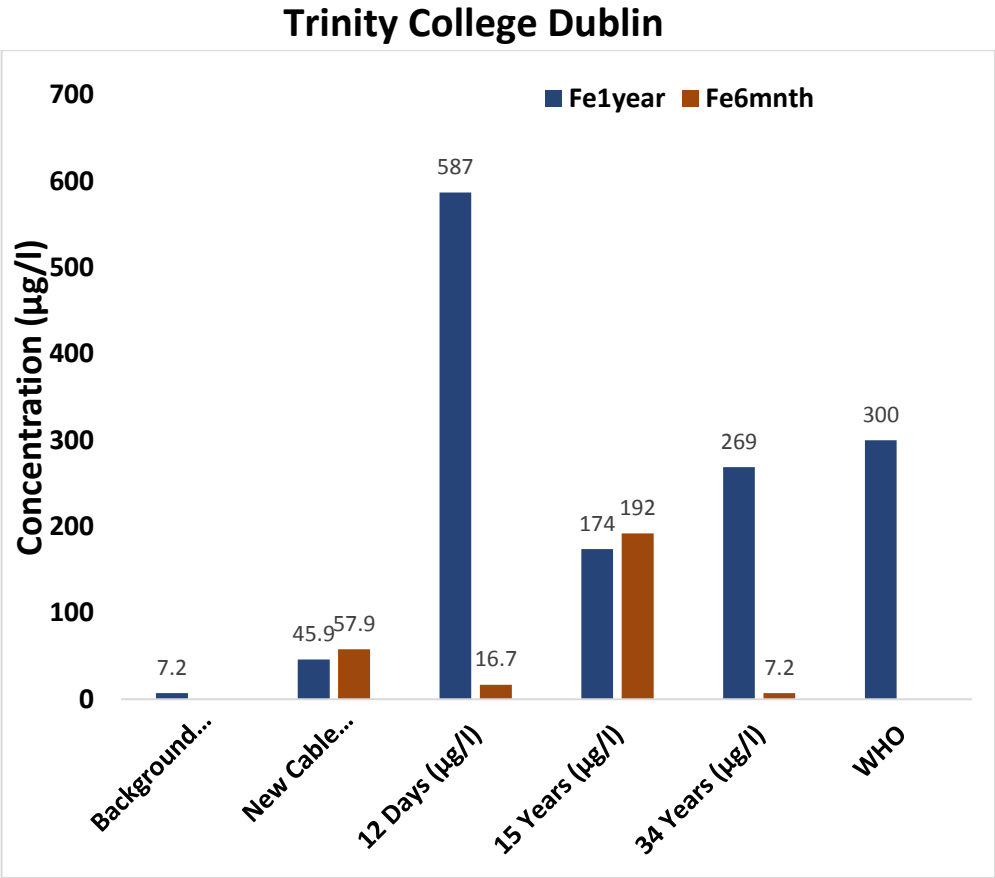

Figure 34d: The concentration of Iron (Fe) in the samples.

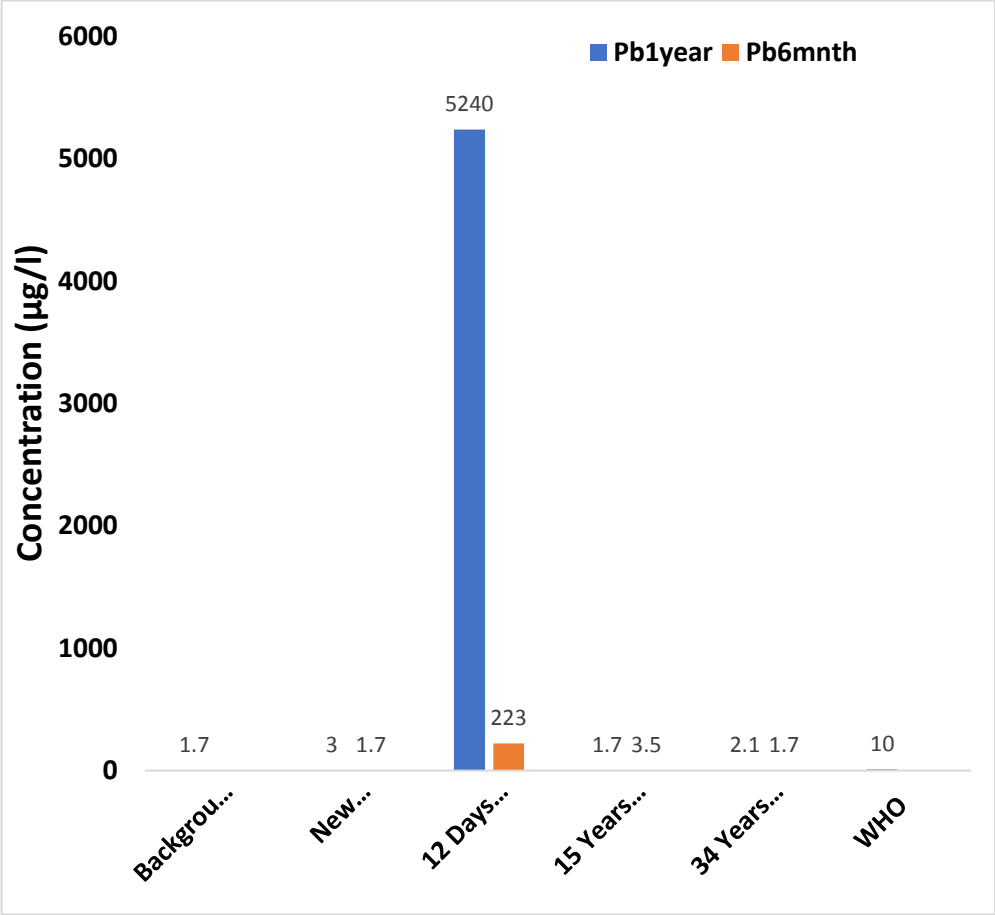

Figure 34e: The concentration of Lead (Pb) in the samples.

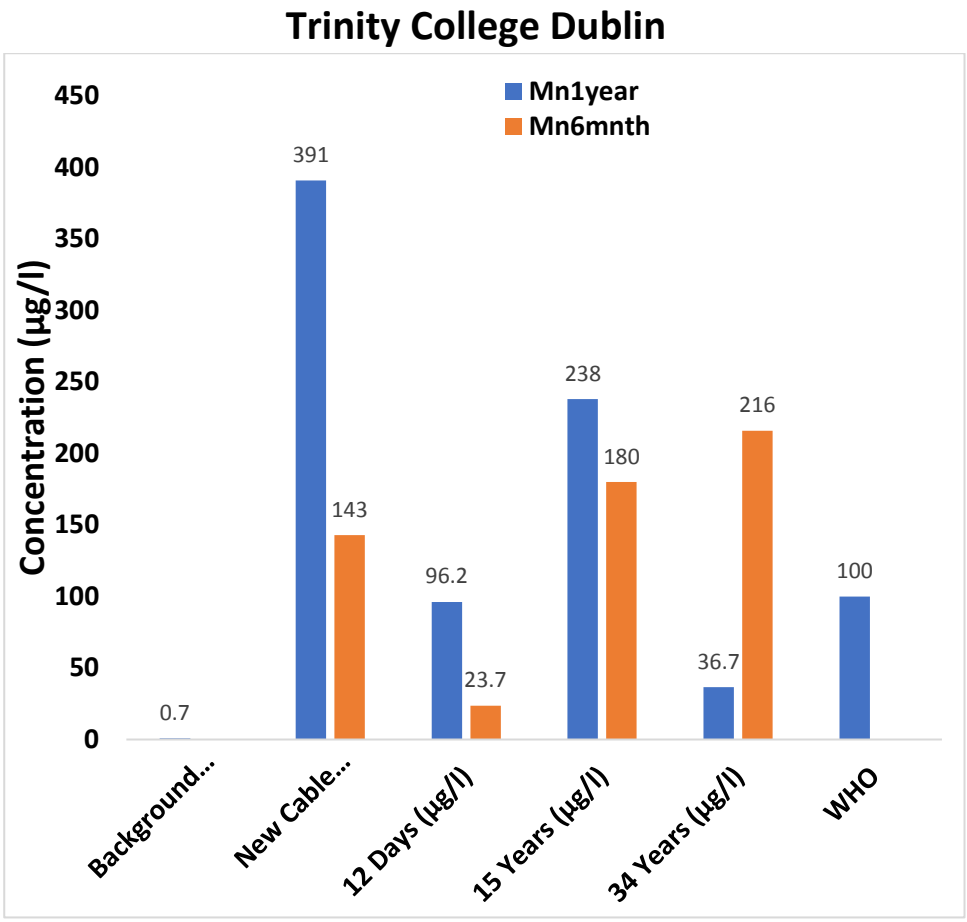

Figure 34f: The concentration of Manganese (Mn) in the samples.

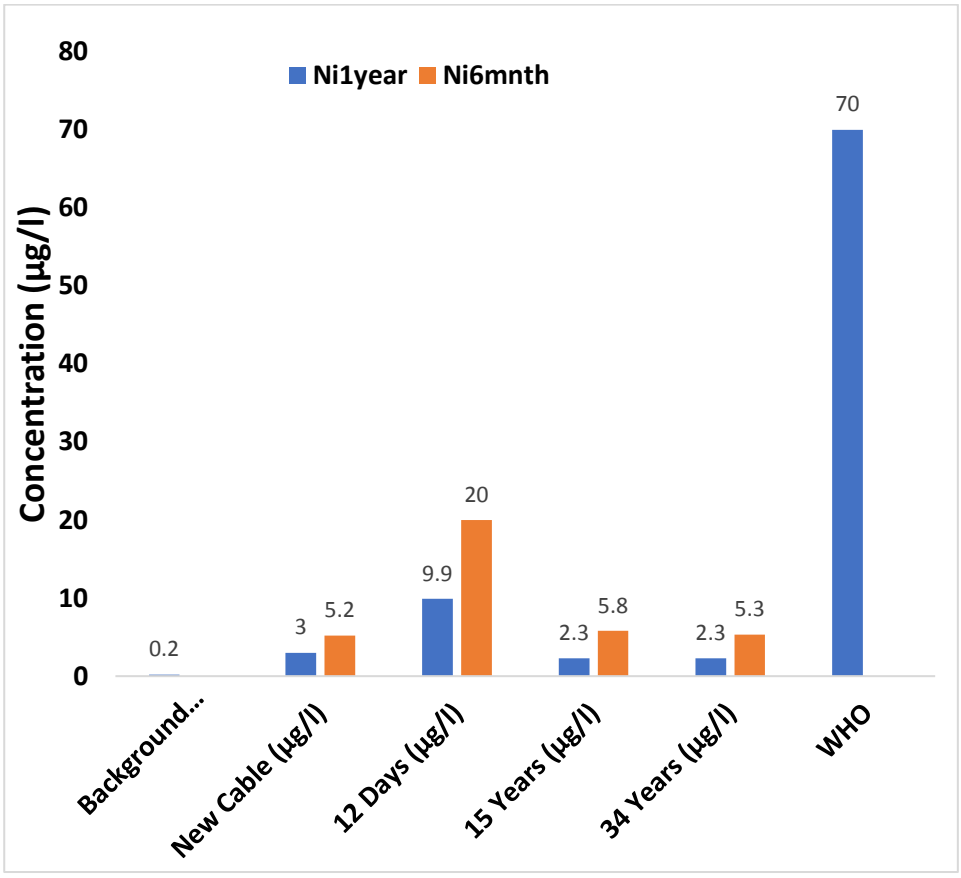

Figure 34g: The concentration of Nickel (Ni) in the samples.

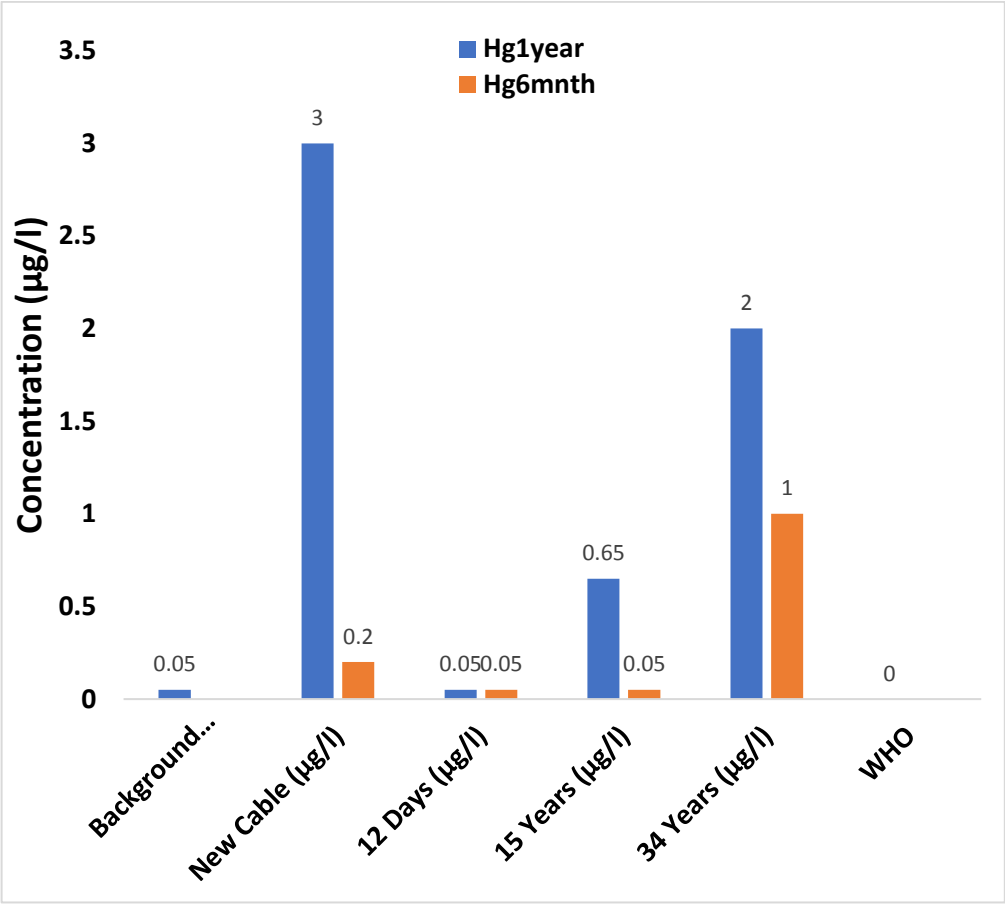

Figure 34h: The concentration of Mercury (Hg) in the samples.

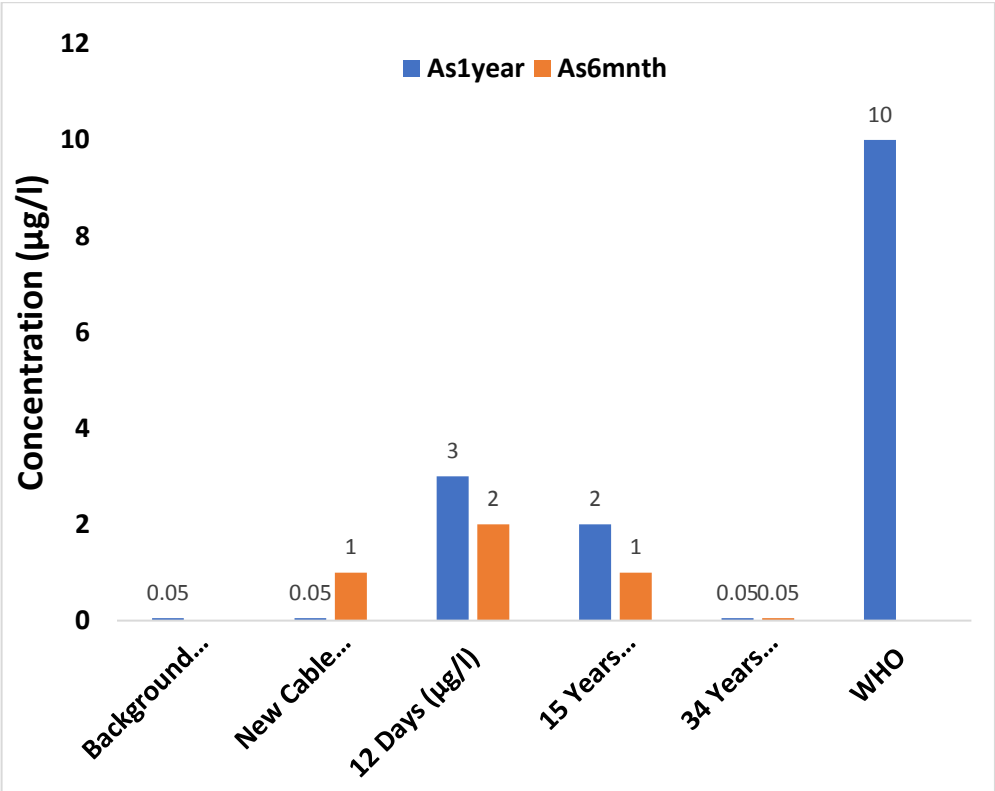

Figure 34i: The concentration of Arsenic (As) in the samples (i)

4.5.2 Individual Cable Contribution to Heavy Metal Pollution Potential

The results of the consequential adjustment with respect to the cable's cross-sectional area and 8 litres of seawater (i.e. the volume of water in the bucket) are presented in Tables 14 and 15. The variation of the HM concentrations per unit cross-sectional area (µg/cm^2) follows a similar pattern as the original results (µg/l) reported in Table 13. For instance, the concentration of Al appears to increase between six months and one year. During the first phase of submersion (6 months), the 12 days cable released 0.803 µg/cm^2 of Al and 29.757 µg/cm^2 of Al in the second phase (1 year).

Table 14: Amount of copper released per cross-sectional area of the subsea power cable submerged for 6 months.

Cables	Cu	Al	Cd	Fe	Pb	Mn	Ni	Hg	As
					$(\mu g/cm^2)$				
New Cable	4.06	3.96	0.03	4.68	0	13.15	0.46	0.01	0.09
12 Days	0.61	0.80	1.28	0.13	3.09	0.32	0.28	0	0.03
15 Years	7.90	2.24	0.05	15.56	0.15	15.09	0.47	0	0.08
34 Years	12.7	0.82	0.04	0	0	27.07	0.64	0.12	0

Table 15: Number of heavy metals released per cross-sectional area of the subsea power cables submerged for 1 year.

Cables	Cu	Al	Cd	Fe	Pb	Mn	Ni	Hg	As
	$(\mu g/cm^2)$								
New Cable	2.20	7.98	0.01	3.58	0.12	36.06	0.26	0.27	0
12 Days	0.04	29.76	0.48	8.1	73.18	1.33	0.14	0	0.04
15 Years	37.46	10.1	0.03	14.04	0	19.97	0.18	0.05	0.16
34 Years	15.84	4.70	0.01	32.92	0.05	4.53	0.26	0.25	0

4.6 Microplastics Results

4.6.1 Microplastics Released by SPCs

After burying the cables (i.e. 0 days, 12 days, 15 years, and 34 years) in the buckets for a year without any interference, seawater samples (20 ml) were filtered and observed under the microscope for the presence of MPs. The images obtained under the microscope are presented in Figures 35(a)-35(d). Following the optical microscopic analysis, three particles were found in the new sample (Figure 35a). On the other hand, one particle was identified in the 34 years sample (Figure 35d). The particles were confirmed using the micro-Raman spectrometer, and the results show that they were not MPs. The particles may be sediments from the seawater. MPs were also not found in the 12 days and 15 years samples. The results suggest that the cables did not emit or release MPs into the seawater for a year during static experimental conditions. A summary of the results following confirmatory analysis is presented in Table 16.

Table 16: Quantity of MPs found during the static experiment.

	Age of cable			
	0 Days	**12 Days**	**15 Years**	**34 Years**
No of MPs	0	0	0	0

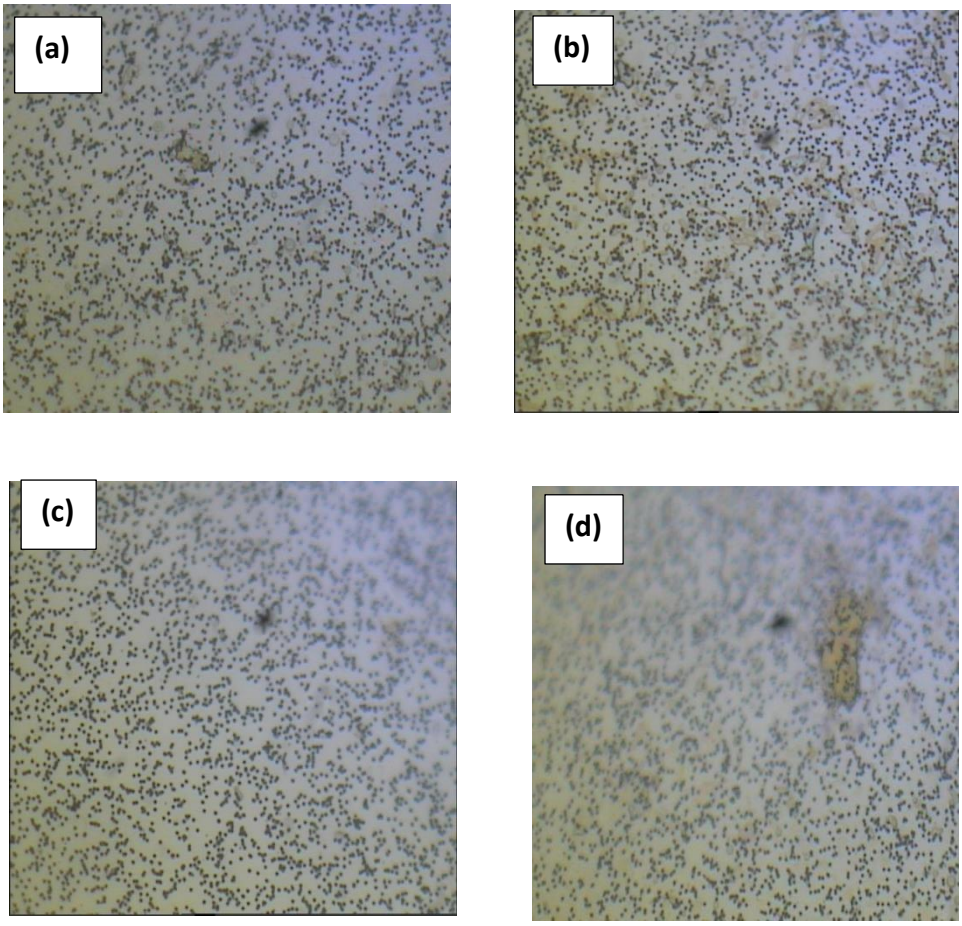

Figure 35: Images obtained under a microscope during the static experiment: (a) 0 days sample, (b) 12 days sample, (c) 15 years sample, and (d) 34 years sample.

In the dynamic experiment, cable fibers (7 cm) were cut and placed into glass bottles containing deionized water. The bottles were then vibrated by a shaker (at 250 RPM) for 15, 45, and 90 minutes, respectively. After filtering and counting, two particles were found in the new sample (45 minutes). Also, one particle was identified in the 12 days sample (45 minutes). The images obtained under the microscope for the different samples are presented in Figures 36 to 39.

(a) 15 mins (b) 45 mins (c) 90 mins

Figure 36: Images obtained under a microscope during the dynamic experiment (0 days sample): (a) 15 mins, (b) 45 mins, and (c) 90 mins.

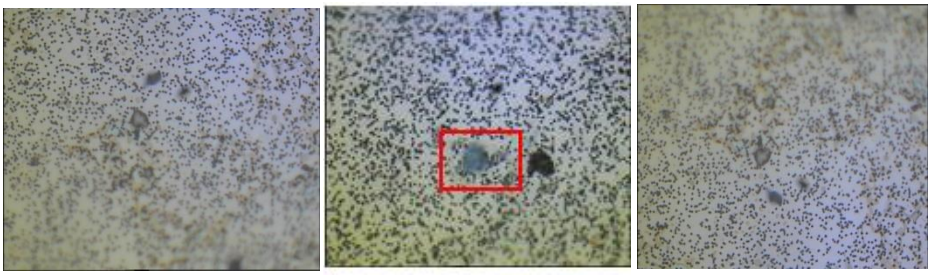

(a) 15 mins (b) 45 mins (c) 90 mins

Figure 37: Images obtained under a microscope during the dynamic experiment (12 days sample): (a) 15 mins, (b) 45 mins, and (c) 90 mins.

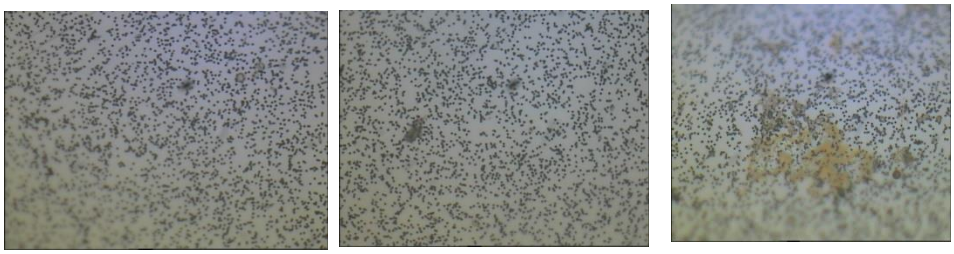

(a) 15 mins (b) 45 mins (c) 90 mins

Figure 38: Images obtained under a microscope during the dynamic experiment (15 years sample): (a) 15 mins, (b) 45 mins, and (c) 90 mins.

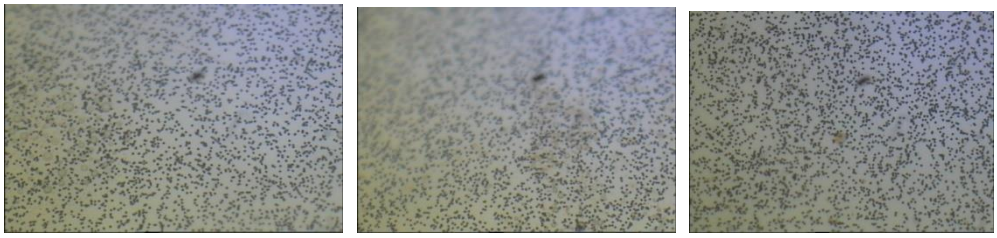

(a) 15 mins **(b) 45 mins** **(c) 90mins**

Figure 39: Images obtained under a microscope during the dynamic experiment (34 years sample): (a) 15 mins, (b) 45 mins, and (c) 90 mins.

The identified particles were confirmed following micro-Raman analysis presented in Figure 40. The spectra obtained were compared with standard ranges from the Infrared and Raman User Group (IRUG) database (Reference no: RSR00021), which confirmed that the particles were made of polypropylene (PP) with > 90 % similarity. No other MP particles were found in the various samples (Table 17). Lastly, the size of the detected MPs ranged between 7.53 and 13.72 µm.

Table 17: Quantity of MPs found during the dynamic experiment.

Duration	Size (µm)	Age of cable				
		0 Days	12 Days	15 Years	34 Years	Total
		No of MPs				
15 mins		0	0	0	0	0
	7.53 to 13.72					
45 mins		2 (PP)	1 (PP)	0	0	3
90 mins		0	0	0	0	0
Total		2	1	0	0	0

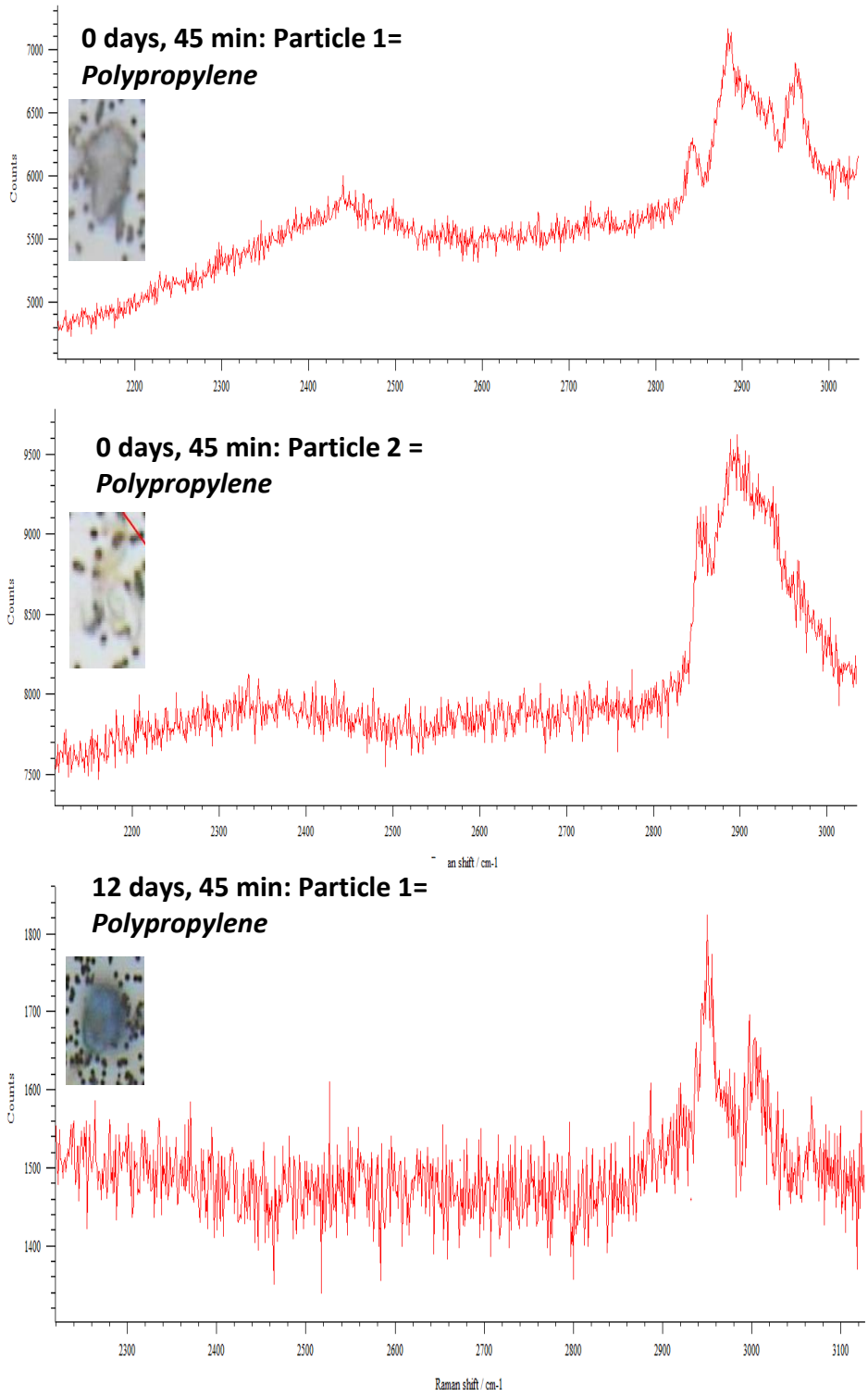

Figure 40: Micro-Raman spectra for identified particles. Particles were made up of polypropylene (PP).

4.6.2 Polymer Risks Assessment

The results of the assessment of the polymeric risks are presented in Figure 41. Accordingly, H_i is classified as low when the MPs are less than 150, medium when they fall between 150 to 300, and high when they exceed 600 (Kabir et al., 2021; Enyoh et al., 2021). Overall, the cables had a polymer risk index value of less than 1.

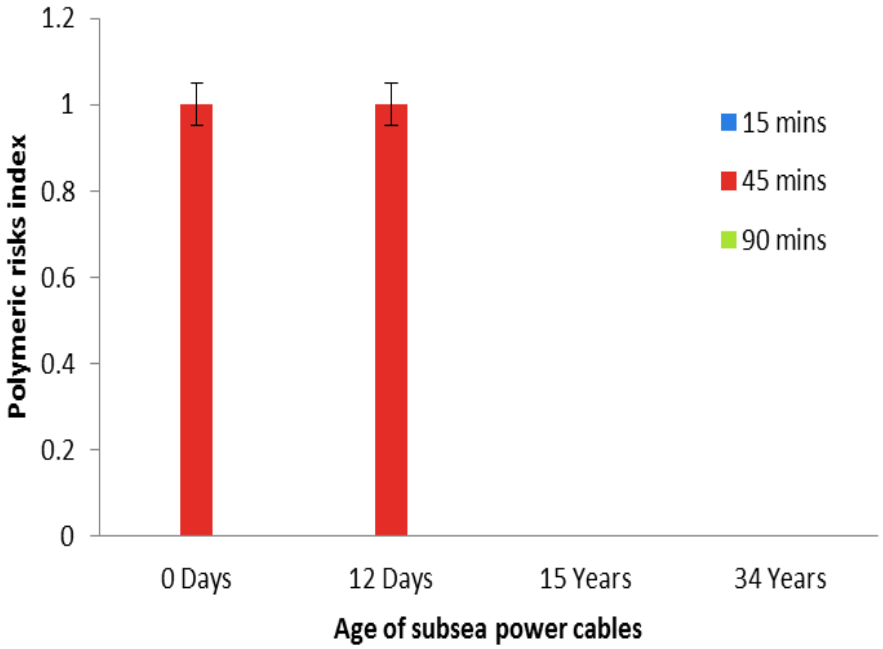

Figure 41: MP polymer risk index (error bars indicates 5 % standard error).

Discussion

5.0 Discussion

5.1 EMF Discussion

5.1.1 EMFs emitted by SPCs

An operational offshore wind turbine generates energy, transported from one point to another, using SPCs. These cables have been found to either temporarily or permanently affect marine life by causing changes in artificial reef effects, noise, heat, chemical and EMF emissions (Petersen and Malm, 2006; Taormina et al., 2018). However, EMF emissions are considered a significant concern compared to other environmental incidences (Taormina et al., 2020). This is because EMFs may alter or mask natural electric and magnetic cues, affecting various ecological processes in marine species such as homing, predation, feeding migrations or spawning, and the ability to detect sexual mates (Tricas and Gill, 2011).

For this reason, it has become pertinent to determine the magnitude and characteristics of EMFs that may be produced by current and potential future SPCs to mitigate the negative impact that cables may have on the wellbeing of marine species. In the first phase of this project, the EMF profiles of 10 AC (3 phase system) SPCs were modelled based on various real-world scenarios. Nine are fully operational among the ten AC cables studied here, while the tenth cable is expected to be commissioned by 2022.

The AC cables have different design configurations in terms of their voltage (i.e. 33 kV to 500 kV) and current carrying capacity. For example, the cables possess different nominal cross-sectional areas ranging between 150 and 1000 mm^2. The EMF strength for each AC cable was

calculated independently by applying Biot-Savart and Lorentz's law. An increase in amperage led to an increase in the strength of the field by the same magnitude because the magnetic field is directly proportional to the current flowing through the cable (Table 9). On the seabed surface (i.e. the default or standard case), the cables had maximum (i.e. at the center of the cable) magnetic field strengths ranging between 0.69 and 4.86 μT, and induced electric field strengths varying between 2.19×10^{-4} and 1.53×10^{-3} V/m, respectively (Figure 19 and 28). The cables solely created these fields.

Induced electric fields are also created by the movement of a marine species over a power cable (Tricas and Gill, 2011). To demonstrate this, a marine animal was modelled to travel over the cables at a speed of 4 m/s, which induced electric fields of $2.78 \times 10^{-6} - 1.94 \times 10^{-5}$ V/m (at the centre of the cable) (Figure 30). While the magnitude of the induced electric field is small in both cases (i.e. the field generated by the cable and movement of a marine species across the cable), the cables induced a much higher electric field than the marine species. However, according to Hirata (1999), some common fish can swim at top speeds of 26.7 m/s (e.g. swordfish). At this speed, the fish may induce electric fields of $1.86 \times 10^{-5} - 1.3 \times 10^{-4}$ V/m, which has a higher magnitude than the fields calculated in this report.

According to a recent study conducted by Hutchinson et al. (2021b), there is a need for researchers to improve the current knowledge base on SPC transmission by predicting the likely EMFs that future larger capacity cables may produce. On this note, the EMF levels emitted by five prospective DC cables were modelled since they generally have a higher current and voltage carrying capacity when compared with AC cables. The models were made using modified and validated EMF equations

developed by CMACS (2003) and Kavet et al. (2016). Without considering the influence of the geomagnetic field, the cables had maximum magnetic field strengths ranging between 7.18 and 57.60 μT (Figure 23). On the other hand, the values rose significantly (56.20-105.59 μT) after considering the influence of the earth's field (Figure 24). Since DC cables do not directly induce electric fields (Exponent, 2014), no calculations were performed. However, the movement of a marine species over the cables will induce electric fields (Tricas and Gill, 2011). This secondary field was modelled based on the assumption that a species was travelling over the cables at a speed of 4 m/s. The fields induced by the species ranged between 2.87×10^{-5} and 2.30×10^{-4} $\mathrm{V/m}$ (at the centre of the cable) (Figure 32). The modelling results show that the DC cables produce far higher emissions than the AC cables.

5.1.2 Impact of Cable Design and configuration on EMF Emission

The design features of any transmission cable will directly influence its emitted EMF intensity (Tricas and Gill, 2011). To investigate this assertion, different cables were chosen to cover a broad spectrum of AC and DC cables (Table 2 and 5).

This study found that small changes in a cable's geometry will affect the E MFs produced around the cable. The cables studied in this report had varying current and voltage carrying capacities. However, the same assumed current was used consistently when modelling the EMF profiles for every cable in each case study. For AC cables, when the current was kept constant, the magnetic field profiles of each cable depended primarily on the cable's nominal cross-sectional area and conductor positioning (or geometry) (Table 2 and Appendix A, Table A-1). In some instances, a cable may have the same cross-sectional area as other cables and still produce different EMF values. To illustrate, cables J (500 kV, 1000

mm^2) and H (170 kV, 1000 mm^2) have identical cross-sectional areas. However, the EMF values around the two cables differed in all cases, even when the same parameters (e.g. current, reference height, and cable burial depth) were used (Figure 19, 21, and 22). This occurred because the two cables had conductors that were positioned at different locations (Appendix A, Table A-1).

On the other hand, the separation distance between the five DC cables (Table 5) influenced the strength of the EMFs generated by the cables (after isolating all other parameters). The intensity of the EMFs increased as the spacing between the conductors got larger.

The burial of a cable is another example of how the positioning of a cable may influence the emitted EMF. Most SPCs are generally buried below the seabed surface to protect against anchoring, trawling, abrasion, or other maritime activities (Albert et al., 2020; Wang et al., 2021). In case 2, calculations were made to show the variation in magnetic fields when the AC cables were trenched to depths of 5 and 10 m, respectively (Figure 21 and 22). The results from this model showed that the strength of the magnetic field decreased with an increase in the burial depth of the cable. However, this does not attenuate the EMF entirely. In a situation where a cable might have been buried close to the topmost region of the ground's surface (e.g. Case 6 – cable buried at 0.5 m), erosion could wash away the topmost soil of the seabed, which may leave parts of the cable exposed. This will ultimately increase the likely EMF level that a marine species will encounter.

In addition, the rotation or twisting of the cable pair will influence the EMF strength. This was shown in case 6, where the average magnetic field strength of the five DC cables was calculated when the cables were positioned at angles of 0, 90, and 180 degrees. The highest magnetic field

of 67.6 µT was produced when the cables were positioned at 0 degrees, with the positive current going into the page. However, when the position of the cables was reversed (180 degrees), the maximum magnetic field decreased by about 51.3%. Likewise, the magnetic field value decreased by 29.7% when the cables were positioned at an angle of 90 degrees.

5.1.3 Comparison with other Studies

Despite the growing increase in ongoing research efforts to understand the effects of electric and magnetic fields on marine fauna, most studies appear to focus only on EMF emissions associated with a single cable type (e.g. a three-core AC cable with a voltage rating of 36 kV) (Vattenfall AB, 2010; Hutchinson et al., 2021a). From the opposite point of view, the general operation of an offshore wind farm requires the use and deployment of different cable types (e.g. array and export cables) (Weerheim, 2018). Therefore, this study focused on the likely emissions generated by various medium, high and ultrahigh voltage cables.

Hutchinson et al. (2021a) emphasized the need for more detailed EMF studies that include all aspects of magnetic and electric field modelling for AC and DC cables. However, achieving this has been challenging because there are no standard procedures or requirements for EMF estimation in most European countries (Vattenfall AB, 2010). For example, in some studies, the induced field is often not calculated (Vattenfall AB, 2010). It was further noted that researchers tend to mix up the properties of electric and magnetic fields. Additionally, after reviewing the relevant scientific literature on this topic, the author of this project found that geomagnetic field calculations were omitted in some studies. Interestingly, Hutchinson et al. (2021b) mentioned that it was of utmost importance for future studies to consider the influence of the geomagnetic field when estimating the magnetic field levels for DC cables. These discrepancies and omissions might make it daunting for

enthusiasts to replicate or perform EMF calculations. Hence, this project carefully details all the methods and basic assumptions needed to quantify EMFs completely. Apart from this, an easy-to-use EMF tool (i.e. The DolphDetch EMF) was developed to assist the Irish public in estimating the EMFs produced by 3-core AC and bipolar DC power cables using the EMF equations described in this project. In addition, this tool is beneficial for creating illustrative models of the EMF intensity around the cables.

General intensities of EMFs associated with SPCs vary for AC and DC cables (WaterProof Marine Consultancy et al., 2016). For instance, a study by Exponent (2018) investigated the magnetic field emissions resulting from a 34.5 kV AC cable trenched to a depth of 1.8 m below the seabed surface. Operating at a capacity of 723 A, the cable generated a magnetic field strength of 2.1 µT. In this project, a cable with a similar voltage capacity (34 kV) created a magnetic field strength that was estimated to be approximately 1.28 µT (at 200 A) (Figure 19). Since the field is directly proportional to the current, the cable will produce emissions of 4.6 µT at 723 A. This emission is more than two magnitudes higher than the calculated field strength identified in the first study. Gill et al. (2009) investigated the emission levels related to a 33 kV cable, with a current-carrying capacity exceeding 500 A. The results of the study showed that the cable produced strengths of 1.5 µT. In another study, a 33 kV cable (with similar loading conditions) generated strengths of 5 µT (Eltra, 2000). This reveals the variability of calculating EMFs, as the strength of the field changed at comparable current and voltage ratings. Despite this, the result (4.6 µT) obtained in this study still falls well within the range of values (2.1 -5 µT) identified by previous studies.

The induced electric fields associated with AC cables can also be compared with intensities reported in other studies. For example, Exponent (2018) estimated the induced electric field created by a 34.5 kV cable after assuming a load current of 723 A and a burial depth of 1.8 m. The study found that the cable produced an electric field of 1.4 mV/m. In this project, the 34 kV SPC generated an intensity of 0.4 mV/m when a load of 200 A was assumed (Figure 28). When this result is scaled up (723 A), the cable will produce a similar field strength of 1.4 mV/m. This result agrees with the findings of Exponent (2018). Contrarily, Vattenfall AB's (2010) publication suggests that a similar-sized cable (36 kV) will produce a larger field of 1.7 mV/m at a lower current carrying capacity (300 A). These discrepancies may be attributed to the different modelling equations and assumptions that the researchers have applied. For example, this project made use of simplified equations for calculating EMFs. These equations tend to overestimate the EMF levels from the cables (Tricas and Gill, 2011). In other modelling studies, researchers fail to include all the parameters, equations, and assumptions made, making it difficult to replicate the models they have created.

Like the AC cable, the DC cables in this project produced magnetic fields that can be compared with results obtained from other studies. To illustrate, this study modelled a ± 320 kV, assuming a load current of 1800 A. The cable generated a magnetic field strength of about 56.2 µT (Figure 24). Supporting the findings of this report is Hutchinson et al. (2021a), who noted that a ± 300 kV cable would emit less than 67 µT. Contrarily, Exponent (2014) modelled a ± 320 kV cable (at a comparable current of 1650 A) and discovered that the cable produced a field of approximately 500 µT. This value is over nine times the magnitude of the fields recorded in the studies mentioned above. Meanwhile, Tricas and Gill (2011) calculated the magnetic fields from nine DC cables (Ranging from ± 75 to 500 kV) and found that the cables produced field strengths between 5 to 160 µT. Interestingly, this project's largest cable (± 500 kV) emitted less

than 106 µT (Figure 24). Based on these findings, one could assume that Exponent might have made calculation errors while modelling. However, on a general scale, the DC SPCs modelled in this project fall with the range of 5 to 160 µT.

As earlier stated, DC cables do not directly induce electric fields; notwithstanding, an electric field may be created by the movement of a marine species over the cable. At a high swimming speed of 4 m/s, the induced electric field from the five DC cables was approximately 0.58 mV/m (Figure 32). At a lower velocity of 2.5 m/s, nine DC cables induced electric field strengths of about 0.19 mV/m (Tricas and Gill, 2011). As aforementioned, the induced electric field calculations are often omitted, making it difficult to compare results across studies.

5.1.4 Marine Species Interactions with EMFs

When investigating EMF emissions from underwater cables, it is imperative to consider the movement of a species within the ocean (Hutchinson et al., 2021b). This is true because the migration of a marine species within the water column may change on an hourly, daily, or seasonal basis (Hutchinson et al., 2021a). Species may swim from one point to the other in search of food. In other cases, relevant ecological sites such as coastal gravel beds may be used by a species (e.g. herring fish) for spawning (Høines et al., 1998). At the bottom of the ocean, a demersal or benthic species are likely to encounter a static SPC. When the cable is operational, a species that possesses electromagnetic sensory abilities is likely to detect EMF emissions from the cable. On the other hand, pelagic species may be impacted by EMFs generated by dynamic cables. In this study, 26 priority species were found to have magneto and electrosensory capabilities. Eight of these species swim in the benthopelagic zones (i.e. pelagic and demersal zones). However, the vast majority (11) are pelagic species, while the rest (7) live and feed in benthic habitats (Table 18).

Table 18: The ecological characteristics of priority species in the Irish sea (Reproduced from Tricas and Gill, 2011; Clarke et al., 2016).

Subgroup	Ordinary name	Habitat (Pelagic (P) or Demersal (D))
Dolphin	Bottle-nose Dolphin	P or D
	Common Dolphin	P
Turtles	Leatherback	P
	Loggerhead	P
	Hawksbill	P
	Kemp's Ridley	P
	Green Turtle	P
Sharks	Spurdog	D
	Tope	P
	Large-spotted dogfish	P or D
	Portuguese dogfish	D
	Basking shark	P
	Small-spotted catshark	D
	Porbeagle shark	P
	Common smooth-hound	P or D
Rays	Thornback ray	P
	Undulate ray	P
Skate	White skate	P or D
	Longnose skate	P or D
	Common (blue) Skate	D
Fish	Pollock	P or D
	Brown trout	P or D
	European seabass	P or D
	Atlantic cod	D
	European plaice	D
	European eel	D

The first set of species that were analysed were the magneto-sensitive bottle-nose and common dolphin. According to Kirschvink (1990), cetaceans (e.g. dolphins) use their sensory abilities to navigate when changing locations. These species can detect geomagnetic fields of about 0.05 µT (Kuznetsov et al., 1990). Modeled results from this study show that the minimum likely field (0.69 µT) from any cable (at its midpoint) far exceeds the sensory threshold for dolphins (Figure 19 and Table 12). Nevertheless, these marine species can detect the fields produced by the 33 kV, 500 mm^2 (0.05 µT) and 34 kV, 500 mm^2 (0.05 µT) cable at a distance of 5 m (to either side of the cable) when the cables are laid on the seafloor (Appendix A, Table A-2). In the case where the dolphins swim directly over a trenched (5 m) cable, they will likely detect the magnetic emissions

surrounding the 150 kV, 800 mm^2 (0.05 µT) cable (Appendix A, Table A-4). However, the existing body of current literature suggests that there is lacking evidence regarding the exact impact of SPCs (Tricas and Gill, 2011). Therefore, by inference, the proximity to the cable was used as a measure for potential EMF exposure or risk. Since this study focuses on static cables, it could be suggested that the bottle-nose dolphin will be more susceptible to the emissions produced by the cables above because it is a benthopelagic animal.

The next group of species is the magneto receptive sea turtles. Sea turtles can detect the magnetic and geomagnetic fields, they use for long-distance migration, navigation, and orientation (Tricas and Gill, 2011). These pelagic animals have demonstrated that they can detect fields ranging from 45 to 49 µT for green turtles and 0.005 to 7400 µT for loggerhead turtles (Table 12). However, not enough is known about Kemp's ridley, leatherback, and hawksbill turtles (Lohmann and Lohmann 1993; Tricas and Gill, 2011). Hence, this study has assumed that these turtles should be responsive to magnetic fields at similar intensities because of their behavioural and anatomical similarities. The modelling results have shown that the green turtles will not perceive any of the total fields from the AC and DC cables (Figure 19, 21, 22, and 24). On the other hand, the other turtles (i.e. Kemp's ridley, leatherback, and hawksbill) will detect emissions when they swim in close proximity (5-10 m) to the AC cables. Contrarily, the turtles will be susceptible to DC emissions from a farther distance (80 m). According to Tricas and Gill (2011), it is difficult to conclude about the risk of underwater cable EMFs. It is unclear how the turtles process or identify changes in the magnetic field. However, this study may suggest minimal potential risks since the sea turtles are pelagic species (Table 18).

Unlike other species, the shortlisted elasmobranch fishes (i.e. sharks, rays, and skates) are receptive to both magnetic and electric stimuli (Table 12). It was demonstrated that the thornback ray would detect magnetic fields of about 36 µT (Brown and Ilyansky, 1978). On the other hand, information about the detection thresholds of the other shortlisted fishes was limited. Most of the experimental studies that were found had focused more on their electrosensory responses to electric fields. The sharks can detect between 0.0001 and 0.2 mV/m, while the rays and skate detect fields ranging from 0.001 to 30 mV/m. These values can be compared with those affiliated with the modelled cables. The induced electric fields created by the rotation of the AC cable conductors will be sensed by the fishes from about 10-20 m away (Figure 28). Conversely, the emissions resulting from the movement of a species travelling across both AC and DC cables will be perceived more by the fishes when swimming directly over the cables (i.e. 10 AC and 5 DC) (Figures 30 and 32). In an experimental study conducted by Gill et al. (2009), the researchers observed changes in the conduct and spatial distribution of actively moving Elasmobranchii fishes when an AC cable became operational. While only a few behavioral studies (i.e. for the small-spotted catshark, basking shark, and thornback ray in Table 12) were found, it may be suggested that the migration of the species (i.e. benthopelagic and demersal elasmobranchs) would possibly be impacted by the cables modelled in this project.

The last group of sea creatures that were analysed is ocean fishes. Fishes such as the brown trout and European seabass are primarily sensitive to magnetic fields, while the pollock and Atlantic cod only respond to electric stimuli (Table 12). Other fishes like the European plaice and eel possess both electro and magneto sensory capabilities. Although the magnetic sensory threshold for the European seabass and plaice are precisely unknown, other species such as the brown trout and European eel can sense emissions of approximately 150-4200 µT, and 0.0126-0.192

µT, respectively. Similarly, the electrosensory levels for the European plaice and eel are yet to be determined; notwithstanding, the pollock and Atlantic code can sense roughly around 30 mV/m and 0.02 mV/m, respectively. Based on the EMF calculations conducted, it was observed that the European eel would have to be within 5-10 m of the AC cable to detect any magnetic emission. Also, the brown trout will not perceive any of the magnetic fields because of its high sensory level, which exceeds the intensity (105.59 µT) from the most prominent cable (i.e. 550 kV, 1 m) (Figure 24). The electrosensitive pollock fish will not detect any of the fields from both AC and DC SPCs. On the other hand, an actively swimming Atlantic cod will sense induced fields that exist directly over the AC (i.e. the induced field from just the cables) and DC cable. Thus, SPCs may impact fish species; however, only a few studies supported this hypothesis (Tricas and Gill, 2011). For instance, it was reported that the European eel tends to reduce its speed while swimming over DC cables (Öhman et al., 2007). Therefore, by inference, the bottom-dwelling Atlantic cod may be identified as the only fish species that the modelled cables might impact. However, more studies (e.g. anatomical, life history, and biological) are needed to assess risk or impact extensively. Finally, it should be noted that it is essential to carefully consider the design (i.e. cable type, loading, and voltage) and configuration (i.e. the position of the conductors, cable orientation, and burial depth) of SPCs as these will have a significant impact on the strength of the EMFs that a cable produces.

5.2 Heavy Metals Discussion

5.2.1 Heavy Metals Released by the SPCs

This study was conducted to determine the concentration of HMs that may be released by four SPCs of different ages (i.e. 0 days, 12 days, 15 years, and 34 years). The concentration of 9 HMs (i.e. Al, Cd, Cu, Fe, Pb, Mn, Ni, Hg, and As) was measured over a period of 6 months and 1 year using the ICP-OES and ICP-MS techniques. The results of the analysis are given in Table 13.

The results reveal varying concentrations of the selected HMs, which are higher than the background values. Expectedly, the mean values of some of the HMs (e.g. Al, Fe, Pb, Mn, As, and Hg) were higher when the cables were submerged for a longer period (i.e. one year) in comparison to the values observed when the cables were placed in the buckets for 6 months. However, the opposite was the case with Cd, Cu, and Ni. These metals were higher over the first phase of submersion compared with the results obtained after 1 year (Figures 34b, c, and g).

Interestingly, recent research conducted by Enyoh et al. (2021) reveals that plastics may serve as adsorbents for the removal of HMs because of their ability to trap pollutants on their surface due to the size of their pores, and surface area. The researchers studied the adsorption of some HMs and other pollutants (e.g. dyes and oils) from aqueous solutions using several plastics. This research observation may explain why some inconsistencies were noticed in the concentration of the HMs identified in this study. It may also pose an interesting likely solution for removing SPC-related pollutants (i.e. heavy metals) since the superior features of modified plastics may serve as excellent adsorbents. However, further research is still required to verify this hypothesis.

So far, this study shows that there is a clear indication of enrichment of the metals from the cables. As stated earlier, these HMs are very toxic and detrimental to the existence of living organisms. They have been known to interrupt intracellular homeostasis, including damage to lipids, proteins enzymes, and DNA as a result of free radical production (Orosun et al., 2020). However, given the dilution capacity of the ocean, the impact of metals released from cables on the ocean ecosystem could be limited.

5.2.2 Assessment of Individual Cable Contributions

The estimated number of HMs released per cm^2 of each cable are provided by Tables 14 and 15. The results indicate that the number of metals released are not completely dependent on the duration of submersion, but also the nature of the electrodes used.

When the new cable was initially submerged (i.e. 6 months), the mean concentrations of Cu, Al, Cd, Fe, Ni, and As appear to be higher than they were in the 1 year period. On the other hand, the values of Pb, Mn, and Hg increased over time. Similar unexpected observations where concentration levels were higher during first phase of submersion were noted for the other cables.

Meticulous examination of the results shows that the oldest cable (i.e. 34 years) had the highest contribution to the total release of HM contents, followed by the 15 years, 12 days, and new cable. The Al contribution of the 12 days cable increased from 0.80 to 29.76 $\mu g/cm^2$ between 6 months and 1 year. The latter concentration is much higher than any other HM released by the other cables. This revelation was expected because the cable (i.e 12 days) was made using aluminum electrodes. This also explains why the other samples had a significantly higher concentration of Cu in comparison to the sample obtained from the 12 days cable since

the other conductors were designed using copper. The pollution of the Irish sea with the heavy metals released by these cables can seriously degrade the health of the species that live in the aquatic ecosystem.

5.3 Microplastics Discussion

5.3.1 Microplastics Released by SPCs

Underwater power cables may affect the marine ecosystem, just like any other man-made installation in the water (Andrulewicz and Otremba, 2011). For example, physical habitat disturbance, sediment resuspension, chemical pollution, and EMF emissions are potential consequences of offshore wind turbine construction, operation, maintenance, and decommissioning (Petersen and Malm, 2006). In addition, cable components include plastics that can degrade and spread into the marine environment when an SPC becomes damaged. Therefore, it is essential to evaluate the emission of MPs from SPCs and estimate risks to marine ecosystems.

In this study, two experiments (i.e. static and dynamic) were carried out to determine the number of microplastics that would be released from four underwater cables. In the static experiment, no MP particles were found (Table 16). The different ages of the various plastic materials did not influence the fragmentation of the polymer. The results show that the static experiment may not be fully applicable for assessing potential MP contaminants. However, it may be possible that the cables may release MPs if left for a more extended period (e.g. five years or more) in the bucket. It is unclear how MPs are distributed or behave dynamically in the water column; nevertheless, it is known that they are influenced by activities such as drilling, trawling, tidal currents, and other processes that cause turbulence in the water column (Moreira et al., 2016; Kane and Clare, 2019). Studies evaluating the presence of MPs (as a result of

the presence of SPCs) were not found for comparison. However, MPs have been reported to be present in the deep and abyssal oceans (Woodall et al., 2014).

Regarding the second experiment, it was demonstrated that the cables have the potential to release MPs when placed under dynamic loading conditions. The vibration of the cables led to the release of MPs in approximately 17% of the water samples. Furthermore, the agitation of the new and 12 days cables resulted in the release of MPs. On the other hand, no MPs were emitted from the different cable samples (i.e 15 and 34 years) (Table 17). The micro-Raman analysis confirmed the MPs to be PP, which corresponded to the insulating material of the SPC (i.e the outer protective covering). SPCs are usually insulated with PP because it is easier to recycle than cross-linked polyethylene, a thermosetting insulation material (Wald et al., 2020). The release of MPs from the cables was generally low, even with dynamic loading conditions. This is particularly good for a submarine environment. Weathering processes (such as UV-light) typically speed up the degradation of a polymer (Kelkar, 2017). However, UV emissions may not reach the bottom of the sea, and a cable may therefore be safe for use.

Despite the widespread distribution of MPs, the risk of MP pollution on the seafloor is still poorly understood. However, they are suspected to enter the food chain through trophic transfer from benthic organisms (Carbery et al., 2018). Damage from MPs to benthic organisms may be biological, physical, or chemical (Enyoh et al., 2020). On a genetic and molecular level (e.g. gene expression and the generation of reactive oxygen species), cellular level (e.g. apoptosis), and population-level (e.g. membrane stability), MPs have the potential to harm large marine species, as well the surrounding environment (Gallo et al., 2018; Santana-Viera, 2021).

The potential risk of MP contamination was very low (i.e Risk index of 1) (Figure 41).

This is because the PP used in insulating the SPCs generally has low toxicity to ecological systems than other polymers (e.g. PVC) (Lithner et al., 2011). However, studies evaluating the direct ecological risks of MP pollution from SPCs were not found. Furthermore, most reports on the risks and impacts of MPs on the benthic environment have been conducted under laboratory conditions. Hence, further studies need to be conducted to understand better SPC-related pollutants (i.e MPs and HMs).

Conclusion and Recommendations

6.0 Conclusion and Recommendations

6.1. Conclusion

This study investigated the impact of electromagnetic fields and chemicals from offshore wind farm submarine power cables on marine species in the Irish Sea. This was achieved by (i) quantifying and characterising the electromagnetic fields produced by current and potential future submarine power cables, (ii) designing an easy-to-use electromagnetic field assessment tool, (iii) identifying priority marine organisms in the Irish Sea that are sensitive to either magnetic or electric fields, (iv) determining the concentration of heavy metals released by four subsea power cables) and (v) determining the abundance of microplastic released by subsea power cables.

The main conclusions from the study are as follows:

1. This study has shown that it is important for cable designers to carefully consider the design (e.g. cable type, loading, and voltage) and configuration (e.g. burial depth, cable orientation, and conductor positioning) of the cables they plan to install in any offshore wind farm as these will have a significant impact on the EMFs that the cables will produce. All aspects of magnetic and induced electric field modelling for AC and DC (including the influence of the geomagnetic field) cables were analysed. The AC cables were found to have generated lower emissions in comparison to DC cables. The different case studies and scenarios that were considered can be used as a guide for other designers and environmentalists interested in identifying or calculating electromagnetic fields from undersea cables.
2. A simple tool was designed to help the general public calculate and predict EMFs from old and future potential subsea cables. Using the tool, EMF calculations can be made for 3-core AC and bipolar DC power cables. Subsequent versions of the tool will include other cable types.

3. 26 priority species were found to possess electromagnetic sensory abilities. From the 26, 7 are mammals (2 dolphins and 5 turtles), 13 are elasmobranchs (8 sharks, 2 rays and 3 skates), and 6 are fishes. They had varying sensitivity levels, which were compared with those associated with the modelled cables. However, there was not enough information available to create an extensive assessment of risk or impact to marine species. Hence, the following inferences were made (1) the bottle-nose dolphin is likely the most susceptible mammal that is at risk of exposure, (2) the potential risks are minimal to sea turtles, (3) the migration of the elasmobranch species would likely be impacted by the emissions from the modelled cables and (4) the Atlantic cod will be affected by the estimated induced electric fields circulating the AC and DC cables, while AC emissions may only impact the European eel.
4. The concentration of 9 heavy metals (i.e. Al, Cd, Cu, Fe, Pb, Mn, Ni, Hg, and As) in 4 subsea cables samples was determined. The results reveal varying concentrations of the selected HMs, which are higher than the background values. Expectedly, the mean values of some of the HMs (e.g. Al, Fe, Pb, Mn, As, and Hg) were higher for the longer time interval (i.e. when the cables were placed in buckets for one year) in comparison to the values observed over six months. However, the opposite was the case with Cd, Cu, and Ni. However, given the dilution capacity of the ocean, the impact of metals released from cables on the ocean ecosystem could be limited. Also, the heavy metal contribution from each cable follows: 34-years-old cable>15 years-old-cable>12-days-old cable>new cable.
5. Cables placed under static conditions failed to release microplastics. However, this study showed that subsea cables could release plastic particles when they are placed under dynamic loading conditions. Notwithstanding, it was demonstrated that the cables pose a low risk of harming the

marine environment because only a few plastic particles were released.

6.2 Recommendations

1. The modelling results could be compared with actual field measurements for similar-sized cables with the same loading conditions.
2. Future reports should also include induced electric field calculations. The influence of the geomagnetic field should be taken into consideration in these reports. Regulatory bodies may help by developing standardised procedures or requirements for EMF estimation.
3. More studies (e.g. anatomical, life history, and biological) are needed to extensively assess risk or impact to marine life from subsea cables.
4. More research should be geared towards testing more cable samples for heavy metal and microplastic pollution. The heavy metal samples should be submerged for longer periods using deionised water. The dynamic experiment should be conducted using the cables complete cross-section.

References

- 4C Offshore (2021). *Submarine Cable Consulting & Market Intelligence | 4C Offshore*. [online] 4coffshore.com. Available at: https://www.4coffshore.com/.
- A. Cozar, F. Echevarria, J. Ignacio Gonzalez-Gordillo, X. Irigoien, B. Ubeda, S. Hernandez-Leon, …, C.M. (2014). Duarte *Plastic debris in the open ocean*Proc. Natl. Acad. Sci. U.S.A., 111 (28), pp. 10239-1024
- Agata, K. and Inoue, T. (2012). Survey of the differences between regenerative and non-regenerative animals. Dev. Growth Diff. 54, 143–152.
- Albert, L., Deschamps, F., Jolivet, A., Olivier, F., Chauvaud, L. and Chauvaud, S. (2020). A current synthesis on the effects of electric and magnetic fields emitted by submarine power cables on invertebrates. *Marine Environmental Research*, 159, p.104958.
- Albert, L., Deschamps, F., Jolivet, A., Olivier, F., Chauvaud, L. and Chauvaud, S. (2020). A current synthesis on the effects of electric and magnetic fields emitted by submarine power cables on invertebrates. Marine Environmental Research, 159, p.104958.
- Alcorn, R. and O'Sullivan, D. (2013). *Electrical design for ocean wave and tidal energy systems*. London: Inst. of Engineering and Technology.
- Ali, H., Khan, E. and Ilahi, I. (2019). Environmental Chemistry and Ecotoxicology of Hazardous Heavy Metals: Environmental Persistence, Toxicity, and Bioaccumulation. *Journal of Chemistry*, 2019, pp.1-14.
- Alomary, A. and Belhadj, S. (2007). Determination of heavy metals (Cd, Cr, Cu, Fe, Ni, Pb, Zn) by ICP-OES and their speciation in Algerian Mediterranean Sea sediments after a five-stage sequential extraction procedure. Environmental Monitoring and Assessment, 135(1-3).

- Alstom (2010). HVDC for beginners and beyond.
- Andrulewicz, E. andOtremba, Z. (2011). Disturbances of natural physical fields by technical activities and their implications for marine life. *Case baltic sea*, 1(1), p.12.
- Ansari, R. and Hei, T. (2000). Effects of 60 Hz extremely low frequency magnetic fields (EMF) on radiation- and chemical-induced mutagenesis in mammalian cells. Carcinogenesis, 21(6), pp.1221-1226.
- Ardelean, M. and Minnebo, P. (2015). HVDC submarine power cables in the world: state-of-the-art knowledge (No. EUR 27527 EN). Joint Research Centre (JRC).
- Ardelean, M. andMinnebo, P. (2015). HVDC Submarine Power Cables in the World; EUR 27527 EN.
- Arthur, C., Baker, J. and Bamford, H. (2009). Proceedings of the International Research Workshop on the Occurrence, Effects, and Fate of Microplastic Marine Debris. NOAA Tech. Memo. NOS-OR&R-48 530.
- ATSDR (2007). U.S. Agency for Toxic Substances and Disease Registry. http://www.atsdr.cdc.gov/mrls/.
- Bardalai, A., Gerada, D., Golovanov, D., Xu, Z., Zhang, X., Li, J., Zhang, H. and Gerada, C. (2019). Reduction of Winding AC Losses by Accurate Conductor Placement in High Frequency Electrical Machines. *IEEE Transactions on Industry Applications*, 56(1), pp.183-193.
- Barnes, D., Galgani, F., Thompson, R. and Barlaz, M. (2009). Accumulation and fragmentation of plastic debris in global environments. *Philosophical Transactions of the Royal Society B: Biological Sciences*, 364(1526), pp.1985-1998.
- Bedore, C. and Kajiura, S. (2013). Bioelectric Fields of Marine Organisms: Voltage and Frequency Contributions to Detectability by Electroreceptive Predators. Physiological and Biochemical Zoology, 86(3), pp.298-311.

- Beggan, C. (2019) Making a Map of the Earth's Magnetic Field. Front. Young Minds. 7:42. doi: 10.3389/frym.2019.00042.
- Benato, R. and Paolucci, A. (2005). Operating capability of long AC EHV transmission cables. Electric Power Systems Research, 75(1), pp.17-27.
- BGS (2020). *An Overview of the Earth's Magnetic Field*. [online] Geomag.bgs.ac.uk. Available at: http://www.geomag.bgs.ac.uk/education/earthmag.html.
- Bochert, R. and Zettler, M. (2004). Long-term exposure of several marine benthic animals to static magnetic fields. *Bioelectromagnetics*, 25(7), pp.498-502.
- Bonta, M., Hegedus, B. and Limbeck, A. (2016). Application of dried-droplets deposited on pre- cut filter paper disks for quantitative LA-ICP-MS imaging of biologically relevant minor and trace elements in tissue samples. Anal. Chim. Acta. 908: 54–62.
- Bromm, B., Hensel, H. and Nier, K. (1975). Response of the ampullae of Lorenzini to static combined electric and thermal stimuli inScyliorhinus canicula. *Experientia*, 31(5), pp.615-618.
- Brown, H. and Ilyinsky, O. (1978). Ampullae of lorenzini in magnetic field. Journal of Comparative Physiology 126:333-341.
- Brown, H., Ilyinsky, O., Muravejko, V., Corshkov, E. and Fonarev, G. (1979). Evidence that geomagnetic variations can be detected by lorenzinian ampullae. Nature, 277(5698), pp.648-649.
- Browne, M., Crump, P., Niven, S., Teuten, E., Tonkin, A., Galloway, T. and Thompson, R. (2011). Accumulation of Microplastic on Shorelines Woldwide: Sources and Sinks. *Environmental Science & Technology*, 45(21), pp.9175-9179.
- Buffett, B. (2014). *Geomagnetic fluctuations reveal stable stratification at the top of the Earth's core*. London, Eng., pp.484-487.

- Bullock, T. and Fessard, A. (1974). *Electroreceptors and other specialized receptors in lower vertrebrates*. Berlin: Springer, p.165.
- Campbell, W. (2003). *Introduction to geomagnetic fields*. 2nd ed. Cambridge: Cambridge Univ. Press.
- Carbery, M., O'Connor, W. and Palanisami, T. (2018). Trophic transfer of microplastics and mixed contaminants in the marine food web and implications for human health. *Environment International*, 115, pp.400-409.
- Carbon Trust (2017). *Floating Wind Joint Industry Project: policy & regulatory appraisal*. Carbon Trust.
- Carter, L., Burnett, D., Drew, S., Marle, G., Hagadorn, L., Bartlett-McNeil, D. and Irvine N. (2009). Submarine Cables and the Oceans – Connecting the World. UNEP-WCMC Biodiversity Series No. 31. ICPC/UNEP/UNEP-WCMC.
- Cathie Group (2018). *An Overview of Cable Burial Risk Assessment Methods*. [online] Cathiegroup.com. Available at: https://cathiegroup.com/article/an-overview-of-cable-burial-risk-assessment-methods/.
- Cavaleiro, P. (2012). Offshore Electric Dynamic Cables [PowerPoint slides]
- Channell, J. and Vigliotti, L. (2019). The Role of Geomagnetic Field Intensity in Late Quaternary Evolution of Humans and Large Mammals. *Reviews of Geophysics*, 57(3), pp.709-738.
- Christian, E., Franklyn, O. Verla, A., Wang, Q., Shafea, L., Veral, E., Isiuku, B., Chowdhury, T., Chizoruo, F. and Chowdhury, A. (2021). "Plasti-remediation": Advances in the potential use of environmental plastics for pollutant removal, Environmental Technology & Innovation, Volume 23, 2021, 101791. https://doi.org/10.1016/j.eti.2021.101791.
- Clarke, M., Farrell, E.D., Roche, W., Murray, T.E., Foster, S. and Marnell, F. (2016) Ireland Red List No. 11: Cartilaginous fish

[sharks, skates, rays and chimaeras]. National Parks and Wildlife Service, Department of Arts, Heritage, Regional, Rural and Gaeltacht Affairs. Dublin, Ireland.

- Clausen, T., and D'Souza, R. (2001). Dynamic risers key component for deepwater drilling, floating production. Offshore, 61(5), 89-90.
- CMACS (2003) A baseline assessment of electromagnetic fields generated by offshore wind farm cables. COWRIE Report EMF - 01-2002 66.
- Cole, M., Lindeque, P., Halsband, C. and Galloway, T. (2011) Microplasticsas contaminants in the marine environment: a review. Mar Pollut Bull 62:2588–2597.
- Corinaldesi, C., Canensi, S., Dell'Anno, A., Tangherlini, M., Di Capua, I., Varrella, S., Willis, T., Cerrano, C. and Danovaro, R. (2021). Multiple impacts of microplastics can threaten marine habitat-forming species. *Communications Biology*, 4(1).
- Creed, J., Brockhoff, C. and Martin, T. (1994). Environmental monitoring systems laboratory office of research and development. U.S. Environmental Protection Agency (U.S. EPA) Cincinnati, Ohio 45268 method 200.8 - Method 200.8, Revision 5.4 (1994). Available at https://www.epa.gov/sites/default/files/2015-06/documents/epa-200.8.pdf
- Curran, R. (2019). *Richard Curran: 'Offshore Wind Investment Will Test Our Climate Change Resolve'*. [online] independent. Available at: https://www.independent.ie/business/irish/richard-curran-offshore-wind-investment-will-test-our-climate-change-resolve-38279902.html.
- DGE (2021). *Coastal and Marine Species Database - data.gov.ie*. [online] Data.gov.ie. Available at: https://data.gov.ie/dataset/coastal-and-marine-species-database.

- Duffus, B. (2001) "Heavy Metals"–A Meaningless Term. Chemistry International -- Newsmagazine for IUPAC, Vol. 23 (Issue 6), pp. 163-167.
- Dunham, A., Pegg, J., Carolsfeld, W., Davies, S., Murfitt, I. and Boutillier, J. (2015). Effects of submarine power transmission cables on a glass sponge reef and associated megafaunal community. *Marine Environmental Research*, 107, pp.50-60.
- EC (2020). FAQ: Low, medium, high, extra high voltage | Eland Cables. [online] Elandcables.com.
- ECE, (European Commission Environment) (1998). Council Directive 98/83/EC of 3 November.
- Eltra (2000). Beregning og maling af magnetfelter omkring kabler og vindmØller. Internt. Notat. 2000:238.
- Emma, B. (2016). A Review of the Evidence of Electromagnetic Field (Emf) Effects on Marine Organisms. *Journal of Ecology and Environmental Sciences*, p.4.
- Enger, P. S., L. Kristensen, and O. Sand. (1976). Perception of weak electric DC currents by European eel (Anguilla anguilla). Comparative Biochemistry and Physiology a-Physiology 54:101-103.
- Enyoh, C. and Isiuku, B. (2020). Determination and Human Health Risk Assessment of Heavy Metals in Floodbasin Soils in Owerri, Southeastern Nigeria. *Chemistry Africa*, 3(4), pp.1059-1072.75
- Enyoh, C. E., Shafea, L., Verla, A. W., Verla, E. N., Qingyue, W., Chowdhury, T., & Paredes, M. (2020). Microplastics Exposure Routes and Toxicity Studies to Ecosystems: An Overview. 35(1), 1–10. https://doi.org/10.5620/eaht.e2020004.
- Enyoh, C., Verla, A., Rakib, K. (2021). Application of Index Models for Assessing Freshwater Microplastics Pollution. WNOFNS 38: 37-48
- Eriksen, M., Lebreton, L., Carson, H., Thiel, M., Moore, C., Borerro, J., Galgani, F., Ryan, P. and Reisser, J. (2014). Plastic Pollution in

the World's Oceans: More than 5 Trillion Plastic Pieces Weighing over 250,000 Tons Afloat at Sea. *PLoS ONE*, 9(12), p.e111913.

- ESB (1999). Electric and Magnetic fields in the Environment. Dublin: ESB.
- ESCA (2021). Submarine Power Cables Ensuring the lights stay on. *European Subsea Cables Association*, p.1.
- EWEA (2020). Wind Energy the Facts. [online] Wind Europe.
- Exponent (2013). *Virigina Offshore Wind Technology Advancement Project*. Magnetic Fields from Submarine Cables. Bowie: Exponent, p.5.
- Exponent (2014). *Submarine Cable DC Magnetic Field in Lake Champlain and Marine Assessment*. Bowie: Exponent, p.4.
- Exponent (2018). *Deepwater wind south fork wind farm*. Offshore electric and magnetic field assessment. New York: Exponent.
- Fahem, M. (2018). 3 Phase High Voltage Submarine Power Cables and their Impact on Marine Ecosystem. EMWORKS.
- Farrell, P. and Nelson, K. (2013). Trophic level transfer of microplastic: Mytilus edulis (L.) to Carcinus maenas (L.). *Environmental Pollution*, 177, pp.1-3.
- Fernandez, E. and Patrick, J. (2021). Magnetic Fields from High Voltage Power Cables. *Electrotechnik Pty Ltd*, 1(1), pp.1-3.
- Fontana, G., Mossotti, R., and Montarsolo, A. (2020). Assessment of microplastics release from polyester fabrics: The impact of different washing conditions. *Environmental Pollution*, 264, p.113960.
- Formicki, K., M. Sadowski, A. Tanski, A. Korzelecka-Orkisz, and A. Winnicki. (2004). Behaviour of trout (*Salmo trutta* L.) larvae and fry in a constant magnetic field. Journal of Applied Ichthyology 20:290.
- Fuxjager, M., Davidoff, K., Mangiamele, L. and Lohmann, K. (2014). The geomagnetic environment in which sea turtle eggs incubate affects subsequent magnetic navigation behaviour of

hatchlings. Proceedings of the Royal Society B: Biological Sciences, 281(1791), p.20141218.

- Gallo, F., Fossi, C., Weber, R., Santillo, D., Sousa, J., Ingram, I., Nadal, A. and Romano, D. (2018). Marine litter plastics and microplastics and their toxic chemicals components: the need for urgent preventive measures. *Environmental Sciences Europe*, 30(1).
- Gilbertson, O. (2000). Electrical cables for power and signal transmission. New York, N.Y.: Wiley.
- Gill, A., Gloyne-Philips, I., Kimber, J. and Sigray, P. (2014). *Marine Renewable Energy, Electromagnetic (EM) Fields And EM-Sensitive Animals*. 1st ed. Dordrecht: Springer, pp.61-79.
- Gill, A., Gloyne-Phillips, I., Neal, K. and Kimber, J. (2005). Cowrie 1.5 Electromagnetic Fields Review. The potential effects of electromagnetic fields generated by sub-sea power cables associated with offshore wind farm developments on electrically and magnetically sensitive marine organisms – a review. Cranfield: Cowrie, pp.12-25.
- Gill, B., Huang, y., Gloyne-Phillips, I., Metcalfe, J., Quayle, V., Spencer, J. and Wearmouth, V. (2009). COWRIE 2.0 Electromagnetic Fields (EMF) Phase 2: EMF-sensitive fish response to EM emissions from sub-sea electricity cables of the type used by the offshore renewable energy industry. Cowrie Ltd. Cowrie-EMF-1-06. 128 pp.
- Gordonnat, J. and Hunt, J. (2020). Subsea cable key challenges of an intercontinental power link: case study of Australia–Singapore interconnector. *Energy Transitions*, 4(2), pp.169-188.
- H. C. (1931). The lower limits of perception of electric currents by fish. Journal of the Marine Biological Association UK 17:415-420.
- Ha, L. C., Sanchez-Vidal, A., Canals, M., Paterson, G. L. J., Coppock, R., Sleight, V., et al. (2014). The deep sea is a major sink for

microplastic debris. R. Soc. Open Sci. 1:140317. doi: 10.1098/rsos.140317

- Hirano, S., Haraguch, J., Mizuno, T. and Nagoya, Y. (2021). Developmentof DC +/- 250 kV Coaxially-Integrated Return Conductor Extruded Cable. p.1.
- Hirata, K. (1999). Swimming speeds of some common fish. Nmri.go.jp.
- Høines, A., Bergstad, O. and Albert, O. (1998). The structure and temporal stability of the fish community on a coastal bank utilized as a spawning ground by herring. *ICES Journal of Marine Science*, 55(2), pp.271-288.
- Huang, Y. (2005). Electromagnetic Simulations of 135-kV Three Phase Submarine Power Cables. Center for Marine and Coastal Studies, Ltd. Prepared for Sweden Offshore.
- Hutchison, Z., Gill, A., Sigray, P., He, H. and King, J. (2020). Anthropogenic electromagnetic fields (EMF) influence the behaviour of bottom-dwelling marine species. *Scientific Reports*, 10(1), p.1.
- Hutchison, Z., Gill, A., Sigray, P., He, H. and King, J. (2021a). A modelling evaluation of electromagnetic fields emitted by buried subsea power cables and encountered by marine animals: Considerations for marine renewable energy development. *Renewable Energy*, 177, pp.72-81.
- Hutchison, Z., Secor, D. and Gill, A. (2021b). The Interaction Between Resource Species and Electromagnetic Fields Associated with Electricity Production by Offshore Wind Farms. *Oceanography*, 33(4), pp.96-107.
- Hydro Quebec (2011). Electric and Magnetic Fields. The Power System and Health. p.3.
- ICPC (2011). *About Submarine Power Cables*.

- IEEE (2019). *IEEE Standard Procedure for Measurement of Power Frequency Electric and Magnetic Field From AC Power Lines*. New York: IEEE, p.21.
- IGRF (2021). *Geomagnetic Data | NCEI*. [online] Ngdc.noaa.gov. Available at: https://www.ngdc.noaa.gov/geomag/data.shtml
- Ikeuchi, M., Sugimoto, K. and Iwase, A. (2013). Plant callus: mechanisms of induction and repression. Plant Cell 25, 3159–3173.
- INNOSEA (2020). Review of the state of the art of dynamic cable system design. INNOSEA.
- International Commission on Non-ionizing Radiation Protection (ICNIRP) (2010). ICNIRP Statement—Guidelines for limiting exposure to time-varying electric and magnetic fields (1 Hz to 100 KHz). Health Phys 99:819-816.
- IRUG (2021). http://www.irug.org/jcamp-details?id=2738.
- Irwin, W. and Lohmann, K. (2005). Disruption of magnetic orientation in hatchling loggerhead sea turtles by pulsed magnetic fields. Journal of Comparative Physiology A, 191(5), pp.475-480.
- Ivanova, D., Vita, G., Steen-Olsen, K., Stadler, K., Melo, P., Wood, R. and Hertwich, E. (2017). Mapping the carbon footprint of EU regions. *Environmental Research Letters*, 12(5), p.054013.
- Jambeck, J., Geyer, R., Wilcox, C., Siegler, T., Perryman, M., Andrady, A., Narayan, R. and Law, K. (2015). Plastic waste inputs from land into the ocean. *Science*, 347(6223), pp.768-771.
- Jayalakshmi, Y. and Deepa, S. (2016). Modelling of Electric and Magnetic Fields Under High Voltage Ac Transmission Line. *Journal of Electrical and Electronics Engineering*, 11(3), pp.24-31.
- Jiwan S., and Ajay K. (2011). Effects of Heavy Metals on Soil, Plants, Human Health and Aquatic Life. International Journal of Research in Chemistry and Environment. 1(2): 15-21.

- Jordan, L., Mandelman, J. and Kajiura, S. (2011). Behavioral responses to weak electric fields and a lanthanide metal in two shark species. Journal of Experimental Marine Biology and Ecology, 409(1-2), pp.345-350.
- Kabir E.A. H. M., Masahiko S., Tsuyoshi I., Koichi Y., Ariyo K., Takaya H. (2021). Assessing small-scale freshwater microplastics pollution, land-use, source-to-sink conduits, and pollution risks: Perspectives from Japanese rivers polluted with microplastics. *Science of the Total Environment*, 768: 144655
- Kalmijn and Adrianus, J., 1972. Bioelectric Fields in Sea Water and the Function of the Ampullae of Lorenzini in Elasmobranch Fishes.
- Kalmijn, A. J. 1971. The electric sense of sharks and rays. Journal of Experimental Biology 55:371-383.
- Kalmijn, J. (1982). "Electric and magnetic-field detection in elasmobranch fishes." Science 218, pp.916–918.
- Kamalapur, G. and Arakeri, K. (2020). A Comparative Study of Monopolar and Bipolar HVDC Transmission Systems. *European Journal of Advances in Engineering and Technology*, 7(8), pp.21-26.
- Kane, I., and Clare M. (2019) Dispersion, Accumulation, and the Ultimate Fate of Microplastics in Deep-Marine Environments: A Review and Future Directions. Front. Earth Sci. 7:80. doi: 10.3389/feart.2019.00080
- Kavet, R., Wyman, M. and Klimley, A. (2016). Modelling Magnetic Fields from a DC Power Cable Buried Beneath San Francisco Bay Based on Empirical Measurements. *PLOS ONE*, 11(2), p.e0148543.
- Kelkar, V. (2017). Analysis of Chlorination & UV Effects on Microplastics Using Raman Spectroscopy. MSc. Arizona State University.
- Kempster, R. and Collin, S. (2011). Electrosensory pore distribution and feeding in the basking shark Cetorhinus

maximus (Lamniformes: Cetorhinidae). *Aquatic Biology*, 12(1), pp.33-36.

- Kirby, N., Siepmann, W., Xu, L. and Luckett, M. (2002). HVDC transmission for large offshore wind farms. *Power Engineering Journal*, 16(3), pp.135-141.
- Kirschvink, J.L. (1990). Geomagnetic sensitivity in cetaceans: an update with live stranding records in the United States, In Sensory Abilities of Cetaceans: Laboratory and Field Evidence (J.A. Thomas and R.A. Kastelein, eds.) Plenum Press, New York, NY. 639-649 pp.
- Koops, F. (2000). Electric and Magnetic fields in Consequence of Undersea Power Cables. Effects of Electromagnetic Fields on the Living Environment: Proceedings of the International Seminar on Effects of Electromagnetic Field on the Living Environment
- Kremers, D., López Marulanda, J., Hausberger, M. and Lemasson, A. (2014). Behavioural evidence of magnetoreception in dolphins: detection of experimental magnetic fields. Naturwissenschaften, 101(11), pp.907-911.
- Kuznetsov, V. B. (1990). Vegetative responses of dolphin to changes in permanent magnetic field. Biofizika 44:496-502.
- Lascelles, B., Notarbartolo Di Sciara, G., Agardy, T., Cuttelod, A., Eckert, S., Glowka, L., Hoyt, E., Llewellyn, F., Louzao, M., Ridoux, V. and Tetley, M. (2014). Migratory marine species: their status, threats and conservation management needs. *Aquatic Conservation: Marine and Freshwater Ecosystems*, 24(S2), pp.111-127.
- Leibfried, T. andZöller, T. (2020). Transmission of electrical power through subsea-cables over long distances. *Karlsruhe Institute of Technology*, pp.1-3.
- Lesaint, C. (2021). High Voltage Subsea Cables: Reducing Costs by Simplifying Design. [online] SINTEF.

- Lewczuk, B., Redlarski, G., Żak, A., Ziółkowska, N., Przybylska-Gornowicz, B. and Krawczuk, M. (2014). Influence of Electric, Magnetic, and Electromagnetic Fields on the Circadian System: Current Stage of Knowledge. BioMed Research International, 2014, pp.1-13.
- Li, X., Shen, H., Zhao, Y., Cao, W., Hu, C. and Sun, C. (2019). Distribution and Potential Ecological Risk of Heavy Metals in Water, Sediments, and Aquatic Macrophytes: A Case Study of the Junction of Four Rivers in Linyi City, China. International Journal of Environmental Research and Public Health, 16(16), 2861. doi:10.3390/ijerph16162861.
- Lithner, D., Larsson, A. and Dave, G. (2011). Environmental and health hazard ranking and assessment of plastic polymers based on chemical composition. Sci. Total Environ. 409 (18), 3309–3324. https://doi.org/10.1016/j.scitotenv.2011.04.038
- Liu, C. (2019). Comparison and Selection of Three-Core Cable and Single-Core Cable. IOP Conference Series: Earth and Environmental Science, 300.
- Liu, G., Fan, M., Wang, P. and Zheng, M. (2021). Study on Reactive Power Compensation Strategies for Long Distance Submarine Cables Considering Electrothermal Coordination. Journal of Marine Science and Engineering, 9(1), p.90.
- Liu, K., Wang, X., Fang, T., Xu, P., Zhu, L. and Li, D. (2019). Source and potential risk assessment of suspended atmospheric microplastics in Shanghai. Science of The Total Environment, 675, pp.462-471.
- Lohmann, K. and Lohmann, C. (1993). A Light-Independent Magnetic Compass in the Leatherback Sea Turtle. The Biological Bulletin, 185(1), pp.149-151.
- Lohmann, K. and Willows, A. (1987). “Lunar-modulated geomagnetic orientation by a marine mollusk.” Science 235:331–334.

- Lohmann, K. J., J. T. Hester, and C. M. F. Lohmann. (1999). Long-distance navigation in sea turtles. Ethology Ecology & Evolution 11:1-23.
- Lohmann, K., Lohmann, C., Ehrhart, L., Bagley, D. and Swing, T. (2004). Geomagnetic map used in sea-turtle navigation. Nature, 428(6986), pp.909-910.
- Lowrie, W. (2007). *Fundamentals of geophysics*. 2nd ed. Cambridge: Cambridge University Press.
- Maekawa, Y., Watanabe, K., Maruyama, S., Murata, Y. and Hirota, H. (2002). Research and Development of DC +/- 500kV Extruded Cables, CIGRE 2002 Session,pp 21-203.
- Malewar, A. (2020). *Earth's magnetic field changes 10 times faster than previously thought*. [online] Tech Explorist. Available at: https://www.techexplorist.com/earth-magnetic-field-changes-10-times-faster-previously-thought/33531/.
- Mandoli, D. (1998). Elaboration of body plan and phase change during development of Acetabularia: how is the complex architecture of a giant unicell built? Ann. Rev. Plant Biol. 49, 173–198.
- Márquez, M. (2020). Our Underwater World Is Full of Cables That Are Sometimes Attacked by Sharks. *Forbes.*
- McCaig, C., Song, B. and Rajnicek, A. (2009). Electrical dimensions in cell science. J. Cell Sci. 122, 4267–4276.
- McLean, S. (2020). *Geomagnetism Frequently Asked Questions*. [online] Ngdc.noaa.gov. Available at: https://www.ngdc.noaa.gov/geomag/faqgeom.shtml#:~:text=Magnetic%20declination%20is%20the%20angle,vector%2C%20measured%20positive%20into%20Earth.
- McManus, T. and Department of Energy. (1988). Electromagnetic fields from high voltage transmission lines: a report to Mr Michael Smith, T.D., Minister for Energy. Dublin: Department of Energy.

- McMullin, E. (2002). The Origins of the Field Concept in Physics. Physics, 4, pp.13-39.
- Meißner, K., Schabelon, H., Bellebaum, J. and Sordyl, H. (2006). *Impacts Of Submarine Cables On The Marine Environment . A Literature Review*.
- Metcalfe, J., Holford, B. and Arnold, G. (1993). Orientation of plaice (Pleuronectes platessa) in the open sea: evidence for the use of external directional clues. *Marine Biology*, 117(4), pp.559-566.
- Mitcheson, J., and Stanfield, P. (2013). "Bioelectricity, ionic basis of membrane potentials and propagation of voltage signals," in Encyclopedia of Biophysics, ed G. C. K. Roberts (Berlin; Heidelberg: Springer), 189–192.
- Moller, P. (1995). Electric fishes. 17th ed. London: Chapman & Hall.
- Moore, A. and Riley, D. (2009). "Magnetic particles associated with the lateral line on the European eel Anguilla anguilla." Journal of Fish Biology 74, pp.1629–1634.
- Moore, G. (1997). *Electric Cables Handbook*. 3rd ed. John Wiley & Sons, pp.20-40.
- Moreira, F. T., Balthazar-Silva, D., Barbosa, L., and Turra, A. (2016). Revealing accumulation zones of plastic pellets in sandy beaches. Environ. Pollut. 218, 313–321. doi: 10.1016/j.envpol.2016.07.006
- National Grid (2018). Electric and Magnetic Fields Report. National Grid (North Wales Connection Project). Warwick, pp.2-4.
- NBDC (2021). *Biodiversity Inventory*. [online] National Biodiversity Data Centre. Available at: https://www.biodiversityireland.ie/projects/biodiversity-inventory/taxonomic-groups/.
- Nishi, T. and G. Kawamura. (2005). *Anguilla japonica* is already magnetosensitive at the glass eel phase. Journal of Fish Biology 67:1213-1224.

- NPWS (2021). *National Parks & Wildlife Service*. [online] Npws.ie. Available at: https://www.npws.ie/.
- Nyqvist, D., Durif, C., Johnsen, M., De Jong, K., Forland, T. and Sivle, L. (2020). Electric and magnetic senses in marine animals, and potential behavioral effects of electromagnetic surveys. *Marine Environmental Research*, 155, p.104888.
- O'Halloran, B. (2019). Energy firms plan to invest billions in Irish Sea wind projects. *The Irish Times.*
- Öhman, M., Sigray, P. and Westerberg, H. (2007). Offshore Windmills and the Effects of Electromagnetic Fields on Fish. AMBIO: A Journal of the Human Environment, 36(8), pp.630-633.
- Oregon Wave Energy Trust (OWET) (2011). Electromagnetic Field Study. p.48.
- Orosun et al. (2020). Monte Carlo approach to risks assessment of heavy metals at automobile spare part and recycling market in Ilorin, Nigeria. Sci. Rep. 10. 22084. https://doi.org/10.1038/s41598-020-79141-0.
- OSPAR (2012) Guidelines on Best Environmental Practice (BEP) in Cable Laying and Operation. OSPAR 12/22/1, Annex 14. 18pp.
- Otremba, Z. and Andrulewicz, E. (2014). Physical Fields During Construction and Operation of Wind Farms by Example of Polish Maritime Areas. *Polish Maritime Research*, 21(4), pp.113-122.
- Pals, N. and Van SchaickZillesen, P. (1982). Exogenous and endogenous influences on metabolic and neural control of respiration, feeding, activity and energy supply in muscles, ion- and osmoregulation, reproduction, perception and orientation. 2nd ed. Oxford u.a., pp.226-227.
- Pals, N., Peters, R. and Schoenhage, A. (1982) Local geo-electric fields at the bottom ofthe sea and their relevance for electrosensitive fish, Netherlands Journal of Zoology, 32 (4): 479-494.

- Peters, R., van Wessel, T., van den Wollenberg, B., Bretschneider, F. and Olijslagers, A. (2002). The bioelectric field of the catfish Ictalurus nebulosus. Journal of Physiology-Paris, 96(5-6), pp.397-404.
- Petersen, J. and Malm, T. (2006). Offshore Windmill Farms: Threats to or Possibilities for the Marine Environment. *AMBIO: A Journal of the Human Environment*, 35(2), pp.75-80.
- Pezy, J., Raoux, A. and Dauvin, J. (2020). The environmental impact from an offshore wind farm: Challenge and evaluation methodology based on an ecosystem approach. *Ecological Indicators*, 114(1), p.1.
- Plodpradit, P., Dinh, V. and Kim, K. (2019). Coupled Analysis of Offshore Wind Turbine Jacket Structures with Pile-Soil-Structure Interaction Using FAST v8 and X-SEA. *Applied Sciences*, 9(8), p.1633.
- Poléo, A., Johannessen, H. and Harboe, M. (2001). High voltage direct current (HVDC)sea cables and sea electrodes: effects on marine life. Dept. of Biology, University of Oslo, Oslo, Norway. N-0316. 50 pp.
- Poletti, W. (2020). The Earth's magnetic field of the last centuries from the perspective of the Jequitinhonha and Mucuri river valleys: A natural observatory of the South Atlantic Anomaly in Brazil. *Journal of South American Earth Sciences*, p.102984.
- Prysmian Group (2020). Wind Turbines and Farms. p.7.
- Putman, N., Lohmann, K., Putnam, E., Quinn, T., Klimley, A. and Noakes, D. (2013). “Evidence for geomagnetic imprinting as a homing mechanism in Pacific salmon.” Current Biology 23:312-316.
- Redlarski, G., Lewczuk, B., Żak, A., Koncicki, A., Krawczuk, M., Piechocki, J., Jakubiuk, K., Tojza, P., Jaworski, J., Ambroziak, D., Skarbek, Ł. and Gradolewski, D. (2015). The Influence of Electromagnetic Pollution on Living Organisms: Historical Trends

and Forecasting Changes. *BioMed Research International*, 2015, pp.1-18.

- Rentschler, M., Adam, F., Chainho, P., Krügel, K. and Vicente, P. (2020). Parametric study of dynamic inter-array cable systems for floating offshore wind turbines. *Marine Systems & Ocean Technology*, 15(1), pp.16-25.
- Republic (2020). *Submarine Power Cables*. [online] Escaeu.org.
- Rizwan, M., Tse, J., Nori, A., Leong, K. and Yim, E. (2019). Principles of Regenerative Medicine. 3rd ed. Academic Press, pp.437-468.
- Sani, U. (2011). Determination of some heavy metals concentration in the tissues of Tilapia and Catfishes U. Sani. 3(2), pp.73-80.
- Santana-Viera, S., Montesdeoca-Esponda, S., Guedes-Alonso, R., Sosa-Ferrera, Z. and Santana-Rodríguez, J. (2021). Organic pollutants adsorbed on microplastics: Analytical methodologies and occurrence in oceans. *Trends in Environmental Analytical Chemistry*, 29, p.e00114.
- Schubert, G. (2007). *Treatise on geophysics*. Amsterdam, Netherlands: Elsevier.
- Scott, K., Harsanyi, P. and Lyndon, A. (2018). Understanding the effects of electromagnetic field emissions from Marine Renewable Energy Devices (MREDs) on the commercially important edible crab, Cancer pagurus (L.). Frontiers in Marine Science, 5.
- Singh, B., Sharma, R., Ajumeera, R. and Mathur, A. (2008). Electromagnetic fields in environment and its health hazards. 2008 International Conference on Recent Advances in Microwave Theory and Applications, pp.558-560.
- Sönnichsen, N. (2020). *Europe: Number Of Offshore Wind Farms 2019 | Statista*. [online] Statista. Available at: https://www.statista.com/statistics/666495/number-of-windfarms-eu/.

- Stolan, R. (2009). Losses and Inductive Parameters in Subsea Power Cables. Masters. Norwegian University of Science and Technology.
- Tamminga, M., Stoewer, S., and Fischer, E. (2019). On the representativeness of pump water samples versus manta sampling in microplastic analysis. *Environmental Pollution*, 254, p.112970.
- Tang, L. (2013). *HVDC Technologies & ABB Experience*
- Tański A. , Korzelecka-Orkisz A. , Grubišić L. , Tičina V. , Szulc J. , Formicki K. (20110. Directional responses of sea bass (*dicentrarchus labrax*) and sea bream (*sparus aurata*) fry under static magnetic field, ejpau 14(4), #08.
- Taormina, B., Bald, J., Want, A., Thouzeau, G., Lejart, M., Desroy, N. and Carlier, A. (2018). A review of potential impacts of submarine power cables on the marine environment: Knowledge gaps, recommendations and future directions. *Renewable and Sustainable Energy Reviews*, 96, pp.380-391.
- Taormina, B., Di Poi, C., Agnalt, A., Carlier, A., Desroy, N., Escobar-Lux, R., D'eu, J., Freytet, F. and Durif, C. (2020). Impact of magnetic fields generated by AC/DC submarine power cables on the behavior of juvenile European lobster (Homarus gammarus). *Aquatic Toxicology*, 220, p.105401.
- Tauxe, L., Butler, R., Van der Voo, R. and Banerjee, S. (2010). *Essentials of paleomagnetism*. Berkeley: University of California Press.
- Tesch, F. (1974). Influence of geomagnetism and salinity on directional choice of eels.Helgolander Wissenschaftliche Meeresuntersuchungen 26:382-395.
- Thomson, C. (2016). *Wind Farms Key to Cutting Carbon Emissions*. [online] The University of Edinburgh. Available at: https://www.ed.ac.uk/news/2016/wind-farms-key-to-cutting-carbon-emissions.

- Tricas, T. and Gill, A. (2011). Effects of EMFs from Undersea Power Cables on Elasmobranchs and Other Marine Species. U.S. Dept. of the Interior, Bureau of Ocean Energy Management, Regulation, and Enforcement, Pacific OCS Region, Camarillo, CA. OCS Study BOEMRE 2011-09.
- U.S. Environmental Protection Agency (EPA) (2004). Risk Assessment Guidance for Superfund Volume I: Human Health Evaluation Manual (Part E, Supplemental Guidance for Dermal Risk Assessment) Final; Office of Emergency and Remedial Response, EPA/540/R/99/005, OSWER 9285.7-02EP PB99-963312.
- U.S. Environmental Protection Agency (EPA) (2007). ProUCL Version 4.00.02 User GuideEPA/600/R-07/038.April.
- U.S. Environmental Protection Agency (EPA) (2009). Risk Assessment Guidance for Superfund Volume I: Human Health Evaluation Manual (Part F, Supplemental Guidance for Inhalation Risk Assessment), Office of Superfund Remediation and Technology Innovation, EPA-540-R-070-002, OSWER 9285.7-82.
- Uihlein, A. and Magagna, D. (2016). Wave and tidal current energy – A review of the current state of research beyond technology. *Renewable and Sustainable Energy Reviews*, 58, pp.1070-1081.
- United States Department of Energy (2013). *Effects of Electromagnetic Fields on Fish and Invertebrates*. Environmental Effects of Marine and Hydrokinetic Energy. United States of America.
- USEPA (2011). National Primary Drinking Water Regulations. Retrieved from http://water.epa.gov/drink/contaminants/index.cfm#List .
- Vattenfall AB (2010). *Impact of EMF from Sub-sea cables on marine organisms*. Vattenfall.

- Verla, A., Enyoh, C., Verla, E. and Nwarnorh, K. (2019). Microplastic–toxic chemical interaction: a review study on quantified levels, mechanism and implication. *SN Applied Sciences*, 1(11).
- Wald, D., Famous, O. and Pasi, R. (2020). Thermoplastic Insulation System for Power Cables. IEEE PES/IAS PowerAfrica. Doi: 10.1109/PowerAfrica49420.2020.9219839
- Walker, M., Kirschvink L., Ahmed, G. and Dizon, E. (1992). "Evidence that fin whales respond to the geomagnetic field during migration." Journal of Experimental Biology 171:67–78.
- Wang, C., Hilburn, I., Wu, D., Mizuhara, Y., Cousté, C., Abrahams, J., Bernstein, S., Matani, A., Shimojo, S. and Kirschvink, J. (2019). Transduction of the Geomagnetic Field as Evidenced from alpha-Band Activity in the Human Brain. *eneuro*, 6(2), pp.ENEURO.0483-18.2019.
- Wang, W., Yan, X., Li, S., Zhang, L., Ouyang, J. and Ni, X. (2021). Failure of submarine cables used in high-voltage power transmission: Characteristics, mechanisms, key issues and prospects. *IET Generation, Transmission & Distribution*, 15(9), pp.1387-1402.
- WaterProof Marine Consultancy, Research BV, and Bureau Waardenburg BV (2016). Potential effects of electromagnetic fields in the Dutch North Sea. Bureau Waardenburg.
- Weerheim, R. (2018). Development of dynamic power cables for commercial floating wind farms. Undergraduate. Technische Universiteit Delft.
- WHO (2003). Aluminum in drinking-water. Background document for preparation of WHO Guidelines for drinking-water quality. Geneva, World Health Organization (WHO/SDE/WSH/03.04/53).
- WHO (2005). Electromagnetic Fields and Public Health (Intermediate Frequencies). International EMF Project Information Sheet. World Health Organization, p.2.

- WHO (2007). Extremely low frequency fields. Environmental Health Criteria 238. Geneva: World Health Organization, pp.1-2.
- WHO (2011). World Health Organization Guidelines for drinking-water. Fourth edition. http://whqlibdoc.who.int/publications/2011/9789241548151_eng.pdf.
- Wilding, T., Gill, A., Boon, A., Sheehan, E., Dauvin, J., Pezy, J., O'Beirn, F., Janas, U., Rostin, L. and De Mesel, I. (2017). Turning off the DRIP ('Data-rich, information-poor') – rationalising monitoring with a focus on marine renewable energy developments and the benthos. *Renewable and Sustainable Energy Reviews*, 74, pp.848-859.
- Wiltschko, W. and Wiltschko, R. (2005). Magnetic orientation and magnetoreception in birds and other animals. *Journal of Comparative Physiology A*, 191(8), pp.675-693.
- Woodruff, D., Irvin, S., Kathryn, M., Jeffrey, W. and Valerie, C. (2013). *Effects Of Electromagnetic Fields On Fish And Invertebrates: Task 2.1.3: Effects On Aquatic Organisms - Fiscal Year 2011 Progress Report - Environmental Effects Of Marine And Hydrokinetic Energy*. United States.
- WPD (2021). *Western Power Distribution - What causes Losses*. [online] Western Power Distribution.
- Wright, S., Rogers, A., Manwell, J. and Ellis, A. (2002). Transmission Options for Offshore Wind Farms in the United States. pp.1-4.
- Xu, Z., Du, C. and Xia, M. (2018). Electromagnetic Fields Due to the Wake of a Moving Slender Body in a Finite-Depth Ocean with Density Stratification. Scientific Reports, 8(1).
- Young, D., Ng, C., Oterkus, S., Li, Q. and Johanning, L. (2018). Assessing the mechanical stresses of dynamic cables for floating offshore wind applications. *Journal of Physics: Conference Series*, 1102, p.1.

- Yujun, Y., Zhifeng. Y, and Shanghong. Z. (2011). Ecological risk assessment of heavy metals in sediment and human health risk assessment of heavy metals in fishes in the middle and lower reaches of the Yangtze River basin. *Environmental Pollution* 159 (2011). 2575 – 2585.
- Zhang, C., Wang, S., Sun, D., Pan, Z., Zhou, A., Xie, S., Wang, J. and Zou, J. (2020). Microplastic pollution in surface water from east coastal areas of Guangdong, South China and preliminary study on microplastics biomonitoring using two marine fish. *Chemosphere*, 256, p.127202.
- Zhang, Y. and Hu, B. (2011). Determination of some refractory elements and Pb by fluorination assisted electrothermal vaporization inductively coupled plasma mass spectrometry with platform and wall vaporization, Spectrochim. Acta B. 66: 163–169.
- Zhao, S., Cheng, Y., Chen, P., Nie, Y. and Fan, K. (2021). A comparison of two dynamic power cable configurations for a floating offshore wind turbine in shallow water. *AIP Advances*, 11(3), p.035302.
- Zheng, Y., Li, J., Sun, C., Cao, W., Wang, M., Jiang, F. and Ju, P. (2021). Comparative study of three sampling methods for microplastics analysis in seawater. *Science of The Total Environment*, 765, p.144495.
- Zoeger, J., J. R. Dunn, and M. Fuller. (1981). Magnetic material in the head of the common pacific Dolphin. Science 213:892-894.

Appendix A
AC and DC EMF Modelling

Table A-1: Cable geometry of the 10 AC SPCs.

Name	Left conductor position (m)	Middle conductor position (m)	Right conductor position (m)
A	-0.0161	0	0.0161
B	-0.0142	0	0.0142
C	-0.0265	0	0.0265
D	-0.0262	0	0.0262
E	-0.03066	0	0.03066
F	-0.0204	0	0.0204
G	-0.0337	0	0.0337
H	-0.0379	0	0.0379
I	-0.0379	0	0.0379
J	-0.1	0	0.1
Line Phasing (Degrees)	**120**	**0**	**-120**

Table A-2: Case 1. The magnetic field strength over the 10 AC SPCs.

Distance along seabed	A (33kV, 185mm2)	B (33kV, 150mm2)	C (33kV, 500mm2)	D (34kV, 500mm2)	E (36kV, 630mm2)	F (115kV, 300mm2)	G (150kV, 800mm2)	H (170kV, 1000mm2)	I (220kV, 1000mm2)	J (500kV, 1000mm2)
Metres	MicroTesla									
80	1.23E-04	1.09E-04	2.03E-04	2.01E-04	2.35E-04	1.56E-04	2.58E-04	2.90E-04	2.90E-04	7.65E-04
75	1.40E-04	1.24E-04	2.31E-04	2.28E-04	2.67E-04	1.78E-04	2.93E-04	3.30E-04	3.30E-04	8.71E-04
70	1.61E-04	1.42E-04	2.65E-04	2.62E-04	3.07E-04	2.04E-04	3.37E-04	3.79E-04	3.79E-04	1.00E-03
65	1.87E-04	1.65E-04	3.07E-04	3.04E-04	3.56E-04	2.36E-04	3.91E-04	4.39E-04	4.39E-04	1.16E-03
60	2.19E-04	1.93E-04	3.61E-04	3.56E-04	4.18E-04	2.78E-04	4.58E-04	5.16E-04	5.16E-04	1.36E-03
55	2.61E-04	2.30E-04	4.29E-04	4.24E-04	4.97E-04	3.30E-04	5.46E-04	6.14E-04	6.14E-04	1.62E-03
50	3.15E-04	2.78E-04	5.19E-04	5.13E-04	6.01E-04	4.00E-04	6.60E-04	7.42E-04	7.42E-04	1.96E-03
45	3.89E-04	3.43E-04	6.41E-04	6.34E-04	7.42E-04	4.93E-04	8.15E-04	9.16E-04	9.16E-04	2.42E-03
40	4.93E-04	4.35E-04	8.11E-04	8.02E-04	9.39E-04	6.24E-04	1.03E-03	1.16E-03	1.16E-03	3.06E-03
35	6.43E-04	5.67E-04	1.06E-03	1.05E-03	1.23E-03	8.15E-04	1.35E-03	1.51E-03	1.51E-03	4.00E-03
30	8.75E-04	7.72E-04	1.44E-03	1.42E-03	1.67E-03	1.11E-03	1.83E-03	2.06E-03	2.06E-03	5.44E-03
25	1.26E-03	1.11E-03	2.07E-03	2.05E-03	2.40E-03	1.60E-03	2.64E-03	2.97E-03	2.97E-03	7.83E-03
20	1.97E-03	1.73E-03	3.24E-03	3.20E-03	3.75E-03	2.49E-03	4.12E-03	4.63E-03	4.63E-03	1.22E-02
15	3.49E-03	3.08E-03	5.74E-03	5.68E-03	6.65E-03	4.42E-03	7.31E-03	8.22E-03	8.22E-03	2.17E-02
10	7.81E-03	6.89E-03	1.29E-02	1.27E-02	1.49E-02	9.90E-03	1.63E-02	1.84E-02	1.84E-02	4.85E-02

Trinity College Dublin

5	3.03E-02	2.68E-02	4.99E-02	4.94E-02	5.78E-02	3.84E-02	6.35E-02	7.14E-02	7.14E-02	1.89E-01
0	7.89E-01	6.96E-01	1.30E+00	1.28E+00	1.50E+00	9.99E-01	1.65E+00	1.85E+00	1.85E+00	4.86E+00
-5	3.03E-02	2.68E-02	4.99E-02	4.94E-02	5.78E-02	3.84E-02	6.35E-02	7.14E-02	7.14E-02	1.89E-01
-10	7.81E-03	6.89E-03	1.29E-02	1.27E-02	1.49E-02	9.90E-03	1.63E-02	1.84E-02	1.84E-02	4.85E-02
-15	3.49E-03	3.08E-03	5.74E-03	5.68E-03	6.65E-03	4.42E-03	7.31E-03	8.22E-03	8.22E-03	2.17E-02
-20	1.97E-03	1.73E-03	3.24E-03	3.20E-03	3.75E-03	2.49E-03	4.12E-03	4.63E-03	4.63E-03	1.22E-02
-25	1.26E-03	1.11E-03	2.07E-03	2.05E-03	2.40E-03	1.60E-03	2.64E-03	2.97E-03	2.97E-03	7.83E-03
-30	8.75E-04	7.72E-04	1.44E-03	1.42E-03	1.67E-03	1.11E-03	1.83E-03	2.06E-03	2.06E-03	5.44E-03
-35	6.43E-04	5.67E-04	1.06E-03	1.05E-03	1.23E-03	8.15E-04	1.35E-03	1.51E-03	1.51E-03	4.00E-03
-40	4.93E-04	4.35E-04	8.11E-04	8.02E-04	9.39E-04	6.24E-04	1.03E-03	1.16E-03	1.16E-03	3.06E-03
-45	3.89E-04	3.43E-04	6.41E-04	6.34E-04	7.42E-04	4.93E-04	8.15E-04	9.16E-04	9.16E-04	2.42E-03
-50	3.15E-04	2.78E-04	5.19E-04	5.13E-04	6.01E-04	4.00E-04	6.60E-04	7.42E-04	7.42E-04	1.96E-03
-55	2.61E-04	2.30E-04	4.29E-04	4.24E-04	4.97E-04	3.30E-04	5.46E-04	6.14E-04	6.14E-04	1.62E-03
-60	2.19E-04	1.93E-04	3.61E-04	3.56E-04	4.18E-04	2.78E-04	4.58E-04	5.16E-04	5.16E-04	1.36E-03
-65	1.87E-04	1.65E-04	3.07E-04	3.04E-04	3.56E-04	2.36E-04	3.91E-04	4.39E-04	4.39E-04	1.16E-03
-70	1.61E-04	1.42E-04	2.65E-04	2.62E-04	3.07E-04	2.04E-04	3.37E-04	3.79E-04	3.79E-04	1.00E-03
-75	1.40E-04	1.24E-04	2.31E-04	2.28E-04	2.67E-04	1.78E-04	2.93E-04	3.30E-04	3.30E-04	8.71E-04
-80	1.23E-04	1.09E-04	2.03E-04	2.01E-04	2.35E-04	1.56E-04	2.58E-04	2.90E-04	2.90E-04	7.65E-04

Table A-3: Case 1. The average magnetic field strength over the 10 AC SPCs.

Distance along seabed	Average magnetic field strength
Metres	microTesla
80	2.63E-04
75	2.99E-04
70	3.43E-04
65	3.98E-04
60	4.67E-04
55	5.56E-04
50	6.73E-04
45	8.31E-04
40	1.05E-03
35	1.37E-03
30	1.87E-03
25	2.69E-03
20	4.20E-03
15	7.45E-03
10	1.67E-02
5	6.48E-02
0	1.68E+00
-5	6.48E-02
-10	1.67E-02
-15	7.45E-03
-20	4.20E-03
-25	2.69E-03
-30	1.87E-03
-35	1.37E-03
s-40	1.05E-03

-45	ss8.31E-04
-50	6.73E-04
-55	5.56E-04
-60	4.67E-04
-65	3.98E-04
-70	3.43E-04
-75	2.99E-04
-80	2.63E-04

Table A-4: Case 2. Modelled magnetic field strength at 5m below seabed.

Distance along seabed	A (33kV, 185mm2)	B (33kV, 150mm2)	C (33kV, 500mm2)	D (34kV, 500mm2)	E (36kV, 630mm2)	F (115kV, 300mm2)	G (150kV, 800mm2)	H (170kV, 1000mm2)	I (220kV, 1000mm2)	J (500kV, 1000mm2)
Metres	microTesla									
65	1.85E-04	1.63E-04	3.05E-04	3.01E-04	3.53E-04	2.35E-04	3.88E-04	4.36E-04	4.36E-04	1.15E-03
60	2.17E-04	1.91E-04	3.57E-04	3.53E-04	4.14E-04	2.75E-04	4.55E-04	5.11E-04	5.11E-04	1.35E-03
55	2.58E-04	2.27E-04	4.24E-04	4.19E-04	4.91E-04	3.26E-04	5.40E-04	6.07E-04	6.07E-04	1.60E-03
50	3.11E-04	2.74E-04	5.12E-04	5.06E-04	5.93E-04	3.94E-04	6.52E-04	7.32E-04	7.32E-04	1.93E-03
45	3.83E-04	3.38E-04	6.30E-04	6.23E-04	7.30E-04	4.85E-04	8.02E-04	9.01E-04	9.01E-04	2.38E-03
40	4.82E-04	4.25E-04	7.94E-04	7.85E-04	9.19E-04	6.11E-04	1.01E-03	1.13E-03	1.13E-03	2.99E-03
35	6.25E-04	5.52E-04	1.03E-03	1.02E-03	1.19E-03	7.93E-04	1.31E-03	1.47E-03	1.47E-03	3.89E-03
30	8.43E-04	7.43E-04	1.39E-03	1.37E-03	1.61E-03	1.07E-03	1.77E-03	1.98E-03	1.98E-03	5.23E-03
25	1.19E-03	1.05E-03	1.96E-03	1.94E-03	2.28E-03	1.51E-03	2.50E-03	2.81E-03	2.81E-03	7.41E-03

20	1.81 E-03	1.60 E-03	2.98E -03	2.94 E-03	3.45 E-03	2.29E -03	3.79E -03	4.26E-03	4.26E -03	1.12E -02
15	3.02 E-03	2.67 E-03	4.97E -03	4.92 E-03	5.76 E-03	3.83E -03	6.33E -03	7.11E-03	7.11E -03	1.88E -02
10	5.80 E-03	5.12 E-03	9.55E -03	9.44 E-03	1.11 E-02	7.35E -03	1.22E -02	1.37E-02	1.37E -02	3.60E -02
5	1.29 E-02	1.14 E-02	2.13E -02	2.10 E-02	2.47 E-02	1.64E -02	2.71E -02	3.04E-02	3.04E -02	8.03E -02
0	2.19 E-02	1.93 E-02	3.61E -02	3.57 E-02	4.18 E-02	2.78E -02	4.59E -02	5.16E-02	5.16E -02	1.36E -01
-5	1.29 E-02	1.14 E-02	2.13E -02	2.10 E-02	2.47 E-02	1.64E -02	2.71E -02	3.04E-02	3.04E -02	8.03E -02
-10	5.80 E-03	5.12 E-03	9.55E -03	9.44 E-03	1.11 E-02	7.35E -03	1.22E -02	1.37E-02	1.37E -02	3.60E -02
-15	3.02 E-03	2.67 E-03	4.97E -03	4.92 E-03	5.76 E-03	3.83E -03	6.33E -03	7.11E-03	7.11E -03	1.88E -02
-20	1.81 E-03	1.60 E-03	2.98E -03	2.94 E-03	3.45 E-03	2.29E -03	3.79E -03	4.26E-03	4.26E -03	1.12E -02
-25	1.19 E-03	1.05 E-03	1.96E -03	1.94 E-03	2.28 E-03	1.51E -03	2.50E -03	2.81E-03	2.81E -03	7.41E -03
-30	8.43 E-04	7.43 E-04	1.39E -03	1.37 E-03	1.61 E-03	1.07E -03	1.77E -03	1.98E-03	1.98E -03	5.23E -03
-35	6.25 E-04	5.52 E-04	1.03E -03	1.02 E-03	1.19 E-03	7.93E -04	1.31E -03	1.47E-03	1.47E -03	3.89E -03
-40	4.82 E-04	4.25 E-04	7.94E -04	7.85 E-04	9.19 E-04	6.11E -04	1.01E -03	1.13E-03	1.13E -03	2.99E -03
-45	3.83 E-04	3.38 E-04	6.30E -04	6.23 E-04	7.30 E-04	4.85E -04	8.02E -04	9.01E-04	9.01E -04	2.38E -03
-50	3.11 E-04	2.74 E-04	5.12E -04	5.06 E-04	5.93 E-04	3.94E -04	6.52E -04	7.32E-04	7.32E -04	1.93E -03
-55	2.58 E-04	2.27 E-04	4.24E -04	4.19 E-04	4.91 E-04	3.26E -04	5.40E -04	6.07E-04	6.07E -04	1.60E -03
-60	2.17 E-04	1.91 E-04	3.57E -04	3.53 E-04	4.14 E-04	2.75E -04	4.55E -04	5.11E-04	5.11E -04	1.35E -03
-65	1.85 E-04	1.63 E-04	3.05E -04	3.01 E-04	3.53 E-04	2.35E -04	3.88E -04	4.36E-04	4.36E -04	1.15E -03

Table A-5: Case 2. Modelled magnetic field strength at 10m below seabed.

Distance along seabed	A (33kV, 185 mm2)	B (33kV, 150 mm2)	C (33kV, 500 mm2)	D (34kV, 500 mm2)	E (36kV, 630 mm2)	F (115kV, 300mm2)	G (150kV, 800mm2)	H (170kV, 1000 mm2)	I (220kV, 1000 mm2)	J (500kV, 1000 mm2)
Metres	microTesla									
80	1.21E-04	1.07E-04	1.99E-04	1.97E-04	2.31E-04	1.53E-04	2.85E-04	2.85E-04	2.85E-04	7.51E-04
75	1.37E-04	1.21E-04	2.26E-04	2.23E-04	2.62E-04	1.74E-04	3.23E-04	3.23E-04	3.23E-04	8.53E-04
70	1.57E-04	1.39E-04	2.59E-04	2.56E-04	3.00E-04	1.99E-04	3.70E-04	3.70E-04	3.70E-04	9.76E-04
65	1.81E-04	1.60E-04	2.99E-04	2.95E-04	3.46E-04	2.30E-04	4.27E-04	4.27E-04	4.27E-04	1.13E-03
60	2.12E-04	1.87E-04	3.49E-04	3.45E-04	4.04E-04	2.69E-04	4.99E-04	4.99E-04	4.99E-04	1.32E-03
55	2.51E-04	2.21E-04	4.13E-04	4.08E-04	4.78E-04	3.18E-04	5.90E-04	5.90E-04	5.90E-04	1.56E-03
50	3.01E-04	2.65E-04	4.95E-04	4.90E-04	5.74E-04	3.81E-04	7.08E-04	7.08E-04	7.08E-04	1.87E-03
45	3.68E-04	3.24E-04	6.05E-04	5.98E-04	7.01E-04	4.66E-04	8.65E-04	8.65E-04	8.65E-04	2.28E-03
40	4.58E-04	4.04E-04	7.54E-04	7.46E-04	8.74E-04	5.81E-04	1.08E-03	1.08E-03	1.08E-03	2.85E-03
35	5.86E-04	5.17E-04	9.65E-04	9.54E-04	1.12E-03	7.42E-04	1.38E-03	1.38E-03	1.38E-03	3.64E-03
30	7.73E-04	6.81E-04	1.27E-03	1.26E-03	1.47E-03	9.79E-04	1.82E-03	1.82E-03	1.82E-03	4.80E-03
25	1.06E-03	9.33E-04	1.74E-03	1.72E-03	2.02E-03	1.34E-03	2.49E-03	2.49E-03	2.49E-03	6.57E-03
20	1.51E-03	1.34E-03	2.49E-03	2.46E-03	2.89E-03	1.92E-03	3.56E-03	3.56E-03	3.56E-03	9.40E-03
15	2.28E-03	2.01E-03	3.75E-03	3.71E-03	4.35E-03	2.89E-03	5.37E-03	5.37E-03	5.37E-03	1.42E-02
10	3.57E-03	3.15E-03	5.87E-03	5.81E-03	6.81E-03	4.52E-03	8.40E-03	8.40E-03	8.40E-03	2.22E-02

5	5.40 E-03	4.76 E-03	8.89 E-03	8.79 E-03	1.03 E-02	6.85E -03	1.27E -02	1.27E-02	1.27E -02	3.36E -02
0	6.52 E-03	5.75 E-03	1.07 E-02	1.06 E-02	1.24 E-02	8.26E -03	1.53E -02	1.53E-02	1.53E -02	4.05E -02
-5	5.40 E-03	4.76 E-03	8.89 E-03	8.79 E-03	1.03 E-02	6.85E -03	1.27E -02	1.27E-02	1.27E -02	3.36E -02
-10	3.57 E-03	3.15 E-03	5.87 E-03	5.81 E-03	6.81 E-03	4.52E -03	8.40E -03	8.40E-03	8.40E -03	2.22E -02
-15	2.28 E-03	2.01 E-03	3.75 E-03	3.71 E-03	4.35 E-03	2.89E -03	5.37E -03	5.37E-03	5.37E -03	1.42E -02
-20	1.51 E-03	1.34 E-03	2.49 E-03	2.46 E-03	2.89 E-03	1.92E -03	3.56E -03	3.56E-03	3.56E -03	9.40E -03
-25	1.06 E-03	9.33 E-04	1.74 E-03	1.72 E-03	2.02 E-03	1.34E -03	2.49E -03	2.49E-03	2.49E -03	6.57E -03
-30	7.73 E-04	6.81 E-04	1.27 E-03	1.26 E-03	1.47 E-03	9.79E -04	1.82E -03	1.82E-03	1.82E -03	4.80E -03
-35	5.86 E-04	5.17 E-04	9.65 E-04	9.54 E-04	1.12 E-03	7.42E -04	1.38E -03	1.38E-03	1.38E -03	3.64E -03
-40	4.58 E-04	4.04 E-04	7.54 E-04	7.46 E-04	8.74 E-04	5.81E -04	1.08E -03	1.08E-03	1.08E -03	2.85E -03
-45	3.68 E-04	3.24 E-04	6.05 E-04	5.98 E-04	7.01 E-04	4.66E -04	8.65E -04	8.65E-04	8.65E -04	2.28E -03
-50	3.01 E-04	2.65 E-04	4.95 E-04	4.90 E-04	5.74 E-04	3.81E -04	7.08E -04	7.08E-04	7.08E -04	1.87E -03
-55	2.51 E-04	2.21 E-04	4.13 E-04	4.08 E-04	4.78 E-04	3.18E -04	5.90E -04	5.90E-04	5.90E -04	1.56E -03
-60	2.12 E-04	1.87 E-04	3.49 E-04	3.45 E-04	4.04 E-04	2.69E -04	4.99E -04	4.99E-04	4.99E -04	1.32E -03
-65	1.81 E-04	1.60 E-04	2.99 E-04	2.95 E-04	3.46 E-04	2.30E -04	4.27E -04	4.27E-04	4.27E -04	1.13E -03
-70	1.57 E-04	1.39 E-04	2.59 E-04	2.56 E-04	3.00 E-04	1.99E -04	3.70E -04	3.70E-04	3.70E -04	9.76E -04
-75	1.37 E-04	1.21 E-04	2.26 E-04	2.23 E-04	2.62 E-04	1.74E -04	3.23E -04	3.23E-04	3.23E -04	8.53E -04
-80	1.21 E-04	1.07 E-04	1.99 E-04	1.97 E-04	2.31 E-04	1.53E -04	2.85E -04	2.85E-04	2.85E -04	7.51E -04

Table A-6: Case 4. Calculated magnetic field produced by 5 DC SPCs (without considering the influence of the geomagnetic field).

Distance along seabed	1 (±320kV, 0.1m)	2 (±500kV, 0.5m)	3 (±500kV, 0.7m)	4 (±500kV, 0.9m)	5 (±550kV, 1m)
Metres			microTesla		
80	1.12E-03	5.62E-03	7.87E-03	1.01E-02	1.12E-02
75	1.28E-03	6.40E-03	8.96E-03	1.15E-02	1.28E-02
70	1.47E-03	7.35E-03	1.03E-02	1.32E-02	1.47E-02
65	1.70E-03	8.52E-03	1.19E-02	1.53E-02	1.70E-02
60	2.00E-03	1.00E-02	1.40E-02	1.80E-02	2.00E-02
55	2.38E-03	1.19E-02	1.67E-02	2.14E-02	2.38E-02
50	2.88E-03	1.44E-02	2.02E-02	2.59E-02	2.88E-02
45	3.55E-03	1.78E-02	2.49E-02	3.20E-02	3.55E-02
40	4.50E-03	2.25E-02	3.15E-02	4.05E-02	4.50E-02
35	5.87E-03	2.94E-02	4.11E-02	5.29E-02	5.87E-02
30	7.99E-03	4.00E-02	5.59E-02	7.19E-02	7.99E-02
25	1.15E-02	5.75E-02	8.05E-02	1.04E-01	1.15E-01
20	1.80E-02	8.98E-02	1.26E-01	1.62E-01	1.80E-01
15	3.19E-02	1.59E-01	2.23E-01	2.87E-01	3.19E-01
10	7.13E-02	3.57E-01	5.00E-01	6.43E-01	7.15E-01
5	2.77E-01	1.39E+00	1.95E+00	2.51E+00	2.79E+00
0	7.18E+00	3.39E+01	4.49E+01	5.39E+01	5.76E+01
-5	2.77E-01	1.39E+00	1.95E+00	2.51E+00	2.79E+00
-10	7.13E-02	3.57E-01	5.00E-01	6.43E-01	7.15E-01
-15	3.19E-02	1.59E-01	2.23E-01	2.87E-01	3.19E-01
-20	1.80E-02	8.98E-02	1.26E-01	1.62E-01	1.80E-01
-25	1.15E-02	5.75E-02	8.05E-02	1.04E-01	1.15E-01
-30	7.99E-03	4.00E-02	5.59E-02	7.19E-02	7.99E-02
-35	5.87E-03	2.94E-02	4.11E-02	5.29E-02	5.87E-02
-40	4.50E-03	2.25E-02	3.15E-02	4.05E-02	4.50E-02

-45	3.55E-03	1.78E-02	2.49E-02	3.20E-02	3.55E-02
-50	2.88E-03	1.44E-02	2.02E-02	2.59E-02	2.88E-02
-55	2.38E-03	1.19E-02	1.67E-02	2.14E-02	2.38E-02
-60	2.00E-03	1.00E-02	1.40E-02	1.80E-02	2.00E-02
-65	1.70E-03	8.52E-03	1.19E-02	1.53E-02	1.70E-02
-70	1.47E-03	7.35E-03	1.03E-02	1.32E-02	1.47E-02
-75	1.28E-03	6.40E-03	8.96E-03	1.15E-02	1.28E-02
-80	1.12E-03	5.62E-03	7.87E-03	1.01E-02	1.12E-02

Table A-7: Case 4. Total magnetic field produced by 5 DC SPCs and the earth.

Distance along seabed	**1 (±320kV, 0.1m)**	**2 (±500kV, 0.5m)**	**3 (±500kV, 0.7m)**	**4 (±500kV, 0.9m)**	**5 (±550kV, 1m)**
Metres			**microTesla**		
80	4.95E+01	4.95E+01	4.95E+01	4.95E+01	4.95E+01
75	4.95E+01	4.95E+01	4.95E+01	4.95E+01	4.95E+01
70	4.95E+01	4.95E+01	4.95E+01	4.95E+01	4.95E+01
65	4.95E+01	4.95E+01	4.95E+01	4.95E+01	4.95E+01
60	4.95E+01	4.95E+01	4.95E+01	4.95E+01	4.95E+01
55	4.95E+01	4.95E+01	4.95E+01	4.95E+01	4.95E+01
50	4.95E+01	4.95E+01	4.95E+01	4.95E+01	4.95E+01
45	4.95E+01	4.95E+01	4.95E+01	4.95E+01	4.95E+01
40	4.95E+01	4.95E+01	4.95E+01	4.94E+01	4.94E+01
35	4.95E+01	4.95E+01	4.94E+01	4.94E+01	4.94E+01
30	4.95E+01	4.94E+01	4.94E+01	4.94E+01	4.94E+01
25	4.95E+01	4.94E+01	4.94E+01	4.94E+01	4.94E+01
20	4.95E+01	4.94E+01	4.94E+01	4.93E+01	4.93E+01
15	4.95E+01	4.93E+01	4.93E+01	4.92E+01	4.92E+01
10	4.94E+01	4.91E+01	4.90E+01	4.89E+01	4.88E+01
5	4.92E+01	4.81E+01	4.75E+01	4.70E+01	4.67E+01

Trinity College Dublin

0	5.62E+01	8.19E+01	9.27E+01	1.02E+02	1.05E+02
-5	4.93E+01	4.85E+01	4.81E+01	4.77E+01	4.75E+01
-10	4.94E+01	4.92E+01	4.91E+01	4.90E+01	4.89E+01
-15	4.95E+01	4.93E+01	4.93E+01	4.92E+01	4.92E+01
-20	4.95E+01	4.94E+01	4.94E+01	4.93E+01	4.93E+01
-25	4.95E+01	4.94E+01	4.94E+01	4.94E+01	4.94E+01
-30	4.95E+01	4.95E+01	4.94E+01	4.94E+01	4.94E+01
-35	4.95E+01	4.95E+01	4.95E+01	4.94E+01	4.94E+01
-40	4.95E+01	4.95E+01	4.95E+01	4.95E+01	4.94E+01
-45	4.95E+01	4.95E+01	4.95E+01	4.95E+01	4.95E+01
-50	4.95E+01	4.95E+01	4.95E+01	4.95E+01	4.95E+01
-55	4.95E+01	4.95E+01	4.95E+01	4.95E+01	4.95E+01
-60	4.95E+01	4.95E+01	4.95E+01	4.95E+01	4.95E+01
-65	4.95E+01	4.95E+01	4.95E+01	4.95E+01	4.95E+01
-70	4.95E+01	4.95E+01	4.95E+01	4.95E+01	4.95E+01
-75	4.95E+01	4.95E+01	4.95E+01	4.95E+01	4.95E+01
-80	4.95E+01	4.95E+01	4.95E+01	4.95E+01	4.95E+01

Table A-8: Case 4. Average magnetic field produced by 5 DC SPCs (without considering the influence of the geomagnetic field).

Distance along seabed	Average magnetic field strength
Metres	microTesla
80	7.20E-03
75	8.19E-03
70	9.40E-03
65	1.09E-02
60	1.28E-02
55	1.52E-02
50	1.84E-02
45	2.27E-02
40	2.88E-02
35	3.76E-02
30	5.12E-02
25	7.36E-02
20	1.15E-01
15	2.04E-01
10	4.57E-01
5	1.78E+00
0	3.95E+01
-5	1.78E+00
-10	4.57E-01
-15	2.04E-01
-20	1.15E-01
-25	7.36E-02
-30	5.12E-02
-35	3.76E-02
-40	2.88E-02
-45	2.27E-02
-50	1.84E-02

-55	1.52E-02
-60	1.28E-02
-65	1.09E-02
-70	9.40E-03
-75	8.19E-03
-80	7.20E-03

Table A-9: Case 4. Average magnetic field produced by 5 DC SPCs and the earth.

Distance along seabed	Average magnetic field strength
Metres	**microTesla**
80	4.95E+01
75	4.95E+01
70	4.95E+01
65	4.95E+01
60	4.95E+01
55	4.95E+01
50	4.95E+01
45	4.95E+01
40	4.95E+01
35	4.95E+01
30	4.94E+01
25	4.94E+01
20	4.94E+01
15	4.93E+01
10	4.90E+01
5	4.77E+01
0	8.75E+01
-5	4.82E+01
-10	4.91E+01
-15	4.93E+01

-20	4.94E+01
-25	4.94E+01
-30	4.94E+01
-35	4.95E+01
-40	4.95E+01
-45	4.95E+01
-50	4.95E+01
-55	4.95E+01
-60	4.95E+01
-65	4.95E+01
-70	4.95E+01
-75	4.95E+01
-80	4.95E+01

Table A-10: Case 5. The average geomagnetic deviation caused by the cables at a location north of the Irish sea.

Distance along seabed	1	2	3	4	5	Average geomagnetic field
Metres				**microTesla**		
40	-4.25E-03	-2.13E-02	-2.98E-02	-3.83E-02	-4.25E-02	-2.72E-02
35	-5.57E-03	-2.78E-02	-3.90E-02	-5.01E-02	-5.57E-02	-3.56E-02
30	-7.60E-03	-3.80E-02	-5.32E-02	-6.84E-02	-7.60E-02	-4.87E-02
25	-1.10E-02	-5.49E-02	-7.69E-02	-9.89E-02	-1.10E-01	-7.03E-02
20	-1.73E-02	-8.63E-02	-1.21E-01	-1.55E-01	-1.73E-01	-1.10E-01
15	-3.09E-02	-1.54E-01	-2.16E-01	-2.78E-01	-3.09E-01	-1.98E-01
10	-7.01E-02	-3.51E-01	-4.91E-01	-6.32E-01	-7.03E-01	-4.49E-01
5	-2.77E-01	-1.39E+00	-1.95E+00	-2.51E+00	-2.79E+00	-1.78E+00
0	6.73E+00	3.24E+01	4.32E+01	5.20E+01	5.57E+01	3.80E+01
-5	-1.98E-01	-9.81E-01	-1.37E+00	-1.76E+00	-1.95E+00	-1.25E+00
-10	-5.96E-02	-2.98E-01	-4.17E-01	-5.37E-01	-5.96E-01	-3.82E-01
-15	-2.78E-02	-1.39E-01	-1.94E-01	-2.50E-01	-2.78E-01	-1.78E-01
-20	-1.59E-02	-7.96E-02	-1.11E-01	-1.43E-01	-1.59E-01	-1.02E-01
-25	-1.03E-02	-5.15E-02	-7.21E-02	-9.28E-02	-1.03E-01	-6.60E-02
-30	-7.21E-03	-3.60E-02	-5.04E-02	-6.49E-02	-7.21E-02	-4.61E-02
-35	-5.32E-03	-2.66E-02	-3.72E-02	-4.79E-02	-5.32E-02	-3.41E-02
-40	-4.09E-03	-2.04E-02	-2.86E-02	-3.68E-02	-4.09E-02	-2.62E-02

Table A-11: Case 5. The average geomagnetic deviation caused by the cables at a location south of the Irish sea.

Distance along seabed	1	2	3	4	5	Average geomagnetic field
Metres				**microTesla**		
40	-4.22E-03	-2.11E-02	-2.95E-02	-3.80E-02	-4.22E-02	-2.70E-02
35	-5.53E-03	-2.76E-02	-3.87E-02	-4.97E-02	-5.53E-02	-3.54E-02
30	-7.54E-03	-3.77E-02	-5.28E-02	-6.79E-02	-7.55E-02	-4.83E-02
25	-1.09E-02	-5.45E-02	-7.64E-02	-9.82E-02	-1.09E-01	-6.98E-02

20	-1.71E-02	-8.57E-02	-1.20E-01	-1.54E-01	-1.71E-01	-1.10E-01
15	-3.07E-02	-1.54E-01	-2.15E-01	-2.77E-01	-3.07E-01	-1.97E-01
10	-6.98E-02	-3.49E-01	-4.89E-01	-6.29E-01	-7.00E-01	-4.47E-01
5	-2.77E-01	-1.39E+00	-1.95E+00	-2.51E+00	-2.79E+00	-1.78E+00
0	6.68E+00	3.23E+01	4.30E+01	5.18E+01	5.55E+01	3.78E+01
-5	-1.93E-01	-9.58E-01	-1.34E+00	-1.71E+00	-1.90E+00	-1.22E+00
-10	-5.87E-02	-2.94E-01	-4.11E-01	-5.28E-01	-5.87E-01	-3.76E-01
-15	-2.74E-02	-1.37E-01	-1.92E-01	-2.47E-01	-2.74E-01	-1.75E-01
-20	-1.57E-02	-7.87E-02	-1.10E-01	-1.42E-01	-1.57E-01	-1.01E-01
-25	-1.02E-02	-5.09E-02	-7.13E-02	-9.17E-02	-1.02E-01	-6.52E-02
-30	-7.13E-03	-3.56E-02	-4.99E-02	-6.42E-02	-7.13E-02	-4.56E-02
-35	-5.26E-03	-2.63E-02	-3.68E-02	-4.74E-02	-5.26E-02	-3.37E-02
-40	-4.04E-03	-2.02E-02	-2.83E-02	-3.64E-02	-4.04E-02	-2.59E-02

Table A-12. Case 6. Average magnetic field produced by 5 DC SPCs (with a twist angle of 0 degrees).

Distance along seabed	1 (±320kV, 0.1m)	2 (±500kV, 0.5m)	3 (±500kV, 0.7m)	4 (±500kV, 0.9m)	5 (±550kV, 1m)	Average magnetic field
Metres			**microTesla**			
25	49.48	49.43	49.41	49.39	49.38	49.42
20	49.47	49.40	49.37	49.33	49.31	49.38
15	49.46	49.33	49.27	49.21	49.18	49.29
10	49.42	49.14	49.00	48.86	48.78	49.04
5	49.23	48.19	47.67	47.15	46.89	47.83
0	52.47	64.20	69.66	74.67	76.98	67.60
-5	49.34	48.75	48.46	48.17	48.03	48.55
-10	49.43	49.21	49.10	49.00	48.94	49.14
-15	49.46	49.36	49.30	49.25	49.22	49.32
-20	49.47	49.41	49.38	49.35	49.33	49.39
-25	49.48	49.44	49.42	49.40	49.39	49.42

Table A-13. Case 6. Average magnetic field produced by 5 DC SPCs (with a twist angle of 90 degrees).

Distance along seabed	1 (±320kV, 0.1m)	2 (±500kV, 0.5m)	3 (±500kV, 0.7m)	4 (±500kV, 0.9m)	5 (±550kV, 1m)	Average magnetic field
Metres			**microTesla**			
25	49.49	49.50	49.51	49.51	49.52	49.51
20	49.49	49.51	49.52	49.52	49.53	49.51
15	49.49	49.52	49.53	49.54	49.55	49.52
10	49.49	49.52	49.53	49.54	49.55	49.53
5	49.44	49.24	49.15	49.08	49.04	49.19
0	48.39	46.00	46.27	47.85	49.23	47.55
-5	49.70	50.57	51.01	51.44	51.65	50.88
-10	49.53	49.71	49.80	49.89	49.93	49.77
-15	49.51	49.57	49.61	49.64	49.66	49.60
-20	49.50	49.53	49.55	49.57	49.58	49.55
-25	49.49	49.52	49.53	49.54	49.54	49.52

Table A-14. Case 6. Average magnetic field produced by 5 DC SPCs (with a twist angle of 180 degrees).

Distance along seabed	1 (±320kV, 0.1m)	2 (±500kV, 0.5m)	3 (±500kV, 0.7m)	4 (±500kV, 0.9m)	5 (±550kV, 1m)	Average magnetic field
Metres			**microTesla**			
25	49.50	49.54	49.57	49.59	49.60	49.56
20	49.51	49.58	49.61	49.64	49.66	49.60
15	49.52	49.64	49.71	49.77	49.80	49.69
10	49.56	49.84	49.98	50.12	50.19	49.94
5	49.75	50.78	51.31	51.83	52.10	51.15
0	46.53	35.50	30.79	26.81	25.13	32.95
-5	49.64	50.25	50.57	50.88	51.04	50.48
-10	49.54	49.76	49.87	49.98	50.04	49.84

-15	49.51	49.62	49.67	49.73	49.75	49.66
-20	49.50	49.57	49.60	49.63	49.64	49.59
-25	49.50	49.54	49.56	49.58	49.59	49.55

Table A-15: Case A. The induced electric field produced by the 10 AC SPCs.

Distance along seabed	A (33kV, 185 mm2)	B (33kV, 150 mm2)	C (33kV, 500 mm2)	D (34kV, 500 mm2)	E (36kV, 630 mm2)	F (115 kV, 300 mm2)	G (150 kV, 800 mm2)	H (170kV, 1000 mm2)	I (220kV, 1000 mm2)	J (500kV, 1000 mm2)
Metres					**Volts per metre**					
80	3.87E-08	3.41E-08	6.37E-08	6.30E-08	7.38E-08	4.91E-08	8.10E-08	9.11E-08	9.11E-08	2.40E-07
75	4.40E-08	3.89E-08	7.25E-08	7.17E-08	8.40E-08	5.58E-08	9.22E-08	1.04E-07	1.04E-07	2.74E-07
70	5.06E-08	4.46E-08	8.32E-08	8.23E-08	9.64E-08	6.41E-08	1.06E-07	1.19E-07	1.19E-07	3.14E-07
65	5.86E-08	5.17E-08	9.65E-08	9.54E-08	1.12E-07	7.43E-08	1.23E-07	1.38E-07	1.38E-07	3.64E-07
60	6.88E-08	6.07E-08	1.13E-07	1.12E-07	1.31E-07	8.72E-08	1.44E-07	1.62E-07	1.62E-07	4.27E-07
55	8.19E-08	7.22E-08	1.35E-07	1.33E-07	1.56E-07	1.04E-07	1.71E-07	1.93E-07	1.93E-07	5.09E-07
50	9.91E-08	8.74E-08	1.63E-07	1.61E-07	1.89E-07	1.26E-07	2.07E-07	2.33E-07	2.33E-07	6.15E-07
45	1.22E-07	1.08E-07	2.01E-07	1.99E-07	2.33E-07	1.55E-07	2.56E-07	2.88E-07	2.88E-07	7.60E-07
40	1.55E-07	1.37E-07	2.55E-07	2.52E-07	2.95E-07	1.96E-07	3.24E-07	3.64E-07	3.64E-07	9.61E-07
35	2.02E-07	1.78E-07	3.33E-07	3.29E-07	3.85E-07	2.56E-07	4.23E-07	4.76E-07	4.76E-07	1.26E-06
30	2.75E-07	2.43E-07	4.53E-07	4.48E-07	5.24E-07	3.49E-07	5.76E-07	6.47E-07	6.47E-07	1.71E-06
25	3.96E-07	3.49E-07	6.52E-07	6.44E-07	7.55E-07	5.02E-07	8.29E-07	9.32E-07	9.32E-07	2.46E-06

20	6.18E-07	5.45E-07	1.02E-06	1.01E-06	1.18E-06	7.83E-07	1.29E-06	1.45E-06	1.45E-06	3.84E-06
15	1.10E-06	9.67E-07	1.80E-06	1.78E-06	2.09E-06	1.39E-06	2.30E-06	2.58E-06	2.58E-06	6.81E-06
10	2.45E-06	2.16E-06	4.04E-06	3.99E-06	4.68E-06	3.11E-06	5.14E-06	5.78E-06	5.78E-06	1.52E-05
5	9.53E-06	8.41E-06	1.57E-05	1.55E-05	1.82E-05	1.21E-05	2.00E-05	2.24E-05	2.24E-05	5.92E-05
0	2.48E-04	2.19E-04	4.08E-04	4.03E-04	4.72E-04	3.14E-04	5.18E-04	5.83E-04	5.83E-04	1.53E-03
-5	9.53E-06	8.41E-06	1.57E-05	1.55E-05	1.82E-05	1.21E-05	2.00E-05	2.24E-05	2.24E-05	5.92E-05
-10	2.45E-06	2.16E-06	4.04E-06	3.99E-06	4.68E-06	3.11E-06	5.14E-06	5.78E-06	5.78E-06	1.52E-05
-15	1.10E-06	9.67E-07	1.80E-06	1.78E-06	2.09E-06	1.39E-06	2.30E-06	2.58E-06	2.58E-06	6.81E-06
-20	6.18E-07	5.45E-07	1.02E-06	1.01E-06	1.18E-06	7.83E-07	1.29E-06	1.45E-06	1.45E-06	3.84E-06
-25	3.96E-07	3.49E-07	6.52E-07	6.44E-07	7.55E-07	5.02E-07	8.29E-07	9.32E-07	9.32E-07	2.46E-06
-30	2.75E-07	2.43E-07	4.53E-07	4.48E-07	5.24E-07	3.49E-07	5.76E-07	6.47E-07	6.47E-07	1.71E-06
-35	2.02E-07	1.78E-07	3.33E-07	3.29E-07	3.85E-07	2.56E-07	4.23E-07	4.76E-07	4.76E-07	1.26E-06
-40	1.55E-07	1.37E-07	2.55E-07	2.52E-07	2.95E-07	1.96E-07	3.24E-07	3.64E-07	3.64E-07	9.61E-07
-45	1.22E-07	1.08E-07	2.01E-07	1.99E-07	2.33E-07	1.55E-07	2.56E-07	2.88E-07	2.88E-07	7.60E-07
-50	9.91E-08	8.74E-08	1.63E-07	1.61E-07	1.89E-07	1.26E-07	2.07E-07	2.33E-07	2.33E-07	6.15E-07
-55	8.19E-08	7.22E-08	1.35E-07	1.33E-07	1.56E-07	1.04E-07	1.71E-07	1.93E-07	1.93E-07	5.09E-07
-60	6.88E-08	6.07E-08	1.13E-07	1.12E-07	1.31E-07	8.72E-08	1.44E-07	1.62E-07	1.62E-07	4.27E-07
-65	5.86E-08	5.17E-08	9.65E-08	9.54E-08	1.12E-07	7.43E-08	1.23E-07	1.38E-07	1.38E-07	3.64E-07
-70	5.06E-08	4.46E-08	8.32E-08	8.23E-08	9.64E-08	6.41E-08	1.06E-07	1.19E-07	1.19E-07	3.14E-07
-75	4.40E-08	3.89E-08	7.25E-08	7.17E-08	8.40E-08	5.58E-08	9.22E-08	1.04E-07	1.04E-07	2.74E-07
-80	3.87E-08	3.41E-08	6.37E-08	6.30E-08	7.38E-08	4.91E-08	8.10E-08	9.11E-08	9.11E-08	2.40E-07

Table A-16: Case A. The average induced electric field produced by the cables.

Distance along seabed	Average induced electric field
Metres	**Volts per metre**
80	8.26E-08
75	9.40E-08
70	1.08E-07
65	1.25E-07
60	1.47E-07
55	1.75E-07
50	2.11E-07
45	2.61E-07
40	3.30E-07
35	4.31E-07
30	5.87E-07
25	8.45E-07
20	1.32E-06
15	2.34E-06
10	5.24E-06
5	2.03E-05
0	5.27E-04
-5	2.03E-05
-10	5.24E-06
-15	2.34E-06
-20	1.32E-06
-25	8.45E-07
-30	5.87E-07
-35	4.31E-07
-40	3.30E-07
-45	2.61E-07
-50	2.11E-07

-55	1.75E-07
-60	1.47E-07
-65	1.25E-07
-70	1.08E-07
-75	9.40E-08
-80	8.26E-08

Table A-17: Case B. The electric field induced over the 10 AC cables by a marine species travelling at a speed of 4 m/s.

Distance along seabed	A (33kV, 185 mm2)	B (33kV, 150 mm2)	C (33kV, 500 mm2)	D (34kV, 500 mm2)	E (36kV, 630 mm2)	F (115 kV, 300 mm2)	G (150 kV, 800 mm2)	H (170kV, 1000 mm2)	I (220kV, 1000 mm2)	J (500kV, 1000 mm2)
Metres	**Volts per metre**									
80	4.93E-10	4.35E-10	8.11E-10	8.02E-10	9.4E-10	6.25E-10	1.03E-09	1.16E-09	1.16E-09	3.06E-09
75	5.61E-10	4.95E-10	9.23E-10	9.13E-10	1.07E-09	7.11E-10	1.17E-09	1.32E-09	1.32E-09	3.48E-09
70	6.44E-10	5.68E-10	1.06E-09	1.05E-09	1.23E-09	8.16E-10	1.35E-09	1.52E-09	1.52E-09	4E-09
65	7.47E-10	6.58E-10	1.23E-09	1.21E-09	1.42E-09	9.46E-10	1.56E-09	1.76E-09	1.76E-09	4.64E-09
60	8.76E-10	7.73E-10	1.44E-09	1.43E-09	1.67E-09	1.11E-09	1.83E-09	2.06E-09	2.06E-09	5.44E-09
55	1.04E-09	9.2E-10	1.72E-09	1.7E-09	1.99E-09	1.32E-09	2.18E-09	2.45E-09	2.45E-09	6.48E-09
50	1.26E-09	1.11E-09	2.08E-09	2.05E-09	2.41E-09	1.6E-09	2.64E-09	2.97E-09	2.97E-09	7.84E-09
45	1.56E-09	1.37E-09	2.56E-09	2.53E-09	2.97E-09	1.97E-09	3.26E-09	3.67E-09	3.67E-09	9.67E-09
40	1.97E-09	1.74E-09	3.24E-09	3.21E-09	3.76E-09	2.5E-09	4.12E-09	4.64E-09	4.64E-09	1.22E-08
35	2.57E-09	2.27E-09	4.24E-09	4.19E-09	4.91E-09	3.26E-09	5.39E-09	6.06E-09	6.06E-09	1.6E-08

30	3.5E-09	3.09E-09	5.76E-09	5.7E-09	6.68E-09	4.44E-09	7.33E-09	8.24E-09	8.24E-09	2.17E-08
25	5.04E-09	4.45E-09	8.3E-09	8.2E-09	9.61E-09	6.39E-09	1.05E-08	1.19E-08	1.19E-08	3.13E-08
20	7.87E-09	6.94E-09	1.29E-08	1.28E-08	1.5E-08	9.97E-09	1.65E-08	1.85E-08	1.85E-08	4.89E-08
15	1.4E-08	1.23E-08	2.3E-08	2.27E-08	2.66E-08	1.77E-08	2.92E-08	3.29E-08	3.29E-08	8.67E-08
10	3.12E-08	2.76E-08	5.14E-08	5.08E-08	5.96E-08	3.96E-08	6.54E-08	7.35E-08	7.35E-08	1.94E-07
5	1.21E-07	1.07E-07	2E-07	1.97E-07	2.31E-07	1.54E-07	2.54E-07	2.86E-07	2.86E-07	7.54E-07
0	3.15E-06	2.78E-06	5.19E-06	5.13E-06	6.01E-06	4E-06	6.6E-06	7.42E-06	7.42E-06	1.94E-05
-5	1.21E-07	1.07E-07	2E-07	1.97E-07	2.31E-07	1.54E-07	2.54E-07	2.86E-07	2.86E-07	7.54E-07
-10	3.12E-08	2.76E-08	5.14E-08	5.08E-08	5.96E-08	3.96E-08	6.54E-08	7.35E-08	7.35E-08	1.94E-07
-15	1.4E-08	1.23E-08	2.3E-08	2.27E-08	2.66E-08	1.77E-08	2.92E-08	3.29E-08	3.29E-08	8.67E-08
-20	7.87E-09	6.94E-09	1.29E-08	1.28E-08	1.5E-08	9.97E-09	1.65E-08	1.85E-08	1.85E-08	4.89E-08
-25	5.04E-09	4.45E-09	8.3E-09	8.2E-09	9.61E-09	6.39E-09	1.05E-08	1.19E-08	1.19E-08	3.13E-08
-30	3.5E-09	3.09E-09	5.76E-09	5.7E-09	6.68E-09	4.44E-09	7.33E-09	8.24E-09	8.24E-09	2.17E-08
-35	2.57E-09	2.27E-09	4.24E-09	4.19E-09	4.91E-09	3.26E-09	5.39E-09	6.06E-09	6.06E-09	1.6E-08
-40	1.97E-09	1.74E-09	3.24E-09	3.21E-09	3.76E-09	2.5E-09	4.12E-09	4.64E-09	4.64E-09	1.22E-08
-45	1.56E-09	1.37E-09	2.56E-09	2.53E-09	2.97E-09	1.97E-09	3.26E-09	3.67E-09	3.67E-09	9.67E-09
-50	1.26E-09	1.11E-09	2.08E-09	2.05E-09	2.41E-09	1.6E-09	2.64E-09	2.97E-09	2.97E-09	7.84E-09
-55	1.04E-09	9.2E-10	1.72E-09	1.7E-09	1.99E-09	1.32E-09	2.18E-09	2.45E-09	2.45E-09	6.48E-09
-60	8.76E-10	7.73E-10	1.44E-09	1.43E-09	1.67E-09	1.11E-09	1.83E-09	2.06E-09	2.06E-09	5.44E-09
-65	7.47E-10	6.58E-10	1.23E-09	1.21E-09	1.42E-09	9.46E-10	1.56E-09	1.76E-09	1.76E-09	4.64E-09
-70	6.44E-10	5.68E-10	1.06E-09	1.05E-09	1.23E-09	8.16E-10	1.35E-09	1.52E-09	1.52E-09	4E-09

-75	5.61E-10	4.95E-10	9.23E-10	9.13E-10	1.07E-09	7.11E-10	1.17E-09	1.32E-09	1.32E-09	3.48E-09
-80	4.93E-10	4.35E-10	8.11E-10	8.02E-10	9.4E-10	6.25E-10	1.03E-09	1.16E-09	1.16E-09	3.06E-09

Table A-18: Case B. The average electric field induced over the 10 AC cables by a marine species travelling at a speed of 4 m/s.

Distance along seabed	Average
Metres	**Volts per metre**
80	1.05E-09
75	1.2E-09
70	1.37E-09
65	1.59E-09
60	1.87E-09
55	2.23E-09
50	2.69E-09
45	3.32E-09
40	4.21E-09
35	5.49E-09
30	7.47E-09
25	1.08E-08
20	1.68E-08
15	2.98E-08
10	6.67E-08
5	2.59E-07
0	6.71E-06
-5	2.59E-07
-10	6.67E-08
-15	2.98E-08
-20	1.68E-08
-25	1.08E-08
-30	7.47E-09
-35	5.49E-09
-40	4.21E-09

-45	3.32E-09
-50	2.69E-09
-55	2.23E-09
-60	1.87E-09
-65	1.59E-09
-70	1.37E-09
-75	1.2E-09
-80	1.05E-09

Table A-19: Case C. The average electric field induced over the 5 DC cables by a marine species travelling at a speed of 4 m/s.

Distance along seabed	1 (±320kV, 0m)	2 (±500kV, 0.5m)	3 (±500kV, 0.7m)	4 (±500kV, 0.9m)	5 (±550kV, 1m)	Average induced electric field
Metres			**Volt per metre**			
20	7.18E-08	3.59E-07	5.03E-07	6.47E-07	7.19E-07	4.60E-07
15	1.27E-07	6.37E-07	8.92E-07	1.15E-06	1.28E-06	8.16E-07
10	2.85E-07	1.43E-06	2.00E-06	2.57E-06	2.86E-06	1.83E-06
5	1.11E-06	5.55E-06	7.79E-06	1.00E-05	1.12E-05	7.13E-06
0	2.87E-05	1.36E-04	1.80E-04	2.16E-04	2.30E-04	1.58E-04
-5	1.11E-06	5.55E-06	7.79E-06	1.00E-05	1.12E-05	7.13E-06

-10	2.85E-07	1.43E-06	2.00E-06	2.57E-06	2.86E-06	1.83E-06
-15	1.27E-07	6.37E-07	8.92E-07	1.15E-06	1.28E-06	8.16E-07
-20	7.18E-08	3.59E-07	5.03E-07	6.47E-07	7.19E-07	4.60E-07

Appendix B
Marine Species

Table B-1: The refined list of marine species in the Irish sea (including endangered and vulnerable species).

Main Group	Subgroup	Ordinary name	Taxon Name
Mammals	Dolphin	Bottle-nosed Dolphin	Tursiops truncatus
Mammals	Dolphin	Common Dolphin	Delphinus delphis
Mammals	Seals	Common Seal	Phoca vitulina
Mammals	Seals	Earless seals	Phocidae
Mammals	Seals	Grey seal	Halichoerus grypus
Reptiles	Turtles	Leatherback	Dermochelys coriacea
Reptiles	Turtles	Loggerhead	Caretta caretta
Reptiles	Turtles	Hawksbill	Eretmochelys imbricata
Reptiles	Turtles	Kemp's Ridley	Lepidochelys kempii
Reptiles	Turtles	Green Turtle	Chelonia mydas
Elasmobranchs	Sharks	Spurdog	Squalus acanthias
Elasmobranchs	Sharks	Tope	Galeorhinus galeus
Elasmobranchs	Sharks	Nursehound or large-spotted dogfish	Scyliorhinus stellaris
Elasmobranchs	Sharks	longnose velvet dogfish	Centroselachus crepidater
Elasmobranchs	Sharks	Portuguese dogfish	Centroscymnus coelolepis
Elasmobranchs	Sharks	Basking shark	Cetorhinus maximus
Elasmobranchs	Sharks	Small-spotted catshark	Scyliorhinus canicula
Elasmobranchs	Sharks	Porbeagle shark	Lamna nasus
Elasmobranchs	Sharks	Angel shark	Squatina squatina
Elasmobranchs	Sharks	Leafscale gulper shark	Centrophorus squamosus
Elasmobranchs	Sharks	kitefin shark	Dalatias licha
Elasmobranchs	Sharks	Common smooth-hound	Mustelus mustelus
Elasmobranchs	Rays	Common Stingray	Dasyatis pastinaca
Elasmobranchs	Rays	Spotted Ray	Raja montagui
Elasmobranchs	Rays	Thornback ray	Raja clavata
Elasmobranchs	Rays	Blonde Ray	Bathyraja brachyurops
Elasmobranchs	Rays	Shagreen ray	Leucoraja fullonica
Elasmobranchs	Rays	Cuckoo ray	Leucoraja naevus
Elasmobranchs	Skate	Longnose skate	Dipturus oxyrinchus
Elasmobranchs	Skate	Undulate skate	Raja undulata
Elasmobranchs	Skate	white skate	Rostroraja alba
Elasmobranchs	Skate	Flapper skate	Dipturus intermedia
Elasmobranchs	Skate	Common (blue) Skate	Dipturus batis
Ocean Fishes	Fish	European flounder	Platichthys flesus
Ocean Fishes	Fish	Pollock	Pollachius virens
Ocean Fishes	Fish	Turbot	Psetta maxima
Ocean Fishes	Fish	Brown trout	Salmo trutta
Ocean Fishes	Fish	European seabass	Dicentrarchus labrax
Ocean Fishes	Fish	Shanny	Lipophrys pholis
Ocean Fishes	Fish	Tompot blenny	Parablennius gattorugine
Ocean Fishes	Fish	European pollock	Pollachius pollachius
Ocean Fishes	Fish	The black faced blenny	Tripterygion delaisi
Ocean Fishes	Fish	Five-bearded rockling	Ciliata mustela
Ocean Fishes	Fish	Armed bullhead	Agonus cataphractus
Ocean Fishes	Fish	Lesser sand eel	Ammodytes tobianus
Ocean Fishes	Fish	Lipped mullet	Chelon labrosus
Ocean Fishes	Fish	Atlantic cod	Gadus morhua
Ocean Fishes	Fish	Shore rockling	Gaidropsarus mediterraneus
Ocean Fishes	Fish	Common dab	Limanda limanda
Ocean Fishes	Fish	Whiting	Merlangius merlangus
Ocean Fishes	Fish	European plaice	Pleuronectes platessa
Ocean Fishes	Fish	Common goby	Pomatoschistus microps
Ocean Fishes	Fish	Turbot	Scophthalmus rhombus
Ocean Fishes	Fish	Common sole	Solea solea

Ocean Fishes	Fish	Sea stickleback	Spinachia spinachia
Ocean Fishes	Fish	The European sprat	Sprattus sprattus
Ocean Fishes	Fish	Greater pipefish	Syngnathus acus
Ocean Fishes	Fish	European eel	Anguilla anguilla
Ocean Fishes	Fish	Tub gurnard	Chelidonichthys lucerna
Ocean Fishes	Fish	Stone loach	Barbatula barbatula
Ocean Fishes	Fish	Bream	Sparus aurata
Ocean Fishes	Fish	Twait shad	Alosa fallax
Ocean Fishes	Fish	Piper gurnard	Trigla lyra
Ocean Fishes	Fish	Butterfish	Pholis gunnellus
Ocean Fishes	Fish	Red scorpionfish	Scorpaena scrofa
Ocean Fishes	Fish	Ballan wrasse	Labrus bergylta
Ocean Fishes	Fish	Stickleback	Gasterosteus aculeatus
Ocean Fishes	Fish	Shorthorn sculpin	Myoxocephalus scorpius
Ocean Fishes	Fish	Leopard-spotted goby	Thorogobius ephippiatus
Ocean Fishes	Fish	Poor cod	Trisopterus minutus
Invertebrates	Crustaceans	Blue striped squat lobster	Galathea strigosa
Invertebrates	Crustaceans	Common lobster	Homarus gammarus
Invertebrates	Crustaceans	Velvet crab	Necora puber
Invertebrates	Crustaceans	Common prawn	Palaemon serratus
Invertebrates	Crustaceans	Green crab	Carcinus maenas
Invertebrates	Crustaceans	Porcelain crab	Porcellana platycheles
Invertebrates	Crustaceans	Risso's crab	Xantho pilipes
Invertebrates	Crustaceans	Edible crab	Cancer pagurus
Invertebrates	Crustaceans	Marine hermit crab	Pagurus bernhardus
Invertebrates	Crustaceans	Northern rock barnacle	Semibalanus balanoides
Invertebrates	Crustaceans	Sand hopper	Talitrus saltator
Invertebrates	Crustaceans	N/A	Xantho incisus
Invertebrates	Crustaceans	Pelagic gooseneck barnacle	Lepas anatifera
Invertebrates	Crustaceans	Harbour crab	Liocarcinus depurator
Invertebrates	Crustaceans	Sea slater	Ligia oceanica
Invertebrates	Crustaceans	Wrinkled swimming crab	Liocarcinus corrugatus
Invertebrates	Crustaceans	Brown shrimp	Crangon crangon
Invertebrates	Crustaceans	Arch-fronted swimming crab	Liocarcinus arcuatus
Invertebrates	Molluscs	Otter shell	Lutraria lutraria
Invertebrates	Molluscs	Sea hare	Aplysia punctata
Invertebrates	Molluscs	Common whelk	Buccinum undatum
Invertebrates	Molluscs	N/A	Gibbula cineraria
Invertebrates	Molluscs	Common periwinkle	Littorina littorea
Invertebrates	Molluscs	Flat periwinkle	Littorina obtusata
Invertebrates	Molluscs	Rough periwinkle	Littorina saxatilis
Invertebrates	Molluscs	Small periwinkle	Melarhaphe neritoides
Invertebrates	Molluscs	Blue mussel	Mytilus edulis
Invertebrates	Molluscs	Common limpet	Patella vulgata
Invertebrates	Molluscs	Flat periwinkle	Littorina obtusata
Invertebrates	Molluscs	The flat top shell	Gibbula umbilicalis
Invertebrates	Molluscs	Patina laevis	Helcion pellucidum
Invertebrates	Molluscs	Common chiton	Lepidochitona cinerea
Invertebrates	Molluscs	Toothed top shell	Osilinus lineatus
Invertebrates	Molluscs	Atlantic dogwinkle	Nucella lapillus
Invertebrates	Molluscs	European painted top shell	Calliostoma zizyphinum
Invertebrates	Molluscs	Common cockle	Cerastoderma edule
Invertebrates	Molluscs	Bristled chiton	Acanthochitona fascicularis
Invertebrates	Molluscs	Chiton	Leptochiton scabridus
Invertebrates	Molluscs	Atlantic bobtail	Sepiola atlantica
Invertebrates	Molluscs	Curled octopus	Eledone cirrhosa
Invertebrates	Annelid	Twin fan worm	Bispira volutacornis
Invertebrates	Annelid	Lugworm	Arenicola marina
Invertebrates	Annelid	Green-leaf worm	Eulalia viridis
Invertebrates	Annelid	Peacock worm	Sabella pavonina
Invertebrates	Annelid	Keelworm	Pomatoceros triqueter
Invertebrates	Annelid	Honeycomb worm	Sabellaria alveolata
Invertebrates	Cnidarians	Snakelocks anemone	Anemonia viridis
Invertebrates	Cnidarians	Dahlia anemone	Urticina felina

Trinity College Dublin

Invertebrates	Cnidarians	Strawberry anemone	Actinia fragacea
Invertebrates	Cnidarians	Beadlet anemone	Actinia equina
Invertebrates	Cnidarians	Firework anemone	Pachycerianthus multiplicatus
Invertebrates	Cnidarians	Tube anemone	Cerianthus lloydii
Invertebrates	Cnidarians	Frilled anemone	Metridium senile
Invertebrates	Cnidarians	Portuguese man o' war	Physalia physalis
Invertebrates	Cnidarians	Barrel jellyfish	Rhizostoma pulmo
Invertebrates	Cnidarians	Compass jellyfish	Chrysaora hysoscella
Invertebrates	Cnidarians	Blue jellyfish	Cyanea lamarckii
Invertebrates	Cnidarians	Lion's mane jellyfish	Cyanea capillata
Invertebrates	Cnidarians	Red sea fingers	Alcyonium glomeratum
Invertebrates	Cnidarians	By-the-Wind Sailor	Velella velella
Invertebrates	Cnidarians	Compass jellyfish	Chrysaora hysoscella